NONLINEAR MODEL FOR REINFORCED CONCRETE SLABS

by

Fuad K. Bashur

David Darwin

A Report on a Research Project Sponsored by
THE NATIONAL SCIENCE FOUNDATION
Research Grant ENG76-09444

University of Kansas
Lawrence, Kansas
December 1976

ACKNOWLEDGEMENTS

This report is based on a thesis submitted by Fuad K. Bashur in partial fulfillment of the requirements for the Ph.D. degree. The support of Mr. Bashur's graduate study by the Syrian Government and the Department of Civil Engineering at the University of Kansas is gratefully acknowledged.

The numerical calculations were performed on the Honeywell 635 and 66/60 systems of the University of Kansas Computation Center.

This study was funded, in part, under National Science Foundation Research Grant No. ENG76-09444.

TABLE OF CONTENTS

LIST OF TABLES

LIST OF FIGURES

LIST OF FIGURES (continued)

LIST OF FIGURES (continued)

Chapter 1

INTRODUCTION

1.1 General

Reinforced concrete is a major construction material. Its properties are not as well known as other more homogeneous structural materials such as steel and aluminum. The difficulties inherent in the analysis of reinforced concrete elements are due to the non-homogeneity of the materials, their nonlinear response to load, the progressive destruction of bond between steel and concrete, progressive cracking and the influence of shrinkage and creep.

These difficulties have not prevented the extensive use of reinforced concrete in structural systems, where many approximate and empirical relations have been applied successfully. The rapid changes in practical design codes show that improved design and analysis procedures continue to be developed. However, more research is needed.

One area where more research is needed is the study of reinforced concrete slabs. Mayer and Rusch (58) indicate that excessive slab deflection is the most common cause of damage in reinforced concrete structures. Serviceability requirements, in particular limitations on cracking and deflection, are becoming more important with the use of high strength steel and concrete.

While a large volume of test data has been generated on the structural behavior of slabs, and relatively accurate procedures have been developed to predict member strength, accurate models for the load-deflection of reinforced concrete slabs are not widely

available.

In this research, a finite element representation is developed for reinforced concrete slabs. Concrete and steel are treated as nonlinear materials, and the variation of material properties through the slab depth is considered.

1.2 Previous Work

Plates are highly indeterminate structures. Difficulties in analysis exist in satisfying equilibrium, stress-strain relations, compatibility of strains and boundary conditions. These difficulties increase when classical theory is applied to reinforced concrete slabs due to the non-homogeneous nature of concrete, the nonlinear response of the material, cracking and time effects. The use of classical elastic thin plate theory, therefore, has been limited to reinforced concrete slabs under low levels of stress. Classical elastic theory fails to predict either the yield moment capacity or the load-deflection behavior of reinforced concrete slabs.

An alternative to elastic analysis is yield line analysis, which provides an estimate of slab bending strength (46,47,52,79). Yield line analysis of slabs gives no information on either shear strength or deflection.

Due to the limitations of the classical and yield line theories, some approximate methods have emerged: The cross beam analogy, the gridwork method, the wide beam method, the equivalent frame method and the finite element method. The most recent state-of-the-art report on deflection of two-way reinforced concrete systems, is given by the ACI committee 435 (3). The paper summarizes the

practical methods for calculating the deflection of two-way slabs.

Of the approximate methods of structural analysis, the finite element method has proved to be an extremely powerful and versatile tool for analysis. In recent years, extensive research has been conducted using the finite element method for the analysis of reinforced concrete structures. Scordelis (85) and Schnobrich (84) provide excellent summaries of this work.

An early application of the finite element method to reinforced concrete was carried out by Ngo and Scordelis (66). They developed an elastic two-dimensional model of reinforced concrete beams with defined crack patterns. Bond slip between concrete and steel bars was modeled by finite spring elements designated as bond links spaced along the bar length. Cracking was modeled by separation of nodal points and a redefinition of structural topology. Nilson (67) extended this work by including nonlinear properties. This approach has not achieved popularity due to the difficulties encountered in redefining the structural topology after each load increment. Mufti, Mirza, McCutcheon and Houde (61,62) used the same model but without modifying the topology. They deleted the cracked element from the overall stiffness; the forces in the cracked element were redistributed during the next cycle.

Rashid (71) introduced another approach in which the cracked concrete was treated as an orthotropic material. The steel elements were assumed to be elastic/perfectly plastic. The Von-Mises yield criterion and the Prandtl-Reuss flow equations were used to define the behavior of the steel in the range of plastic deformation. This

approach proved to be more popular and many investigators have used it with variations in material properties and modes of failure.

Isenberg and Adham (43) introduced a nonlinear orthotropic model and demonstrated its use on tunnel problems. The nonlinear stress-strain behavior of concrete and steel was idealized with bilinear stress-strain curves. Bond and the effect of lateral confinement on compression and tensile strength were considered.

Franklin (32) analyzed reinforced concrete frames with and without infilled shear panels using quadrilateral plane stress elements under monotonic and cyclic loading and compared the analytical studies with the experimental results.

Valliappan and Doolan (90) studied the stress distribution in reinforced concrete structures (beams, haunches, hinges), using an elasto-plastic model for steel and concrete. The concrete was represented as a brittle material in tension.

Other relevant studies include the work done by Yuzugullu and Schnobrich (94) in which reinforced concrete shear wall-frame systems were analyzed. Suidan and Schnobrich (87) used a three-dimensional isoparametric element to study cracking, crushing and yielding of reinforced concrete beams. Their analysis included a shear retention factor for post cracking behavior. Darwin and Pecknold (26,27,28) introduced a nonlinear constitutive model for plain concrete subject to cyclic biaxial stresses, and the concept of equivalent uniaxial strain, in order to separate the Poisson effect from the cumulative strain. They analyzed shear walls under monotonic and cyclic loading and compared their results with experimental results; a good match

was obtained. Salem and Mohraz (75) analyzed planar reinforced structures, deep beams and multiple opening conduits. They employed linear isoparametric quadrilateral elements with incompatible deformation modes. The concrete in compression was modeled as a nonlinear material using the formulation developed by Mikkola and Schnobrich (60). In tension, the concrete followed a descending stress-strain curve after cracking.

Nam and Salmon (64) compared the constant stiffness and the variable stiffness approaches for nonlinear problems. Using a combination of isoparametric elements and bar elements they found the variable stiffness approach to be far superior for problems involving the prediction of cracking in reinforced concrete structures.

Reinforced concrete slabs and shells have received considerable attention from investigators. Two basic approaches have been used: the modified stiffness approach (9,45) and the layered element approach (36,37,53,54,81,82,83,92).

Bell and Elms (9) presented a method for computer analysis of reinforced concrete slabs which produces deflections and crack patterns for the total range of loading from zero to ultimate. Triangular bending elements and the method of successive approximations were used. Cracking normal to the principal moment direction was accounted for by using a reduced stiffness. Theoretical and experimental displacement curves did not match. Later (10) they developed a partially cracked element, but they found that this element was neither as accurate nor as well behaved as an analysis based on either an elastic or a totally cracked element.

Jofriet and McNeice (45) used a quadrilateral plate bending element with four corner nodes and three degrees of freedom at each node. Cracking on normals to the principal moment directions were accounted for by using a reduced stiffness suggested by Beeby (8) for beams. Their research did not take into account load history or post-yielding behavior.

Scanlon (81,82) presented a finite element analysis to determine the effects of cracking, creep and shrinkage on reinforced concrete slabs. The finite element consisted of a series of layers, each with a different plane stress constitutive relationship. Cracks progressed through the thickness of the element, layer by layer, parallel or perpendicular to the orthogonal reinforcement steel. The concrete was modeled as a linear elastic material in compression and an elastic brittle material in tension. The modulus in tension, after cracking, was obtained using a stepped stress-strain diagram. The stiffness of a layer was evaluated by superposing the stiffnesses of steel and concrete. The shear modulus of a layer, whether cracked or uncracked was taken to be that of an uncracked plain concrete layer. It was found that the use of tensile stiffening for concrete in cracked zones was a significant factor in the accuracy of deflection computations and that a significant redistribution of moments occurred as the result of cracking. Comparison was made with the experimental and theoretical analyses of Jofriet and McNeice (45) and good agreement was obtained. Scanlon and Murry (83) extended this work to include time-dependent deflection and the effect of creep, and shrinkage.

Lin and Scordelis (53,54) extended the work of Scanlon to include

elasto-plastic behavior for the steel in tension and compression and for the concrete in compression. For tension in concrete, they replaced the actual curve by a triangular shaped curve with a descending slope after initial tensile failure. The post-yielding behavior obeyed the Von-Mises yield criterion. Incremental loading was used with iteration within each increment.

Hand, Pecknold and Schnobrich (36,37) used a layered element to determine the load-deflection history of reinforced concrete plates and shells of uniform thickness. The nonlinear behavior of steel and concrete was considered in the analysis. Steel was modeled as elasto-plastic; concrete was assumed to be elastic brittle in tension and to have a bilinear stress-strain relationship up to yield in biaxial compression. They used the strength envelope obtained by Kupfer, Hilsdorf and Rüsch (48) as a yield criterion. A shear retention factor was introduced to provide torsional and shear stiffness after cracking. The layered finite element allowed the material properties to vary through the element depth. Bending and membrane forces were considered and a doubly curved rectangular shallow shell element with twenty degrees of freedom was used in the analysis. The authors stated that their numerical results were as good or better than the modified stiffness approaches used by Jofriet and McNiece or by Bell.

Wanchoo and May (92) introduced a layered model with concrete in compression and steel following the Von-Mises criteria. Concrete was elastic brittle in tension. The rectangular finite element developed by Bogner, Fox and Schmit (11) was used. Their analytical results were compared with a test slab and a good match was obtained.

1.3 Object and Scope

The object of this research is to develop a model for reinforced concrete slabs using the finite element technique and appropriate constitutive relations. The model may be used to simulate the load-deflection behavior of slabs under monotonic load. In the analysis, the reinforced concrete slabs are modeled as incrementally elastic, anisotropic bodies. Nonlinear behavior is introduced through the material properties of concrete and reinforcing steel. Concrete is modeled as inelastic material in compression and as an elastic brittle material in tension. Steel is modeled as an uniaxial material with a bilinear stress-strain curve. Bond slip between steel and concrete, creep, shrinkage, temperature, long term loading, cyclic loading and membrane stresses are not included. Loads are applied incrementally, and the solution is corrected using successive iterations.

The proposed model is compared with experimental results for beams, and one-way and two-way slabs.

The model should prove to be a useful research tool and may be used in limited design problems to check stresses and deflections of reinforced concrete slabs for various combinations of load and geometry.

Chapter 2

MATERIAL AND SLAB MODELS

2.1 General

Reinforced concrete is far from being homogeneous, isotropic, elastic material. It is a composite of many materials which behave linearly and elastically only under low loads. The object of this chapter is to introduce the material models used to represent the composite slab (plain concrete and reinforcing steel) and to describe the slab model in which the material models are combined. The resulting model is designed to represent the load-deformation behavior of reinforced concrete slabs up to failure.

In this analysis, slabs are considered as anisotropic plates. Moment-curvature relations are developed and used to determine the resisting moments in the slabs. The assumptions used for bending of thin plates are used. Straight sections, normal to the middle surface before bending, remain straight and normal to the surface after bending; and normal stresses in sections parallel to the middle surface are assumed to be small compared with stresses in the transverse sections.

The slab model introduced in this chapter is designed to be used with the finite element technique. The properties of the model are evaluated at the centroid of each element.

The behavior of reinforced concrete slabs is controlled by the behavior of the constituent materials, steel and concrete. The anisotropic behavior of these slabs is modeled by treating the concrete

as a stress-dependent, orthotropic material and the steel as an uniaxial material. For the concrete, the axes of orthotropy coincide with the yield lines of the slab; the steel axes coincide with the steel directions.

As used in this study, the stiffness and moment-curvature relations are formulated along the yield lines, which do not, in general, coincide with the steel axes. The steel forces and stiffnesses must therefore be transformed to the yield axes. Sectional analyses are then carried out along the concrete material axis. This approach is used with the finite element approach together with the concept of "Initial Stresses" to solve the nonlinear load-deflection problem.

2.2 Material Model

2.2.1 Concrete

2.2.1.1 Orthotropic Constitutive Relations

In this study, concrete is modeled as an incrementally linear, orthotropic material. The stress-strain relations may be written in differential form as follows:

$$\begin{Bmatrix} d\sigma_1 \\ d\sigma_2 \\ d\tau_{12} \end{Bmatrix} = \frac{1}{1 - \nu_1 \nu_2} \begin{bmatrix} E_1 & \nu_2 E_1 & 0 \\ \nu_1 E_2 & E_2 & 0 \\ 0 & 0 & (1-\nu_1\nu_2)G \end{bmatrix} \begin{Bmatrix} d\varepsilon_1 \\ d\varepsilon_2 \\ d\gamma_{12} \end{Bmatrix} \qquad (2.1)$$

where E_1, E_2, ν_1, ν_2 and G are stress-dependent material properties, and 1 and 2 are the current material axes.

Only four of the five material properties are independent; due

to energy considerations,

$$\nu_1 E_2 = \nu_2 E_1 \tag{2.2}$$

Darwin and Pecknold (26,27,28) reduced the four independent properties to three by insuring that neither direction is favored, either for Poisson's ratio, ν, or for shear modulus, G. They used an "equivalent" Poisson's ratio, ν:

$$\nu^2 = \nu_1 \nu_2 \tag{2.3}$$

and the following constitutive equations for plain concrete:

$$\begin{Bmatrix} d\sigma_1 \\ d\sigma_2 \\ d\tau_{12} \end{Bmatrix} = \frac{1}{1-\nu^2} \begin{bmatrix} E_1 & \nu\sqrt{E_1 E_2} & 0 \\ & E_2 & 0 \\ \text{sym.} & & \frac{1}{4}(E_1+E_2-2\ \nu\sqrt{E_1 E_2}) \end{bmatrix} \begin{Bmatrix} d\varepsilon_1 \\ d\varepsilon_2 \\ d\gamma_{12} \end{Bmatrix} \tag{2.4}$$

The three values, E_1, E_2 and ν, are determined as functions of the state of stress and strain at each point.

Although the changes in the direction of the material axes between successive increments are small for most cases, rotations of the material axes are permitted in order to reflect the latest changes in stress and strain.

2.2.1.2 Equivalent Uniaxial Strain

In plate bending problems, the state of stress is essentially two-dimensional, and the strain in one direction is a function, not only of the stress in that direction, but also of the stress in the

orthogonal direction, due to Poisson's effect. It is convenient to analyze the two directions individually by separating that portion of strain due to the nonlinear behavior in each direction from that due to Poisson's effect.

The device of "equivalent uniaxial strain", developed by Darwin and Pecknold (26,27,28) to keep track of the degradation of the stiffness and the strength of concrete under cyclic loading, is used to help establish this directional behavior along the material axes. The equivalent uniaxial strain is used, in conjunction with "equivalent uniaxial curvature" (Section 2.3.2.1), to establish concrete stiffness and strength through the depth of the slab. Once the moment-curvature relations are established on the material axes, the equivalent uniaxial strains on the surface of the slab may be transformed to true strains which are used in conjunction with the slab curvature to compute the strains in the reinforcing steel.

By definition, the equivalent uniaxial strain, ε_{Iu}, is:

$$\varepsilon_{Iu} = \int d\varepsilon_{Iu} = \int \frac{d\sigma_I}{E_I} \tag{2.5}$$

or incrementally:

$$\varepsilon_{Iu} = \Sigma \Delta\varepsilon_{Iu} = \sum_{\substack{\text{load} \\ \text{increment}}} \frac{\Delta\sigma_I}{E_I} \tag{2.6}$$

where $\Delta\sigma_I$ is the incremental change in stress, σ_I, and E_I represents the tangent modulus in the I-direction at the start of the load increment. An increment of equivalent uniaxial strain, $\Delta\varepsilon_{Iu}$, represents the change in strain in the I-direction that would occur for a change

in stress of $\Delta\sigma_I$, with $\Delta\sigma_J = 0$. Equivalent uniaxial strains are not transformable, as are true strains. However, for a fixed set of axes, equivalent uniaxial strains may be converted to true strains, which are transformable. For an orthotropic material, the differential changes in strain are a function of the changes in stress.

$$d\varepsilon_1 = \frac{d\sigma_1}{E_1} - \nu_2 \frac{d\sigma_2}{E_2}$$
$$d\varepsilon_2 = -\nu_1 \frac{d\sigma_1}{E_1} + \frac{d\sigma_2}{E_2} \tag{2.7}$$

Solving Eqs. (2.2) and (2.3) for Poisson's ratios, ν_1 and ν_2 gives:

$$\nu_1 = \nu \left(\frac{E_1}{E_2}\right)^{\frac{1}{2}}$$
$$\nu_2 = \nu \left(\frac{E_2}{E_1}\right)^{\frac{1}{2}} \tag{2.8}$$

Substituting these values in Eq. (2.7) and using the definition of equivalent uniaxial strain given in Eq. (2.5), the differential changes in the true strain may be expressed in terms of differential changes in equivalent uniaxial strain:

$$d\varepsilon_1 = d\varepsilon_{1u} - \nu \left(\frac{E_2}{E_1}\right)^{\frac{1}{2}} d\varepsilon_{2u}$$
$$d\varepsilon_2 = -\nu \left(\frac{E_1}{E_2}\right)^{\frac{1}{2}} d\varepsilon_{1u} + d\varepsilon_{2u} \tag{2.9}$$

The total strains in the material axes at any level of the slab may be written in incremental form as:

$$\varepsilon_1 = \sum_{\substack{\text{load}\\ \text{increment}}} \left(\Delta\varepsilon_{1u} - \nu\left(\frac{E_2}{E_1}\right)^{\frac{1}{2}}\Delta\varepsilon_{2u}\right)$$

$$\varepsilon_2 = \sum_{\substack{\text{load}\\ \text{increment}}} \left(-\nu\left(\frac{E_1}{E_2}\right)^{\frac{1}{2}}\Delta\varepsilon_{1u} + \Delta\varepsilon_{2u}\right) \qquad (2.10)$$

2.2.1.3 Uniaxial Stress-Strain Curves

In spite of extensive research, knowledge of the behavior of concrete subject to multiaxial states of stress in incomplete. Therefor, empirical formulations are basic in both design and research. Of the many equations proposed for representing of stress-strain relations for concrete (39,69,76), the equation suggested by Saenz (74) is adapted for this study. Its parameters are modified here to include the descending portion of the stress-strain curve. The Saenz equation is presented in Fig. 2.1,and in nondimensional coordinates with an experimental curve, in Fig. 2.2. The Saenz equation for concrete under uniaxial compression is:

$$\sigma = \frac{\varepsilon}{A + B\varepsilon + C\varepsilon^2 + D\varepsilon^3} \qquad (2.11)$$

where

ε is the strain at any point in the concrete section; and

σ is the stress in concrete corresponding to strain ε.

The strain, ε, for most applications in this study is the "equivalent uniaxial strain", ε_{Iu}, described above. A, B, C, and D are parameters determined by imposing the following boundary conditions:

At the origin, the stress and the strain are zero and the tangent equals the initial modulus of elasticity for the concrete; at the maximum stress, σ_o, the strain is ε_o and the tangent is zero; and at maximum strain, ε_f, the stress is σ_f.

Thus:

$$A = \frac{1}{E_o}$$

$$B = \frac{R_E + R - 2}{R_E \sigma_o}$$

$$C = \frac{1 - 2R}{R_E \sigma_o \varepsilon_o}$$

$$D = \frac{R}{R_E \sigma_o \varepsilon_o^2}$$

$$R = \frac{R_E (R_f - 1)}{(R_\varepsilon - 1)^2} - \frac{1}{R_\varepsilon}$$

$$R_E = \frac{E_o \sigma_o}{\sigma_o} \qquad (2.12)$$

$$R_f = \frac{\sigma_o}{\sigma_f} \text{ ; and}$$

$$R_\varepsilon = \frac{\varepsilon_f}{\varepsilon_o}$$

E_o is the initial tangent modulus of elasticity as determined from uniaxial compression tests; the approximate formula given by ACI (318-71) (2) is used.

σ_o is the maximum concrete strength (= f'_c for the uniaxial case).

ε_o is the strain at which the peak compressive stress is attained.

In this study its value varies between 0.0020 and 0.0021 (Fig. 2.3) for concrete strength varying between 3500 psi and 5700 psi; in this range $\varepsilon_o = 0.002$ is satisfactory; however, for higher or lower strength the following formula may be used:

$$\varepsilon_o = \frac{\sigma_o}{363000 + 400\ \sigma_o} \tag{2.13}$$

This formula is obtained by curve fitting using the experimental results given in Reference 70.

ε_f is the maximum strain.

For the descending portion of the stress-strain curve, the maximum strain is three to four times the strain at maximum strength. For this study:

$$\varepsilon_f = 4\varepsilon_o \tag{2.14}$$

σ_f the strength at ε_f, is approximated by:

$$\sigma_f = 450 + 0.25\ \sigma_o - 3.4\ \sigma_o^2 \times 10^{-5} \tag{2.15}$$

Eq. (2.15) is empirical and obtained by interpolation methods, using the experimental results of Reference 70.

The effect of concrete strength on the shape of the ascending portion of the stress-strain diagrams is small, but is quite noticeable on the descending portion, as shown in Fig. 2.2. As will be seen later, only part of the descending curve is used.

Eq. (2.11) is used to represent stress as a function of strain

through the portion of the slab depth in which the concrete is in compression. No attempt is made to model the effect of strain gradient on strength or stiffness.

The modulus of elasticity for concrete in compression is a function of strain and is obtained by differentiating Eq. (2.11):

$$E = \frac{d\sigma}{d\varepsilon} = \frac{A - C\varepsilon^2 - 2D\varepsilon^3}{(A + B\varepsilon + C\varepsilon^2 + D\varepsilon^3)} \tag{2.16}$$

2.2.1.4 Biaxial Stress-Strain Relationships

The increase in strength of concrete under biaxial stress has been reported by many investigators (48,56,65,72,93). However, the importance of this increase on the behavior of reinforced concrete slabs has been questioned (44,52,79). The biaxial effect is included in this analysis to help determine its importance in the load-deflection behavior of reinforced concrete slabs.

To determine the shape of the stress-strain curves under biaxial stress, an approach similar to the one used for uniaxial stresses is followed. The equation suggested by Saenz is used. It is only necessary to include the effect of biaxial stresses on the maximum strength of concrete and on strain at maximum strength.

a) Determination of Maximum Strength

Kupfer and Gerstle (49) introduced the following approximate equation for biaxial compressive strength:

$$\left(\frac{\sigma_{1c}}{f'_c} + \frac{\sigma_{2c}}{f'_c}\right)^2 - \frac{\sigma_{2c}}{f'_c} - 3.65\,\frac{\sigma_{1c}}{f'_c} = 0 \tag{2.17}$$

where σ_{1c} and σ_{2c} are the minor and major principal compressive strengths, respectively (see Fig. 2.4). Using $\alpha = \sigma_1/\sigma_2$, Eq. (2.17) may be rewritten as (26):

$$\sigma_{2c} = \frac{1 + 3.65\alpha}{(1 + \alpha)^2} f'_c \tag{2.18}$$

The peak compressive stress in the minor direction is:

$$\sigma_{1c} = \alpha\sigma_{2c} \tag{2.19}$$

b) Determination of the Equivalent Uniaxial Strain at Peak Stress, ε_{Ic}:

Investigators (48,56,72,92) have reported larger values of strain at maximum stress for biaxial compression than for uniaxial compression. This increase in real strain occurred in spite of the Poisson effect. Darwin and Pecknold (26,27,28) gave the following equations for the equivalent uniaxial strain at the maximum compressive stress:

1) $\sigma_{Ic} > f'_c$

$$\varepsilon_{Ic} = \varepsilon_o \left(\frac{\sigma_{Ic} R}{f'_c} - (R-1)\right) \tag{2.20}$$

where

ε_o = Strain at peak stress for uniaxial compression.

R = 3 : This value was derived from experimental curves for $\alpha = 0$ and $\alpha = 1$.

2) $\sigma_{Ic} \leq f'_c$

$$\varepsilon_{Ic} = \varepsilon_o \left[-1.6 \left(\frac{\sigma_{Ic}}{f'_c}\right)^3 + 2.25 \left(\frac{\sigma_{Ic}}{f'_c}\right)^2 + 0.35 \left(\frac{\sigma_{Ic}}{f'_c}\right)\right] \tag{2.21}$$

The biaxial effect is included by substituting ε_{Ic}, σ_{Ic} and ε_{Iu} for ε_o, σ_o and ε in Eqs. (2.11) and (2.12), respectively. Comprehensive discussion and comparison with both experimental and analytical work is given in References (26,27) and should be referred to for more details.

This approach was originally developed for use in plain stress problems. For bending problems in this study, where stresses change through the depth in a nonlinear manner, the ratio of principal stresses, α, at the extreme compression fibers of the cross section is evaluated and used as the representative value to calculate the maximum compressive strength.

2.2.1.5 Tensile Behavior

Reinforced concrete members are rarely employed in pure tension. Most design procedures and codes of practice neglect the tensile strength of concrete. However, the tensile strength of concrete is important in predicting the location and width of cracks, and plays an important role in the load-deflection behavior of reinforced concrete members.

Concrete in tension behaves as a linear brittle material, as shown in Fig. 2.1. The modulus of elasticity for concrete in tension

is approximately equal to the initial tangent modulus in compression. Cracks form perpendicular to the material axes whenever the tensile stresses exceed the tensile strength of the concrete.

Of the various methods of determining the tensile strength of concrete, the modulus of rupture seems to give a better prediction of structural behavior for members employed in flexure than does either the splitting tensile or direct tensile strengths. This is due to the fact that plain concrete can undergo larger stresses and strains when subjected to a strain gradient (73,75,86), a situation more closely matched in the modulus of rupture test than in the other tests. The effect of biaxial tension on tensile strength is very small and neglected in this work.

In this study, concrete in tension is modeled as a linear, elastic, brittle material with a modulus of elasticity equal to the initial modulus in compression and with a maximum tension strength suggested by the ACI (2) Building Code:

$$f_{rt} = 7.5\sqrt{f'_c} \tag{2.22}$$

2.2.2 Stress-Strain Relations for Steel Reinforcement

The stress-strain relations and mechanical properties of steel are usually obtained from tensile tests. A sharply defined yield point and yield plateau can be obtained for mild and intermediate grades of steel. In this study, reinforcing steel is idealized as an uniaxial material with the bi-linear stress-strain curve shown

in Fig. 2.5.

2.3 Slab Model

2.3.1 Flexural Stiffness of Reinforced Concrete Slabs

In this study, reinforced concrete slabs are analyzed as incrementally linear, anisotropic plates. The concrete material axes (yield lines), (N,T), are considered to be the axes of anisotropy. The concrete material properties vary through the depth of the slab. If u, v and w are the translational components of displacements in N, T and Z (normal to surface) coordinates, then the strains in the (N,T) system are*:

$$\varepsilon_n = \frac{\partial u}{\partial n} \quad , \quad \varepsilon_t = \frac{\partial v}{\partial t}$$
$$\gamma_{nt} = \frac{\partial v}{\partial n} + \frac{\partial u}{\partial t} \tag{2.23}$$

From the assumption of straight sections,

$$u = - Z'_n \frac{\partial w}{\partial n}$$
$$v = - Z'_t \frac{\partial w}{\partial t} \tag{2.24}$$

where Z'_n and Z'_t are the distances from a point in the section to the

* N (n) and T (t) are used interchangeably with 1 and 2 to represent material axes in this report.

neutral axes in the N and T directions, respectively. By substituting Eq. (2.24) in (2.23), the following is obtained:

$$\varepsilon_n = - Z'_n \frac{\partial^2 w}{\partial n^2} = - Z'_n \kappa_n$$

$$\varepsilon_t = - Z'_t \frac{\partial^2 w}{\partial t^2} = -Z'_t \kappa_t \qquad (2.25)$$

$$\gamma_{nt} = - (Z'_n + Z'_t) \frac{\partial^2 w}{\partial n \partial t} = - (Z'_n + Z'_t)\kappa_{nt}$$

where κ_n, κ_t and κ_{nt} are the curvatures on the (N,T) axes. Incrementally:

$$\Delta\varepsilon_n = -Z_n \Delta\kappa_n$$

$$\Delta\varepsilon_t = - Z_t \Delta\kappa_t \qquad (2.26)$$

$$\Delta\gamma_{nt} = - (Z_n + Z_t) \Delta\kappa_{nt}$$

Z_n and Z_t in Eq. (2.26) are the distances from any point in the section to the instantaneous neutral axes in the N and T directions, respectively. The instantaneous neutral axis is the point of zero incremental change in stress and is located at a distance ΔZ from the neutral axis, (Fig. 2.6):

$$\Delta Z = \frac{\int EZ' dZ}{\int E dZ} \qquad (2.27)$$

where E is a function of Z.

For an anisotropic slab, the incremental stress-strain relations may be written as follows:

$$\begin{Bmatrix} \Delta\sigma_n \\ \Delta\sigma_t \\ \Delta\tau_{nt} \end{Bmatrix} = \begin{bmatrix} C_{11} & C_{12} & C_{13} \\ & C_{22} & C_{23} \\ \text{Sym.} & & C_{33} \end{bmatrix} \begin{Bmatrix} \Delta\varepsilon_n \\ \Delta\varepsilon_t \\ \Delta\gamma_{nt} \end{Bmatrix} \tag{2.28}$$

where C_{ij} are functions of depth, as well as location in the plate. By substituting the incremental changes in strain from Eqs. (2.26) in Eqs. (2.28), the incremental changes in stress are expressed as functions of the incremental changes in curvature.

$$\begin{Bmatrix} \Delta\sigma_n \\ \Delta\sigma_t \\ \Delta\tau_{nt} \end{Bmatrix} = - \begin{bmatrix} Z_n C_{11} & Z_t C_{12} & \frac{1}{2}(Z_n+Z_t)C_{13} \\ & Z_t C_{22} & \frac{1}{2}(Z_n+Z_t)C_{23} \\ \text{Sym.} & & \frac{1}{2}(Z_n+Z_t)C_{33} \end{bmatrix} \begin{Bmatrix} \Delta\kappa_n \\ \Delta\kappa_t \\ 2\Delta\kappa_{nt} \end{Bmatrix} \tag{2.29}$$

The changes in bending and twisting moments per unit length are:

$$\begin{aligned} \Delta M_n &= \int \Delta\sigma_n Z_n \, dZ \\ \Delta M_t &= \int \Delta\sigma_t Z_t \, dZ \\ \Delta M_{nt} &= \int \Delta\tau_{nt} Z_{nt} \, dZ \end{aligned} \tag{2.30}$$

where

$$Z_{nt} = \frac{1}{2}(Z_n + Z_t)$$

The incremental moment-curvature relations for an anisotropic

plate are obtained by substituting Eqs. (2.29) in Eqs. (2.30):

$$\begin{Bmatrix} \Delta M_n \\ \Delta M_t \\ \Delta M_{nt} \end{Bmatrix} = -\begin{bmatrix} \int C_{11} Z_n^2 dZ & \int C_{12} Z_n Z_t dZ & \int C_{13} Z_n Z_{nt} dZ \\ & \int C_{22} Z_t^2 dZ & \int C_{23} Z_t Z_{nt} dZ \\ \text{Sym.} & & \int C_{33} Z_{nt}^2 dZ \end{bmatrix} \begin{Bmatrix} \Delta\kappa_n \\ \Delta\kappa_t \\ 2\Delta\kappa_{nt} \end{Bmatrix} \quad (2.31)$$

Eq. (2.31) may be expressed more simply as:

$$\begin{Bmatrix} \Delta M_n \\ \Delta M_t \\ \Delta M_{nt} \end{Bmatrix} = -\begin{bmatrix} D_{11} & D_{12} & D_{13} \\ & D_{22} & D_{23} \\ \text{Sym.} & & D_{33} \end{bmatrix} \begin{Bmatrix} \Delta\kappa_n \\ \Delta\kappa_t \\ 2\Delta\kappa_{nt} \end{Bmatrix} \quad (2.32)$$

or:

$$\{\Delta M\} = -[D]\{\Delta\kappa\} \quad (2.33)$$

Eqs. (2.31), (2.32) and (2.33) are modified below to be used with reinforced concrete slabs.

2.3.1.1 Steel Contribution to Flexural Stiffness

Since steel occurs only at limited points through the depth of the section, Eq. (2.30) may be rewritten as follows:

$$\begin{aligned} \Delta M_n &= \int Z_n \Delta\sigma_n dZ_n + \Sigma \Delta f_n \bar{Z}_n \\ \Delta M_t &= \int Z_t \Delta\sigma_t dZ_t + \Sigma \Delta f_t \bar{Z}_t \\ \Delta M_{nt} &= \int Z_{nt} \Delta\tau_{nt} dZ_{nt} + \Sigma \Delta f_{nt} \bar{Z}_{nt} \end{aligned} \quad (2.34)$$

where Δf_n, Δf_t and Δf_{nt} are the incremental changes in the steel force per unit length and $\bar{Z}_n$, $\bar{Z}_t$ and $\bar{Z}_{nt}$ are measured from the centroid of the steel area to the instantaneous neutral axes. The intergration terms in Eq. (2.34) are evaluated for the concrete only.

The incremental changes in the steel force are functions of the incremental strains in the steel.

$$\begin{Bmatrix} \Delta f_x \\ \Delta f_y \end{Bmatrix} = \begin{bmatrix} E_x A_x & 0 \\ 0 & E_y A_y \end{bmatrix} \begin{Bmatrix} \Delta \varepsilon_x \\ \Delta \varepsilon_y \end{Bmatrix} \tag{2.35}$$

where X and Y are the steel axes:

A_x, A_y are the areas of steel reinforcement per unit length in the X and Y directions;

E_x, E_y are the tangent moduli of steel in the X and Y directions; and

$\varepsilon_x, \varepsilon_y$ are the strains in the steel in the X and Y directions.

The components of the changes in steel force in the N and T directions can be obtained by transformation from the X, Y system:

$$\begin{Bmatrix} \Delta f_n \\ \Delta f_t \\ \Delta f_{nt} \end{Bmatrix} = \begin{bmatrix} \cos^2\theta & \sin^2\theta \\ \cos^2\theta & \cos^2\theta \\ -\sin\theta\cos\theta & \sin\theta\cos\theta \end{bmatrix} \begin{Bmatrix} \Delta f_x \\ \Delta f_y \end{Bmatrix} \tag{2.36}$$

where θ is the angle between the steel direction, (X,Y), and the material axes, (N,T).

Likewise the incremental strains in the (X,Y) system may be expressed in terms of the incremental strains in the (N,T) coordinates:

$$\begin{Bmatrix} \Delta \varepsilon_x \\ \Delta \varepsilon_y \end{Bmatrix} = \begin{bmatrix} \cos^2\theta & \sin^2\theta & -\sin\theta\cos\theta \\ \sin^2\theta & \cos^2\theta & \sin\theta\cos\theta \end{bmatrix} \begin{Bmatrix} \Delta \varepsilon_n \\ \Delta \varepsilon_t \\ \Delta \gamma_{nt} \end{Bmatrix} \tag{2.37}$$

Substituting Eqs. (2.37) and (2.35) in Eq. (2.36), the following

expression is obtained:

$$\begin{Bmatrix} \Delta f_n \\ \Delta f_t \\ \Delta f_{nt} \end{Bmatrix} = \begin{bmatrix} (A_x E_x \cos^4\theta + A_y E_y \sin^4\theta) & (A_x E_x + A_y E_y)\sin^2\theta\cos^2\theta & (-A_x E_x \cos^2\theta + A_y E_y \sin^2\theta)\sin\theta\cos\theta \\ & (E_x A_x \sin^4\theta + A_y E_y \cos^4\theta) & (-A_x E_x \sin^2\theta + A_y E_y \cos^2\theta)\sin\theta\cos\theta \\ \text{Sym.} & & (E_x A_x + A_y E_y)\ \sin^2\theta\cos^2\theta \end{bmatrix} \begin{Bmatrix} \Delta\varepsilon_n \\ \Delta\varepsilon_t \\ \Delta\gamma_{nt} \end{Bmatrix} \tag{2.38}$$

The strains at the level of the steel reinforcement are obtained in terms of the incremental changes in curvature from Eq. (2.26):

$$\begin{aligned} \Delta\varepsilon_n &= -\bar{Z}_n \Delta\frac{\partial^2 w}{\partial n^2} = -\bar{Z}_n \Delta\kappa_n \\ \Delta\varepsilon_t &= -\bar{Z}_t \Delta\frac{\partial^2 w}{\partial t^2} = -\bar{Z}_n \Delta\kappa_t \\ \Delta\gamma_{nt} &= -(\bar{Z}_n + \bar{Z}_t)\Delta\frac{\partial^2 w}{\partial n \partial t} = -(\bar{Z}_n + \bar{Z}_t)\ \Delta\kappa_{nt} \end{aligned} \tag{2.39}$$

By substituting Eqs. (2.39) in Eqs. (2.38), the contribution of steel to the moments in Eqs. (2.34) may be written as follows:

$$\begin{Bmatrix} \Sigma\Delta f_n\ \bar{Z}_n \\ \Sigma\Delta f_t\ \bar{Z}_t \\ \Sigma\Delta f_{nt}\ \bar{Z}_{nt} \end{Bmatrix} = \begin{bmatrix} D^s_{11} & D^s_{12} & D^s_{13} \\ & D^s_{22} & D^s_{23} \\ \text{Sym.} & & D^s_{33} \end{bmatrix} \begin{Bmatrix} \Delta\kappa_n \\ \Delta\kappa_t \\ 2\Delta\kappa_{nt} \end{Bmatrix} \tag{2.40}$$

where:

D^s = is the contribution of steel to the flexural stiffness matrix

in the (N,T) system; and

$$D^s_{11} = (A_x E_x \cos^4\theta + A_y E_y \sin^4\theta)\ \bar{Z}_n^2$$

$$D^s_{12} = (A_x E_x + A_y E_y)\ \sin^2\theta\ \cos^2\theta\ \bar{Z}_n \bar{Z}_t$$

$$D^s_{13} = (-A_x E_x \cos^2\theta + A_y E_y \sin^2\theta)\ \sin\theta\ \cos\theta\ \bar{Z}_n \bar{Z}_{nt}$$

$$D^s_{22} = (A_x E_x \sin^4\theta + A_y E_y \cos^4\theta)\ \bar{Z}_t^2$$

$$D^s_{23} = (-A_x E_x \sin^2\theta + A_y E_y \cos^2\theta)\ \sin\theta\ \cos\theta\ \bar{Z}_n \bar{Z}_{nt}$$

$$D^s_{33} = (A_x E_x + A_y E_y)\ \sin^2\theta\ \cos^2\theta\ \bar{Z}_{nt}^2 \qquad (2.41)$$

2.3.1.2 Concrete Contribution to Flexural Stiffness

The contribution of concrete to the flexural stiffness is obtained by substituting the incremental constitutive equations for concrete, Eqs. (2.4), in the first term of the right hand side of Eqs. (2.34) and expressing incremental changes in strain in terms of incremental changes in curvature (Eq. (2.36))

$$\begin{Bmatrix} \int Z_n \Delta\sigma_n dZ \\ \int Z_t \Delta\sigma_t dZ \\ \int Z_{nt} \Delta\tau_{nt} dZ \end{Bmatrix} = - \begin{bmatrix} D^c_{11} & D^c_{12} & 0 \\ & D^c_{22} & 0 \\ \text{Sym.} & & D^c_{33} \end{bmatrix} \begin{Bmatrix} \Delta\kappa_n \\ \Delta\kappa_t \\ 2\Delta\kappa_{nt} \end{Bmatrix} \qquad (2.42)$$

where:

$$D^c_{11} = \frac{1}{1-\nu^2}\int E_1\ Z_n^2\ dZ$$

$$D^c_{12} = \frac{1}{1-\nu^2}\int \sqrt{E_1 E_2}\ Z_n Z_t\ dZ$$

$$D^c_{22} = \frac{1}{1-\nu^2}\int E_2 Z_t^2\ dZ$$

$$D^c_{33} = \frac{1}{4(1-\nu^2)}\int (E_1 + E_2 - 2\nu\sqrt{E_1 E_2})\ Z_{nt}^2\ dZ$$

The final incremental moment-curvature relations for the slab may be written by substituting Eqs. (2.40) and Eqs. (2.42) in Eqs. (2.34):

$$\begin{Bmatrix} \Delta M_n \\ \Delta M_t \\ \Delta M_{nt} \end{Bmatrix} = - \begin{bmatrix} D_{11} & D_{12} & D_{13} \\ & D_{22} & D_{23} \\ \text{Sym.} & & D_{33} \end{bmatrix} \begin{Bmatrix} \Delta \kappa_n \\ \Delta \kappa_t \\ 2\Delta \kappa_{nt} \end{Bmatrix} \tag{2.43}$$

where:

$$D_{ij} = D^s_{ij} + D^c_{ij} \tag{2.44}$$

D^s_{ij} is given by Eqs. (2.41)

D^c_{ij} is given by Eqs. (2.43)

Eqs. (2.43) are integrated using Gauss Quadrature with six integration points through the depth of the slab.

As developed, the flexural stiffness matrix, D, automatically includes a "shear retention factor", negating the need for an arbitrary value to insure stability after cracking.

The flexural stiffness matrix in the global coordinate system, $\bar{D}$, is obtained as follows (98):

$$[\bar{D}] = [T]^T [D] [T] \tag{2.45}$$

where:

$$[T] = \begin{bmatrix} \cos^2\bar{\theta} & \sin^2\bar{\theta} & \sin\bar{\theta}\cos\bar{\theta} \\ \sin^2\bar{\theta} & \cos^2\bar{\theta} & -\sin\bar{\theta}\cos\bar{\theta} \\ -2\sin\bar{\theta}\cos\bar{\theta} & 2\sin\bar{\theta}\cos\bar{\theta} & \cos^2\bar{\theta} - \sin^2\bar{\theta} \end{bmatrix} \tag{2.46}$$

and $\bar{\theta}$ is the angle between the global coordinate system and the material axes.

2.3.2 Moment-Curvature Relationships

The moment-curvature relations for plate problems play the same role in bending problems as do the stress-strain relations in plane stress problems. Using a relationship of the form $M = f(\kappa)$ allows the "initial stress" technique to be expanded to an "initial moment" approach.

In this section, the concept of "equivalent uniaxial curvature", analogous to equivalent uniaxial strain, is introduced. This concept allows the moments on the yield lines to be treated independently. The moment-curvature relations are determined along the yield lines using concrete stresses and transformed steel forces. These relations are the equilibrium equations for forces and moments. They are non-linear and are solved by iteration. The moments, the location of the neutral axis, the strains and the stresses, at the section corresponding to the equivalent uniaxial curvature are obtained.

2.3.2.1 Equivalent Uniaxial Curvature

The object of introducing the concept of "equivalent uniaxial curvature" is to allow the moment-curvature relations along each material axis to be followed independently. In general, the moment in one direction depends not only on the curvature in that direction, but also on the curvature in the orthogonal direction, due to Poisson's effect, as can be seen in Eqs. (2.32). Expressing the moment-curvature relations in terms of equivalent uniaxial curvature allows a substantial simplification of what would otherwise be a complex interaction problem.

By definition, the "equivalent uniaxial curvature" in the I

direction is:

$$\kappa_{Iu} = \int d\kappa_{Iu} = \int \frac{dM_I}{D_{II}} \tag{2.47}$$

or incrementally:

$$\kappa_{Iu} = \sum_{\substack{\text{load} \\ \text{increment}}} \Delta\kappa_{Iu} = \sum_{\substack{\text{load} \\ \text{increment}}} \frac{\Delta M_I}{D_{II}} \tag{2.48}$$

$I = 1,2$

where:

ΔM_I is the incremental change in the moment per unit length in the I direction during a load increment (from finite element analysis); and D_{II} is the flexural stiffness in the I direction at the start of the load increment.

An increment of equivalent uniaxial curvature, $\Delta\kappa_{Iu}$, represents the change in curvature along the I axis that would occur for a change in moment of ΔM_I, with $\Delta M_J = 0$.

2.2.2.2 Steel Forces

In general, the yield lines do not coincide with the principal moment axes nor with the direction of steel reinforcement. The steel forces, f_x and f_y, are calculated using the true strains in the steel (Eq. (2.35)). The true strains in the steel directions are obtained using an iteration technique described in the next section.

Required in the solution of the moment-curvature relations, the components of the steel forces along the (N,T) axes are:

$$f_n = f_x \cos^2\theta + f_y \sin^2\theta$$
$$f_t = f_x \sin^2\theta + f_y \cos^2\theta \qquad (2.49)$$

where:

f_x, f_y are the steel forces per unit length in the (X,Y) axes;

f_n, f_t are the components of the steel forces in the (N,T), axes; and

θ is the angle between the steel axes, (X,Y), and the material axes, (N,T).

2.3.2.3 Moment-Curvature Equations

The moment-curvature relations are derived at the material axes, (N,T). All strains are equivalent uniaxial strains, (Section 2.2.1.2). These relations are used to obtain the resisting moment corresponding to the equivalent uniaxial curvature, (Section 2.3.2.1), so that residual moment at the centroid of the element can be obtained. The following notation, shown in Fig. 2.7.

ε = equivalent uniaxial strain at distance Z' from the neutral axis.

ε_c = equivalent uniaxial strain at the extreme compressive fiber of concrete.

$\varepsilon_1, \varepsilon_2$ = equivalent uniaxial strains at the extreme fibers of the section, limits of integration.

σ_I = stress in the concrete at distance Z' from the neutral axis in the I direction, I = 1,2.

f'_I = component of the compression steel forces per unit length in the N and T directions.

f_I = component of the tensile steel forces per unit length in the N and T directions.

kH = depth of the neutral axis; and

M_{IR} = the resisting moment in the I direction.

From statics, the following equilibrium equations are obtained:

$$\Sigma_I F = 0, \quad \Sigma_I M = 0 \qquad I = 1,2 \tag{2.50}$$

where

$\Sigma_I F$ sum of forces in the I direction.

$\Sigma_I M$ sum of the moments around the neutral axis in the I direction.

Using material properties, Eq. (2.50) becomes:

$$\begin{aligned} &\int \sigma_I dA + f'_I - f_I = 0 \\ &\int \sigma_I Z' dA + f'_I(kH-d'_s) + f_I((1-k)H-d_s) - M_{IR} = 0 \end{aligned} \tag{2.51}$$

The resisting moment in the I direction, M_{IR}, is obtained by solving Eqs. (2.51) as shown below.

From Fig. 2.7, the following is obtained:

$$\begin{aligned} Z' &= \frac{\varepsilon}{\kappa_{Iu}} \\ dZ' &= \frac{d\varepsilon}{\kappa_{Iu}} \\ k &= \frac{\varepsilon_c}{\kappa_{Iu} H} \\ \varepsilon_1 &= \varepsilon_c \\ \varepsilon_2 &= H\kappa_{Iu} - \varepsilon_c \end{aligned} \tag{2.52}$$

In order to solve Eq. (2.51), the stress in the concrete, σ_I, is rewritten in terms of the equivalent uniaxial strain: $\sigma_I = f(\varepsilon)$ (Eq. (2.11)); after substituting Eq. (2.52) in Eq. (2.51) and changing the limits of integration, the following expressions are obtained:

$$\frac{1}{\kappa_{Iu}} \int_{\varepsilon_2}^{\varepsilon_1} \sigma_I(\varepsilon)\, d\varepsilon + f'_I - f_I = 0 \qquad \text{(a)}$$

$$\frac{1}{\kappa_{Iu}^2} \int_{\varepsilon_2}^{\varepsilon_1} \sigma_I(\varepsilon)\varepsilon d\varepsilon + f'_I(kH-d'_s) + f_I((1-k)H-d_s) - M_{IR} = 0 \qquad \text{(b)} \qquad (2.53)$$

The components of the steel forces, f_I, (f_n and f_t), must be known in advance to solve Eq. (2.53). In fact, the true strains, ε_x and ε_y, and therefore the steel forces, f_x and f_y, in the steel directions are not known, but are functions of the strains, ε_n, ε_t and γ_{nt} (Eq. (2.37)). The strains, ε_x and ε_y, are obtained by trial and error, using the iteration technique summarized below.

For any iteration, the most recent values of the steel forces, f_x and f_y, are used as approximate starting values to calculate the components of the steel forces, f_I, (I = 1,2), in the N and T directions, (Eq. (2.49)). The components of the steel forces are approximated, and the equivalent uniaxial curvature, κ_{Iu}, is known; Eq. (2.53(a)) is then solved, using the Newton-Raphson method, for the equivalent uniaxial strain, ε_c, at the extreme compression fiber in the section in the N and T directions. These equivalent uniaxial strains are then converted to true strains, ε_I, using Eq. (2.10).

The true strains at the surface of the slab in the X and Y directions, are obtained by transforming the strains, ε_n, ε_t and γ_{nt}, from the (N,T) system to the (X,Y) system using Eq. (2.37).

The strains in the steel, ε_x and ε_y, can be obtained using the true strains and curvatures in the X and Y directions. The strains in the steel are used to calculate the forces in the steel reinforcement. The updated steel forces are transformed back to the (N,T) axes to obtain the steel forces f_I which are again used to solve Eq. (2.53(a)) for ε_c. Convergence is obtained if the ratio of the change in steel force to its original value is less than one percent:

$$\frac{f_{x2} - f_{x1}}{f_{x1}} \leq 0.01$$

$$\frac{f_{y2} - f_{y1}}{f_{y1}} \leq 0.01 \qquad (2.54)$$

where f_{x2} and f_{y2} are the most recent values of the steel forces in the X and Y directions and f_{x1} and f_{y1} are the previous values.

Following convergence of the steel forces and Eq. (2.53(a)), the resisting moments are obtained from Eq. (2.53(b)). In most cases, convergence is obtained in less than five iterations. More iterations are required when large deflections are reached, and excessive strains in concrete and steel occur.

As stated above, Eq. (2.53(a)) is solved for the equivalent uniaxial strain in the N and T directions using the Newton-Raphson method. The integrals in Eq. (2.53) are evaluated numerically, using

Gaussian quadrature. The solution of Eq. (2.53(a)) is considered to have converged if both the strain, ε_c, and the location of the neutral axis, k, satisfy the following criteria:

a) Strains:

$$\varepsilon_{c\ new} - \varepsilon_{c\ old} \leq 10^{-7} \tag{2.55}$$

b) Location of neutral axis:

$$k_{new} - k_{old} \leq 10^{-4} \tag{2.56}$$

Convergence is obtained within 2 to 3 iterations because the most recent values of ε_c and k are used as starting values. In addition, the Newton-Raphson method has a second order convergence which assures fast convergence.

2.3.3 Material Axes and Cracking of Reinforced Concrete Slabs

The anisotropic properties of reinforced concrete slabs are due primarily to cracking concrete and yielding reinforcing steel. For orthotropically reinforced concrete slabs, the crack directions (yield lines) do not necessarily coincide with the direction of principal moments or with the direction of steel reinforcement, and only in isotropically reinforced slabs do the directions of the cracks coincide with those of the principal moments.

In this study, the material coordinate system coincides with the yield lines. The yield line criteria follows the work of Kemp (47), Save (79) and Braestrup (12,13).

Save (79) expressed the yield line criteria in terms of the applied bending moments in the X and Y directions. Kemp (47), Lenschow and Sozen (15,52) and Jain and Kennedy (44) expressed this criterion in terms of principal moments acting in any direction relative to the reinforcement. The same principles are used to derive these two approaches and either one can be obtained from the other. In this work Kemp's (47) approach is used to determine the yield line directions.

Yielding occurs at the orientation in the slab where the ratio of the applied moment to the resisting moment is maximum, regardless of the absolute value of the external moment. A yield line forms when the applied and the resisting bending moments and the applied and the resisting twisting moments are equal at a particular orientation or:

$$M_1' \cos^2\psi + M_2' \sin^2\psi = M_{XR} \cos^2\theta + M_{YR} \sin^2\theta \qquad (2.57)$$

$$(M_2' - M_1') \sin\psi \cos\psi = (M_{YR} - M_{XR}) \sin\theta \cos\theta \qquad (2.58)$$

where:

M_1' and M_2' are the principal bending moments per unit length (see Fig. 2.8).

M_{XR} and M_{YR} are the resisting moments per unit length in the X and Y (steel) directions at yield.

ψ is the angle between X1, the normal to the principal moment, and N, the normal to the yield line direction.

θ is the angle between the X axis and the normal to the yield line.

$$\theta = \psi + \phi$$

ϕ is the angle between steel direction, X, and the normal to the principal moment, M_1'.

The orientation of the yield lines can be obtained by rearranging Eq. (2.58):

$$\tan 2\psi = \frac{(M_{XR} - M_{YR}) \sin 2\phi}{[(M_1' - M_2') - (M_{XR} - M_{YR}) \cos 2\phi]} \tag{2.60}$$

Eliminating ψ from Eqs. (2.57) and (2.58), the yield criterion is obtained:

$$M_{XR} M_1' (\sin^2\phi + \mu \cos^2\phi) + M_{XR} M_2' (\cos^2\phi + \mu \sin^2\phi) - M_1' M_2' - \mu M_{XR}^2 = 0 \tag{2.61}$$

where, $\mu = M_{YR}/M_{XR}$

Eqs. (2.60) and (2.61) can be rewritten as:

$$\tan 2\psi = \frac{(1-\mu) \sin 2\phi}{\beta(1-\omega)-(1-\mu) \cos 2\phi} \tag{2.62}$$

$$\beta = \frac{P+\omega Q-\sqrt{(P+\omega Q)^2-4\mu\omega}}{2\omega} \tag{2.63}$$

where:

$$\omega = M_2'/M_1'$$

$$\beta = M_1'/M_{XR}$$

$$P = \sin^2\phi + \mu \cos^2\phi$$

$$Q = \cos^2\phi + \mu \sin^2\phi$$

Before yielding, rotation of the material axes is permitted and the directions determined using Eq. (2.60). After yielding, this material axes are fixed. Therefore, in the proposed model, initial cracking does not start perpendicular to the principal moments, but follows the orientation of the principal curvatures (Eq. (2.60)). This has not been confirmed experimentally; probably because cracking does not occur on a single line whose inclination may be easily measured. The direction of principal moment and principal curvature are very close at this level of loading.

Eqs. (2.62) and (2.63) determine the yield line direction at any point in the slab. Equations similar to (2.62) and (2.63) were given by Kemp (47), Jain and Kennedy (13,44) and Lenschow and Sozen (15,52).

This theory has been confirmed by extensive testing programs carried out by Lenschow and Sozen (52), Lenkei (15), Cardenas and Sozen (16) and recently by Jain and Kennedy (44).

According to this theory, twisting moments may exist on the yield lines. Cracks coincide with the direction of principal moments only in isotropically reinforced concrete slabs. Tests

show that the reorientation, or kinking, of reinforcing bars, is so small that it can be neglected (15,16,44,52). Kinking, therefore, is not included in this model. In addition, (15,16,52) the the effect of biaxial bending appears to have no measurable influence on flexural strength in under-reinforced slabs. This last point is verified in this study, as will be shown in Chapter 4.

Chapter 3

FINITE ELEMENT PROCEDURE

3.1 Plate Bending Element

The finite element used in this study is a compact, rectangular, plate bending element with sixteen degrees of freedom. This element was developed by Bogner, Fox and Schmit (11), using first degree Hermitian polynominals. The element is widely used and has been checked extensively (1,33). For elastic problems, the deflection converges to the exact value with a low number of elements (nine to sixteen elements per quarter plate).

Bogner, Fox and Schmit (11) obtained the stiffness matrix for isotropic thin plates. In this study their work is extended to cover anisotropic, elastic thin plates. The stiffness matrix is written in a partitioned form and integrated item by item. Details of the element and the adaptation for anisotropic plates are presented in Appendix A.

3.2 Solution Procedure

Linear strain-displacement relationships are adequate for most reinforced concrete slabs. Therefore, geometric nonlinearities are neglected and only nonlinearities due to material behavior are considered in this study.

To obtain the load-deflection behavior of slabs to failure, loads are applied incrementally. During the course of loading, the original load increments are reduced to smaller values after cracking

of the concrete and/or yielding of the steel. For each increment of load, iterations are performed until the solution converges. Loads are corrected using one of two adaptations of the Initial Stress Method (95,96,98). Both the constant stiffness and the variable stiffness approaches are used, (see Figs. 3.1 and 3.2). The constant stiffness approach is used before cracks form in the slab. The initial stiffness of the structure is used for each load increment and iteration. Upon the initiation of cracking, the variable stiffness approach is used. This approach treats the problem as a series of linear problems and updates the stiffness matrix following each iteration.

In general, the number of iterations required for convergence is greater when the constant stiffness method is used. The actual number of calculations and the amount of computation time required per iteration is less than when the variable stiffness approach is used, since the structure stiffness matrix is not recalculated during each step. However, in a nonlinear problem, the constant stiffness approach may prove less efficient due to slow convergence. For reinforced concrete slabs prior to cracking, nonlinearity due to material behavior is minor; the slab is practically linear and convergence is reached within two iterations using the constant stiffness method. After cracking, a large number of iterations are required to achieve a satisfactory degree of accuracy using the constant stiffness approach. This proves to be more expensive than the variable stiffness approach. Of more importance, after cracking, the problem is highly path dependent, and convergence is assurred

only with small load increments and continual updating of the stiffness matrix. Since only a portion of the structure may be softened by cracking, realistic load-deflection behavior is modeled only by recalculating the structure stiffness to account for the cracks. Observations made early in this study show that when stiffness properties are used, that are not as accurate as those presented in Chapter 2, some load-deflection curves can be produced, but that at times, convergence and stability of the solution are extremely poor.

Immediately after cracking starts, five to twelve iterations are required for convergence. Thereafter, two or three iterations are satisfactory to achieve convergence in most cases.

The procedure used in this work is outlined below: Upon convergence of a load increment, the remaining residual nodal forces, are added to the next increment of load to obtain the new incremental load vector, $\{\Delta f^n\}$.

The element stiffness matrices, [k], are updated to reflect the current material properties. The structure stiffness matrix, [K], is assembled from the element matrices.

The incremental nodal displacement vector, $\{\Delta\delta^n\}$, is obtained by solving the system of equilibrium equations, using the incremental load vector and the updated stiffness of the structure:

$$\{\Delta\delta^n\} = [K]^{-1} \{\Delta f^n\} \tag{3.1}$$

The total nodal displacements are:

$$\{\delta^n\} = \{\delta^{n-1}\} + \{\Delta\delta^n\} \tag{3.2}$$

The superscript, n, is the number of the current iteration.

The apparent or calculated moments at the centroids of the elements in the global coordinate system are obtained by adding the incremental changes in moment as follows:

$$\{\Delta\bar{M}^n\} = [\bar{D}]\ [B]\ \{\Delta\sigma^n\} \tag{3.3}$$

$$\{\bar{M}^n\} = \{\bar{M}^{n-1}\} + \{\Delta\bar{M}^n\} \tag{3.4}$$

where:

$\{\Delta\bar{M}^n\}$ is the incremental change in the moment vector for the current iteration;

$\{\bar{M}^n\}$ is the total moment vector;

$[\bar{D}]$ is the updated flexure and torsional stiffness; and

$[B]$ is the matrix relating curvatures to nodal displacements.

The moments on the material axes are obtained by transforming Eqs. (3.3) and (3.4) from the global coordinate system to the material axes as follows:

$$\{\Delta M^n\} = [T_\sigma]\ \{\Delta\bar{M}^n\} \tag{3.5}$$

$$\{M^n\} = \{M^{n-1}\} + \{\Delta M^n\} \tag{3.6}$$

where:

$\{\Delta M^n\}$ is the incremental change in moment vector for the current iteration, in material axes (Fig. 3.3);

$\{M^n\}$ is the total moment vector in material axes;

$[T_\sigma]$ is the transformation matrix for stresses:

$$[T_\sigma] = \begin{bmatrix} \cos^2\bar{\theta} & \sin^2\bar{\theta} & 2\sin\bar{\theta}\cos\bar{\theta} \\ \sin^2\bar{\theta} & \cos^2\bar{\theta} & -2\sin\bar{\theta}\cos\bar{\theta} \\ -\sin\bar{\theta}\cos\bar{\theta} & \sin\bar{\theta}\cos\bar{\theta} & \cos^2\bar{\theta}-\sin^2\bar{\theta} \end{bmatrix} \tag{3.7}$$

$\bar{\theta}$ is the angle between the global and material axes.

For each element, the incremental and total equivalent uniaxial curvatures (Chapter 2) on the material axis are then obtained:

$$\{\Delta\kappa^n_{Iu}\} = \{\frac{\Delta M^n_I}{D^n_{II}}\} \quad I = 1,2 \tag{3.8}$$

$$\{\kappa^n_{Iu}\} = \{\kappa^{n-1}_{Iu}\} + \{\Delta\kappa^n_{Iu}\} \tag{3.9}$$

$I = 1,2$

where:

$\{\Delta\kappa^n_{Iu}\}$ is the current change in the equivalent uniaxial curvature in the I direction;

$\{\kappa^n_{Iu}\}$ is the total equivalent uniaxial curvature in the I direction;

$\{\Delta M^n_I\}$ is the current change in the moment in the I direction; and

$[D^n_{II}]$ is the updated tangent flexural stiffness in the I direction.

The resisting moments, M^n_R, corresponding to the nonlinear material behavior, are calculated using the equivalent uniaxial curvatures (Section 2.3.2.3). Residual moments, Δm^n, which represent the lack

of satisfaction of equilibrium due to nonlinear material behavior, are obtained by subtracting the resisting moments from the apparent moments:

$$\{\Delta m^n\} = \{M^n\} - \{M_R^n\} \tag{3.10}$$

The residual moments are then converted to nodal forces to be applied to the structure:

$$\{\Delta f^n\} = \iint_A [B]^T \{\Delta \bar{m}^n\} \, d\bar{x} \, d\bar{y} \tag{3.11}$$

If the incremental displacements have converged, or if the prescribed number of iterations has been reached, another increment of load is applied and the solution continues; if the problem has not converged, the solution is repeated using the residual loads and the updated structure stiffness. Calculations terminate when the strain in the concrete or in the steel exceeds a specific limit.

The input data for the program used in this study includes a description of the geometry of the structure and the properties of the materials used. The program permits the use of varying element thicknesses, reinforcing ratios, and directions of steel.

As output, the program gives the total deflection, the total load vector and the residual nodal forces at nodal points. At the element centroids the program provides the total moments, the total curvatures, the stress and strain in the concrete at the extreme compressive fiber, the stress and strain in the steel, and the cracking level and direction. Numerical examples for beams and slabs are presented in Chapter 4.

3.3 Convergence Criteria

Convergence criteria play a key role in nonlinear problems. The accuracy of the solution and the speed of convergence depend on the magnitude and type of criteria selected. If the limits are loose, accuracy and convergence to the right roots are questionable; the structure appears to be too stiff. If very tight limits are imposed, the number of iterations increases and the incremental deflections may change sign with each iteration. In some problems, the solution may even diverge. A middle ground must be established.

Convergence criteria can be based on displacements and/or on forces. In this study, the convergence criteria are based on displacements only.

The convergence criteria imposed here use the Euclidian norms (square root of the sum of the squares) of the total nodal deflections, TD, and the change in nodal deflections for the last iteration, RD. The Euclidian norms are defined as follows:

$$N_2(\delta) = \sqrt{\delta_1^2 + \delta_2^2 + \cdots + \delta_n^2} \tag{3.12}$$

$$\begin{aligned} TD &= N_2(\delta^n) \\ RD &= N_2(\Delta\delta^n) \end{aligned} \tag{3.13}$$

The solution is considered to have converged, if one of the following two criteria is satisfied:

a) The ratio of the norm of the incremental nodal deflection vector from the last iteration to the norm of the total deflection vector is less than one percent, and the ratio

of the norms of the last two incremental nodal deflection vectors is less than fifteen percent.

$$\frac{RD}{TD} \leq 0.01 \quad \text{and} \quad \frac{RD\ new}{RD\ old} \leq 0.15 \tag{3.14}$$

b) The ratio of the norm of the last incremental nodal deflection vector to the norm of the total deflection vector is less than seven thousandths.

$$\frac{RD}{TD} \leq 0.007 \tag{3.15}$$

In this study, case (b) controlled for most iterations (more than 90%). Case (a) controlled for the early load increments. When tighter criteria were used for case (b) (0.005), case (a) was found to control in many cases; the solution required a greater number of iterations without improving the accuracy of the results.

Chapter 4

NUMERICAL EXAMPLES

4.1 General

In this chapter the applicability and the usefullness of the proposed model are demonstrated. Numerical examples are selected and presented in a sequence of increasing complexity: Two singly reinforced concrete beams, tested by Gaston, Siess and Newmark (34), two slabs tested by Cardenas and Sozen (16), three slabs tested by Jain and Kennedy (44), and two slabs tested by McNeice (59).

In each case, the analytical solution is compared with the experimental results. Several examples include additional comparisons with analytical results obtained by other investigators.

The material properties of the test specimens are presented in Table 4.1. These values were used by the original investigators. Estimates are made in cases where specific data are not available.

The model demonstrated in Sections 4.2 and 4.3 does not include the effect of biaxial stresses on concrete strength. The minor importance of the biaxial strength effect on slabs is demonstrated in Section 4.4.

4.2 Beams

4.2.1 Simply Supported Beams--Gaston, Siess and Newmark

Gaston, Siess and Newmark (34) conducted a series of tests on simply supported reinforced concrete beams. The beams were loaded at the third points. Load-deflection curves were obtained

experimentally with deflections measured at the loading points and at the span center line. Two beams, T1MA (Fig. 4.1) and T3MA (Fig. 4.2), demonstrate the ability of the proposed model to simulate load-deflection behavior. T1MA is under-reinforced, while T3MA has a balanced reinforcement ratio.

Due to symmetry, only half of each beam is analyzed. For the analytical solution, the beams are loaded incrementally with an initial load increment of 2000 lbs. The load increment is reduced to 1000 lbs. after the initiation of cracking, and to 400 lbs. once yielding occurs. Although the load-deflection behavior of the proposed model is, for the most part, independent of the size of the load increment, these reductions in the size of the load increment give stability to the programmed calculations. If large increments are used, the analysis over-shoots the ultimate load, and corrections must be made to attain the equilibrium configuration at large displacements. In some cases, the analysis falsely indicates that the concrete has been crushed at a very early stage. Decreasing the size of the load increments, has only a small effect on the total computation time, since large load increments require a higher number of iterations.

The load deflection curves in Figs. 4.1 and 4.2 show a good match with experimental results. Figs. 4.3 and 4.4 show the analytical crack depths in beams T1MA and T3MA immediately before and after yielding of the steel reinforcement.

The analytical solutions for both beams, indicate that only very small changes in the resisting moments occur after yielding of the

steel, independent of the stresses in the concrete when yielding begins. This observation is in concert with the well known fact that in balanced and under-reinforced concrete sections, the ultimate moments are controlled by the reinforcing steel and that higher concrete strength adds very little to the ultimate strength. The stresses in the concrete reach a maximum immediately after yielding of the steel in balanced reinforced beams and after a few additional small load increments in under-reinforced beams. The concrete stresses then begin to decrease on the downward portion of the stress-strain curve, demonstrating the "softer" nature of the model as compared to an elasto-plastic representation.

The moments and deflections at yielding are compared with the experimental and analytical work of Gaston, Siess and Newmark (34), and Hsu and Mirza (40) in Table 4.2. The proposed model provides a good match with the experimental results.

4.3 Slabs

4.3.1 Slabs Subjected to Uniaxial Bending Moments--Cardenas and Sozen

An extensive experimental investigation of flexural yield criteria has been carried out by Lenschow and Sozen (52) and Cardenas and Sozen (16). A series of slabs, simply supported on two edges and free on the other two, are subjected to uniaxial bending moments. The proposed model is used to simulate the moment-curvature behavior of two slabs, B7 and B10. The model also matches the change in steel strain and concrete strain with increasing moment. The slabs are isotropically reinforced (equal steel percentages) with slab B10

reinforced parallel to slab edges, and slab B7 reinforced at an angle of 45° with the slab edges (Fig. 4.5). Due to symmetry, one half of the slab is used in the analysis. This half is divided into either three or nine elements, as shown in Fig. 4.6. The material properties used in the analysis are given by Cardenas and Sozen and shown in Table 4.1.

For the analysis, load increments of 1000 in. lb. per in. are used. After cracking begins, the load increment is reduced to 250 in-lb per inch. This change assures convergence and programming stability.

The proposed model is compared with the results obtained experimentally by Cardenas and Sozen (16) and analytically by Hand, Pecknold and Schnobrich (36) in Figs. 4.7 through 4.12.

Hand, Pecknold and Schnobrich (36,37) analyze B7 and B10 using a layered, twenty degree of freedom, shallow shell finite element. Each layer is assumed to be in a state of plane stress and the material properties are assumed to be constant over the layer thickness. Slabs B7 and B10 are represented by a single finite element.

The proposed model shows good agreement with the experimental results, for moment-curvature and moment-strain (concrete and steel) behavior. The improved results, as compared with Hand, et. al., may be due in part to the higher number of finite elements used. However, because the moment field in these problems is essentially uniform, a larger number of elements provides no particular advantage. In fact, little difference is apparent when three and nine elements are used to model the slabs (Fig. 4.6).

Moments and curvatures at cracking and yielding, and moments at ultimate, are compared with those obtained both experimentally and analytically (16,34) in Table 4.3.

Cracking in slab B7 occurs at an applied moment of 1625 in-lb/in. All elements in the proposed model start cracking during the same load increment due to the uniformity of the applied moment. For the nine element model, the middle elements crack perpendicular to the applied uniaxial moment (Fig. 4.13), while Poisson's effect and the boundary conditions at the edges, cause a gradual change in the orientation of the cracks for the exterior elements. A completely uniform field for moments and curvatures is perceived when three elements are used resulting in the uniform cracking pattern shown in Fig. 4.13. Slab B10 exhibits a similar crack pattern (not shown).

A discontinuity in the analytical moment-curvature curves occurs approximately at one-third of the ultimate load, and is due to the development of cracks in the concrete. During this load increment, the bending moment in the section drops to a lower value after cracking (Fig. 4.14), due to the release of the tensile forces across the crack. Equilibrium is restored after redistribution of these forces as explained in Chapter 3.

Prior to yielding, the direction of the reinforcing steel has a significant effect on the load-deflection and moment-curvature curves. The greater the inclination of the steel direction with respect to the edges of the slab, the greater the deflections and curvatures. This is due to the reduced contribution of inclined steel to the flexural stiffness of a reinforced concrete slab (see

Eqs. (2.41)). As predicted by yield line theory, the orientation of steel in an isotropically reinforced slab has no influence on the ultimate loads. The same ultimate moments are obtained for both slabs, as may be seen by comparing Figs. 4.7 and 4.10.

4.3.2 Micro-Concrete Slabs Under Line Loads--Jain and Kennedy

The problems investigated in the preceeding sections consider full size concrete specimens. In this and the following section, micro-concrete slabs are investigated.

Recently, Jain and Kennedy (44) conducted a series of tests on micro-concrete slabs to investigate the parameters that control the formation of yield lines. Their experimental results are represented by moment-deflection curves at the mid-span of the slab. Three of the slabs, A1, A2 and A3, are studied. The reinforcement is isotropic (equal moment capacities) in each slab and makes an angle of 0^{o} (A1), 30^{o} (A2) or 45^{o} (A3) with the direction of the applied uniaxial moment. The moments are generated by means of two uniformly distributed line loads (Fig. 4.15). The steel reinforcement was annealed in order to lower the yield stress and obtain a distinct yield plateau. The average yield stress is 32 ksi. The material properties are given in Table 4.1, and the finite element grid and dimensions are shown in Fig. 4.15. Due to the lack of symmetry in the reinforcing, the full slab is modeled analytically for slab A2.

Analytically, the slabs are loaded incrementally with a line load of 10 lbs/in. The load increment is reduced to 5 lbs/in after

the initiation of cracks, and to 2.5 lbs/in when yielding occurs. The analytical results are compared with the experimental moment-deflection curves in Fig. 4.16. The curves for the proposed model exhibit a marked discontinuity due to cracking and look somewhat softer than the experimental curves.

Both experimental and analytical results reinforce the conclusions reached in the previous section concerning the effect of reinforcement direction on the deflections, curvatures and ultimate moments. Fig. 4.16 shows that the deflection increases with increased inclination of steel reinforcement with respect to the applied moments and reaches its maximum at an angle of 45°. The value of the ultimate moment is constant and is independent of the steel inclination.

4.3.3 Slabs Under Concentrated Load--McNeice

a) One-Way Slab

McNeice (59) tested a one-way slab under a concentrated load (Fig. 4.17). The details of the slab properties are taken from reference (45); the yield strength of the steel reinforcement is not given and is assumed as 50 ksi.

Jofriet and McNeice (45) analyze this slab and a corner supported slab (discussed in Section 4.3.3(b)). Their analysis is "intended to deal with slabs in the service load range"; steel and concrete are treated as elastic materials, and nonlinear behavior is modeled by changes in slab stiffness during the monotonic increase in applied load. They use two empirical

formulas to approximate the moment of inertia of the section. The first formula is due to Branson and is similar to the one adopted by the ACI (2), but the ratio of moments is taken to the fourth power. The second formula is due to Beeby (8); he assumed the modulus of elasticity of the cracked section to be reduced to $0.57\ E_o$. Jofriet and McNeice use a quadrilateral plate bending element. In their work, a unit load is applied and scaled down to the value at which the first region cracks; the stiffness matrix is changed appropriately; the unit load is reapplied and the results are scaled to the next crack observation. This procedure is repeated until the desired load level is reached. They had difficulty in matching the experimental results in this problem and felt that this was due to excessive bond slip between the flat reinforcing bars and the concrete.

In this study, due to symmetry, only half of the slab is analyzed. The slab is divided into four elements. The slab is loaded incrementally with a concentrated load of 100 lbs. and reduced to 50 lbs. after the initiation of cracks. The slab model starts cracking, perpendicular to the direction of the principal applied moment at a total load of 650 pounds. Fig. 4.18 shows the cracking level immediately before and after yielding of the steel reinforcement. As shown in Fig. 4.17, an extremely good match is obtained with the experimental curve up to a total load of 1400 pounds. These results are obtained assuming zero bond slip between the concrete and the reinforcing

steel.

b) Two-Way Slab Supported at the Corners

The two-way slab tested by McNeice (59) is square, supported at the four corners and reinforced with an isotropic mesh. The slab is subjected to a central concentrated load. The steel yield point is assumed to be 50 ksi. The material properties are given in Table 4.1, and the finite element grid is shown in Fig. 4.19.

This problem is of special interest: first because it is a two-way slab with moments varying through the slab in two directions; second, because this slab has been analyzed by many investigators, Jofriet and McNeice (45), Scanlon (80, 83), Hand, Pecknold and Schnobrich (35) and Lin and Scordelis (53), and comparison between their models and the one introduced in this study can be made. A key disadvantage is the lack of detailed test data (i.e., the yield point of the steel).

For his analytical work, Scanlan (82) uses a layered rectangular plate bending element with four degrees of freedom at each corner node. Cracks are assumed to progress through the thickness of the element, layer by layer, parallel and perpendicular to the orthogonal reinforcement. Steel and concrete are taken as linear materials with no post-yield behavior or failure considered.

Lin and Scordelis (53) extend Scanlon's approach to include elasto-plastic behavior for steel and concrete. They

account for the coupling effect between membrane and bending action. A triangular element with fifteen degrees of freedom is used. Both of these studies include a tension stiffening effect for concrete between cracks.

Jofriet and McNeice's (45) model and Hand, Pecknold and Schnobrich's (36) model are described in Sections 4.3.3(a) and 4.3.1, respectively.

For the proposed model, one-quarter of the slab is considered, due to symmetry. Sixteen elements per quarter are used. With this number of elements, deflections in simply supported, isotropic elastic plates converged to the exact series solution. In the nonlinear analysis, single-precision provides satisfactory accuracy for the computer solution. If a higher number of elements had been used, double-precision would have been required, due to increase in the number of round-off errors in the solution of the larger system of equations. This would have increased the program storage requirement and the computational time by more than fifty percent, without changing the results significantly.

Deflections at points A and B, located 3 and 9 inches from the concentrated load (Fig. 4.19), are used to compare the analytical and experimental results. The deflection at point A is obtained approximately from deflections at nodal points 20 and 25. Point B concides with nodal point 15.

In the model, the slab is loaded incrementally with an

initial load increment of 400 lbs. This is reduced to 200 lbs., after initiation of cracks. Cracks start at a load of approximately 1200 lbs. As loading progresses to yield, the material axes rotate slightly. The rotation averages approximately three degrees in this problem and is due to changes in the principal moments caused by cracking. Fig. 4.20 shows the levels and directions of the cracks at a load of 2800 lbs.

The proposed solution is compared with the experimental curves and analytical models proposed by others (Figs. 4.21, 4.22). It is in good agreement with the experimental solution and with the solution of Jofriet and McNeice (Beeby). The model provides a better match than the three layered models shown. The ability to represent cracking as a continuous process, not limited to distinct layers, is viewed as a strong point of the proposed model. It also has the ability to represent a wider range of test results than that offered by Jofriet and McNeice.

4.4 Biaxial Stresses

The effect of the behavior of concrete under biaxial stresses on the behavior of reinforced concrete slabs is studied in this work. The slab in Section 4.3.3(b) is ideal for this purpose since the slab is subjected to positive biaxial moments over nearly its entire surface. The slab is analyzed using the portion of the concrete model presented in Section 2.2.1.4. The results are compared (Fig. 4.23) with the analytical curve obtained in Section 4.3.3.(b), which did not include a biaxial strength effect. The two analytical curves

are very close; the biaxial model is slightly stiffer, as may be expected. This minor difference supports the experimental observations of other investigators (16,44,52).

The fact that the increase in concrete strength due to biaxial compression has little effect on the load-deflection behavior of the model is due to the fact that the slab is under-reinforced and therefore, the effect of varying concrete strength ($\pm$ 20%) has very little effect on the resisting moment arm after the reinforcing steel yields. Because of the relatively minor effect on slab behavior of the biaxial strength increase, this portion of the model is not used in the other problems discussed in this chapter. Those results are, therefore, obtained with a somewhat simpler representation of concrete.

Chapter 5

SUMMARY AND CONCLUSIONS

5.1 Summary

A nonlinear model is developed to analyze reinforced concrete slabs under monotonically increasing loads. The model is used in conjunction with a compact, rectangular, plate bending finite element to trace elastic and inelastic load-deformation behavior of slabs up to failure.

Concrete is represented as a linear, brittle material in tension and a nonlinear, softening material in compression. Yield line theory is used to establish material axes. Reinforcing steel is modeled as a uniaxial, elasto-plastic material. Perfect bond is assumed between the steel and the concrete. The influences of temperature, shrinkage, creep and cyclic loading are not considered.

The slabs are analyzed as incrementally linear, anisotropic plates. Loads are applied incrementally and corrected using the initial stress method. Crack level and direction, and stresses and strains in concrete and steel are obtained using the nonlinear material and moment-curvature relationships.

The validity of the model is studied by comparing analytical results for beams and slabs with the analytical and experimental results of others. The effect of the increase in concrete strength, due to biaxial compression, on the load-deflection behavior of the model is also studied. A computer program is developed to implement the analysis.

5.2 Conclusions

The proposed model and method of analysis give satisfactory results for predicting the flexural behavior of reinforced concrete beams and slabs. The slab model is designed to analyze under-reinforced, balanced and over-reinforced concrete flexural members. However, over-reinforced concrete slabs are not common in practice, and are not investigated in this work.

The ability to represent cracking as a continuous process, appears to be a strong point of the model. The softening of concrete in compression appears to be a less critical, though significant, portion of the model.

The numerical examples indicate that the effect of biaxial stresses on concrete plays an insignificant role in modeling the behavior of reinforced concrete slabs. The load-deflection behavior of under-reinforced concrete slabs is not sensitive to the exact shape of the stress-strain curve for concrete in compression.

Good matches with test data are obtained for the numerical examples presented without modeling bond slip between steel and concrete or kinking of the steel at the yield lines.

The accuracy of the structural stiffness used in the incremental finite element analysis is an important factor in controlling the speed of convergence and the stability of the solution. The accuracy of the structural stiffness plays an important role in controlling the shape of the load-deflection curves, especially where highly inelastic behavior is involved, such as cracking or yielding. The variable stiffness approach proved to be a satisfactory procedure for handling these nonlinearities. In addition, reducing the size of

the load increment, after cracking and yielding, helps to insure an accurate analysis.

As used in this model, the yield line theory proved to be an excellent tool, not only for predicting the ultimate strength of the slabs, but for formulating the full load-deflection curves of the members.

The study demonstrates analytically, that the orientation of steel in isotropically reinforced slabs effects slab stiffness, but not strength. The conclusion matches experimental observations.

5.3 Recommendations for Further Study

The method of analysis introduced in this work, the concepts of uniaxial strain and curvature, and the calculation of strains and forces in the reinforcing steel are more general than applied in this study. They may be used with the finite element technique to analyze prestressed, as well as, reinforced concrete, and to analyze structural members such as shells. The proposed model may be easily extended to include in-plane stresses.

Shear failure is likely to occur in thin reinforced concrete slabs under concentrated loads and over supports. Three-dimensional analysis is required to solve these problems. Extending the proposed model to include shear requires experimental, as well as analytical, research. The proposed model is limited to "thin slabs". The nonlinear analysis of thick slabs and deep beams requires a different approach, using three-dimensional material representations and finite elements.

Experimental work on hollow slabs is needed, and the technique introduced here can be used to compare the analytical and experimental findings.

REFERENCES

1. Abel, J. F., and Desai, C. S., "Comparison of Finite Elements for Plate Bending", Journal of the Structural Division, ASCE, Vol. 98, No. ST9, Sept. 1972, pp. 2143-2154.

2. ACI: Building Code Requirements for Reinforced Concrete (318-71), American Concrete Institute, 1971.

3. ACI Committee 435, "State of the Art Report, Deflection of Two Way Reinforced Concrete Floor Systems", American Concrete Institute, SP-43, 1974.

4. ACI: Causes, Mechanism and Control of Cracking in Concrete, American Concrete Institute, SP-20, 1968.

5. ACI: Deflections of Concrete Structures, American Concrete Institute, SP-43, 1974.

6. Backlund, J., "Limit Analysis of Reinforced Concrete Slabs by a Finite Element Method", Presented at the June 1-2, 1972, Speciality Conference on the Finite Element Method in Civil Engineering, McGill University, Montreal, Canada, pp. 803-840.

7. Barnard, P. R., "Research into the Complete Stress-Strain Curve for Concrete," Magazine of Concrete Research, Vol. 16, No. 49, Dec. 1964, pp. 203-210.

8. Beeby, A. W., "Short-Term Deformation of Reinforced Concrete Members", Cement and Concrete Association, Technical Report No. TRA 408, London, England, March, 1968.

9. Bell, J. C., and Elms, D. G., "A Finite Element Approach to Post-Elastic Slab Behavior", American Concrete Institute, SP-30, 1971.

10. Bell, J. C., and Elms, D., "Partially Cracked Finite Elements", Journal of the Structural Division, ASCE, Vol. 97, No. ST7, July 1971.

11. Bogner, F. K., Fox, R. L., and Schmit, L. A., "The Generation of Interelement, Compatible Stiffness and Mass Matrices by the Use of Interpolation Formula", Proceedings Conference on Matrix Methods in Structural Mechanics, Wright-Patterson AFB, Ohio 1965.

12. Braestrup, M. W., "Yield-Line Theory and Limit Analysis of Plates and Slabs, Magazine of Concrete Research, Vol. 22, No. 71, June 1970, pp. 99-106.

13. Braestrup, M. W., Discussion of "Yield Criterion for Reinforced Concrete Slabs," by Satish C. Jain and John B. Kennedy, ASCE, Structural Division, Vol. 101, No. ST1, Jan. 1975, pp. 353-355.

14. Branson, D. E., "Instantaneous and Time-Dependent Deflections of Simple and Continuous Reinforced Concrete Beams," Alabama Highway Research Report No. 7, Bureau of Public Roads, Aug. 1963.

15. Cardenas, A., Clyde, D. H., Hilleboy, A., Lenkei, P., and Authors, Discussion of the Paper by Rolf J. Lenschow and M. A. Sozen "A Yield Criterion for Reinforced Concrete Slabs," Journal of the American Concrete Institute, Vol. 64, No. 11, 1967, pp. 784-785.

16. Cardenas, A., and Sozen, M. A., "Strength and Behavior of Isotropically and Nonisotropically Reinforced Concrete Slabs Subjected to Combinations of Flexural and Torsional Moments," Structural Research Series, No. 336, University of Illinois, Urbana, Illinois, 1968.

17. Cardenas, A., Lenschow, R. J., and Sozen, M. A., "Stiffness of Reinforced Concrete Plates," Journal of the Structural Division, ASCE, Vol. 98, No. ST11, November, 1972, pp. 2587-2603.

18. Cervenka, V., "Inelastic Analysis of Reinforced Concrete Panels Under In-Plane Loads," Thesis presented to the University of Colorado, at Boulder, Colorado, in 1970, in partial fulfillment of the requirements fo the degree of the Doctor of Philosophy.

19. C.E.B. F.I.P. International Recommendation for the Design and Construction of Concrete Structures, London, Cement and Concrete Association, 1970.

20. Chen, A.C.T., and Chen, Wai, F., "Constitutive Relations for Concrete," Journal of the Engineering Mechanics Division, ASCE, Vol. 101, No. EM4, August, 1975, pp. 465-481.

21. Clark, L. E., Gerstle, K. H., and Tulin, L. G., "Effect of Strain Gradient on the Stress-Strain Curve of Mortar and Concrete," Journal of the American Concrete Institute, Vol. 64, No. 9, Sept. 1967, pp. 580-586.

22. Clark, V., Neville, A. M., and Houghton-Evans, W., "Deflection Problems and Treatment in Various Countries," American Concrete Institute, SP-43, 1974, pp. 129-179.

23. Comité Europeen du Beton: "Recommendation for an International Code of Practice for Reinforced Concrete," published Jointly by American Concrete Institute, Detroit, and Cement and Concrete Association, London, 1963.

24. Corley, W. G., and Jirsa, J. O., "Equivalent Frame Analysis for Slab Design," Journal of the American Concrete Institute, Vol. 67, No. 11, Nov. 1970, p. 875.

25. Coon, M. D., and Evans, R. J., "Incremental Constitutive Laws and Their Associated Failure Criteria with Application to Plain Concrete," International Journal of Solid Structures, Vol. 8, 1972, pp. 1169-1183.

26. Darwin, D., and Pecknold, D. A., "Inelastic Model for Cyclic Biaxial Loading of Reinforced Concrete," Structural Research Series, No. 409, University of Illinois, Urbana, Illinois, July, 1974.

27. Darwin, D., and Pecknold, D. A., "Analysis of RC Shear Panels Under Cyclic Loading," Journal of the Structure Division, ASCE, Vol. 102, No. ST2, February, 1967, pp. 355-369.

28. Darwin, D., and Pecknold, D. A., "Analysis of Cyclic Loading of Plane R/C Structures," Second National Symposium on Computerized Structural Analysis and Design, George Washington University, March 29-31, 1976. Accepted for publication in Computers and Structures.

29. Desayi, P., and Krishnan, S., "Equation for the Stress-Strain Curve of Concrete," Journal of the American Concrete Institute, Vol. 61, No. 3, Mar. 1964, pp. 345-350.

30. Desayi, P., "A Model to Simulate the Strength and Deformation of Concrete in Compression," Material and Structures, Research and Testing (Paris); Vol. 1, 1968, pp. 49-56.

31. Echiverria-Gomez, A., and Schnobrich, W. C., "Lumped Parameter Analysis of Cylindrical Prestressed Concrete Reactor Vessels," Structural Research Series No. 340, University of Illinois, Urbana, Illinois, July, 1968.

32. Franklin, H. A., "Non-Linear Analysis of Reinforced Concrete Frames and Panels," Thesis presented to the University of California, at Berkeley, Calif., in March, 1970; in partial fulfillment of the requirements for the degree of Doctor of Philosophy.

33. Gallagher, R. H., "Analysis of Plates and Shell Structures," Proceeding of the Symposium on Application of Finite Element Methods in Civil Engineering, ASCE, Nov. 13-14, 1969, Vanderbilt University, Nashville, Tennessee.

34. Gaston, J. R., Siess, C. P., and Newmark, N. M., "An Investigation of the Load-Deformation Characteristics of Reinforced Concrete Beams up to the Point of Failure," Structural Research Series, No. 40, University of Illinois, Urbana, Illinois, Dec. 1952.

35. Gupta, A. K., Mohraz, B., and Schnobrich, W. C., "Elasto-Plastic Analysis of Three Dimensional Structures Using the Isoparametric Element," Structural Research Series, No. 381, University of Illinois, Urbana, Illinois, Aug. 1971.

36. Hand, R. A., Pecknold, D. A., and Schnobrich, W. C.,"A Layered Finite Element Non-Linear Analysis of Reinforced Concrete Plates and Shells," Structural Research Series, No. 389, University of Illinois, Aug. 1972.

37. Hand, F. R., Pecknold, D. A., and Schnobrich, W. C., "Nonlinear Layered Analysis of RC Plates and Shells," Journal of the Structural Division, ASCE, Vol. 99, No. ST7, July, 1973, pp. 1491-1505.

38. Hearmon, R. F. S., An Introduction to Applied Anisotropic Elasticity, Oxford University Press, London, England, 1961.

39. Hognestad, E., "Confirmation of Inelastic Stress Distribution in Concrete," Journal of the Structural Division, ASCE, Vol. 83, No. ST2, March 1957, pp. 17.

40. Hsu, C. T. and Mirza, M. S., "A Study of Post Yielding Deflection in Simply Supported Reinforced Concrete Beams," American Concrete Institute, SP-43, 1974.

41. Huber, M. T., Probleme Der Static Technisch Wichtiger Orthotroper Platte, Warsawa, 1929.

42. Isaacson, E., and Keller, H. B., Analysis of Numerical Methods, John Wiley & Sons, New York, 1966.

43. Isenberg, J. and Adham, S., "Analysis of Orthotropic Reinforced Concrete Structure," Journal of the Structural Division, ASCE, Vol. 96, No. ST12, December 1970, pp. 2607-2624.

44. Jain, S. and Kennedy, J., "Yield Criterion for Reinforced Concrete Slabs," Journal of the Structural Division, ASCE, Vol. 100, No. ST3, March, 1974, pp. 631-644.

45. Jofreit, J. C.. and McNeice, G. M., "Finite Element Analysis of Reinforced Concrete Slabs," Journal of Structural Division, ASCE, Vol. 97, No. ST3, March 1971, pp. 785-806.

46. Johansem, K. W., "Yield Line Theory," Cement and Concrete Association, London, 1962.

47. Kemp, K. O., "The Yield Criterion for Orthotropically Reinforced Concrete Slabs," International Journal of Mechanical Sciences, Vol. 7, November 1965, pp. 737-746.

48. Kupfer, H., Hilsdorf, H. K., and Rusch, H.,"Behavior of Concrete Under Biaxial Stresses,"Journal of the American Concrete Institute, Vol. 66, No. 8, August, 1969 pp. 656-666.

49. Kupfer, H. B., and Gerstle, K. H., "Behavior of Concrete Under Biaxial Stresses," Journal of Engineering Mechanics Division, ASCE, Vol. 99, No. EM4, Aug. 1973, pp. 852-866.

50. Lekhnitskii, S. G., Anisotropic Plates, Gordon and Breach: Science Publishers, New York, 1968.

51. Lekhnitskii, S. G., Theory of Elasticity of an Anisotropic Elastic Body, Holden Day Inc., San Francisco, 1963.

52. Lenshow, R. and Sozen, M. A., "A Yield Criterion for Reinforced Concrete Under Biaxial Moments and Forced," Civil Engineering Studies, Structural Research Series, No. 311, University of Illinois, Urbana, Illinois, July 1966.

53. Lin, C. S. and Scordelis, A. C., "Nonlinear Analysis of RC Shells of General Form," Journal of Structural Division, ASCE, Vol. 101, No. ST3, March 1975, pp. 523-538.

54. Lin, C. S., and Scordelis, A. C., "Finite Element Study of a Reinforced Concrete Cylindrical Shell Through Elastic, Cracking and Ultimate Ranges," Journal of the American Concrete Institute, Vol. 72, No. 11, Nov. 1975, pp. 628-633.

55. Liu, T. C. Y., Nilson, A. H., and Slate, F. O., "Biaxial Stress-Strain Relations for Concrete", Journal of Structural Division, ASCE, Vol. 98, No. ST5, May 1972, pp. 1025-1034.

56. Liu, T. C. Y., Nilson, A. H. and Slate, F. O., "Stress-Strain Response and Fracture of Concrete in Uniaxial and Biaxial Compression," Journal of the American Concrete Institute, Vol. 69, No. 5, May 1972, pp. 291-295.

57. Mallett, R. H., and Marcal, P. B., "Finite Element Analysis of Non-Linear Structures", Journal of the Structural Division, ASCE, Vol. 94, No. ST9, 1968, pp. 2081-2105.

58. Mayer, H., and Rusch, H., "Building Damage Caused by Deflection of Reinforced Concrete Building Components," Technical Translation 1412, National Research Council, Ottawa, Canada.

59. McNeice, G. M, "Elastic-Plastic Bending of Plates and Slabs by Finite Element Method", Thesis presented to the University of London, at London, England, in 1967 in partial fulfillment of the requirement for the degree of Doctor of Philosophy.

60. Mikkola, M. J., and Schnobrich, W. C., "Material Behavior Characteristics for Reinforced Concrete Shells Stressed Beyond the Elastic Range," Structural Research Series, No. 367, University of Illinois, Urbana, Illinois, August 1970.

61. Mufti, A. A., Mirza, M. S., McCutcheon, J. O., and Houde, J., "A Study of the Behavior of Reinforced Concrete Elements," Structural Concrete Series No. 70-5, McGill University, 1970.

62. Mufti, A. A., Mirza, N. S., McCutcheon, J. O., and Houde, J., "A Study of the Non-Linear Behavior of Structural Concrete Elements," Proceedings of the Specialty Conference of Finite Element Method in Civil Engineering, Montreal, Canada, June, 1972.

63. Murray, D. W., and Wilson, E. L., "Large Deflection Plate Analysis by Finite Element," Journal of the Engineering Mechanics Division, ASCE, Vol. 95, No. EM1, Feb. 1969, pp. 143-166.

64. Nam, C. H., and Salmon, C. G., "Finite Element Analysis of Concrete Beams," Journal of the Structural Division, ASCE, Vol. 100, No. ST12, December 1974, pp. 2419-2432.

65. Nelissen, L. J. M., "Biaxial Testing of Normal Concrete," Heron, Netherlands, Vol. 18, No. 1, 1972.

66. Ngo, D., and Scordelis, A. C., "Finite Analysis of Reinforced Concrete Beams," Journal of the American Concrete Institute, Vol. 64, No. 3, March, 1967, pp. 152-163.

67. Nilson, A. H., "Nonlinear Analysis of Reinforced Concrete By the Finite Element Method," Journal of the American Concrete Institute, Vol. 65, No. 9, Sept. 1968.

68. Oden, J. T., "Finite Element Applications in Nonlinear Structural Analysis,"Proceedings Symposium on Application of Finite Element Methods in Civil Engineering, ASCE, No. 13-14, 1969, Nashville, Tennessee, Vanderbilt University.

69. Popovics, S., "A Review of Stress-Strain Relationships for Concrete," Journal of the Structural Division, ASCE, Vol. 67, No. 3, March 1970, pp. 243-248.

70. Ramaley, D., and McHenry, D., "Stress-Strain Curves for Concrete Strained Beyond the Ultimate Load," Laboratory Report No. Sp-12 U.S. Bureau of Reclamation, Denver, March 1947.

71. Rashid, Y. R., "Ultimate Strength Analysis of Prestressed Concrete Pressure Vessels," Nuclear Engineering Design, Vol. 7, p. 334, 1968.

72. Romstad, K. M., Taylor, M. A., and Herrman, L. R., "Numerical Biaxial Characterization for Concrete," Journal of the Engineering Mechanics Division, ASCE, Vol. 100, No. EM5, Oct. 1974, pp. 935-948.

73. Rusch, H., "Researches Toward a General Flexural Theory for Structural Concrete," Journal of the American Concrete Institute, Vol. 57, No. 1, July 1960, pp. 1-28.

74. Saenz, L. P., Discussion of "Equation for the Stress-Strain Curve of Concrete," by Desayi and Krishnan, Journal of the American Concrete Institute, Vol. 61, No. 9, Sept. 1964, pp. 1229-1235.

75. Salem, M. H. and Mohraz, B. M., "Nonlinear Analysis of Planar Reinforced Concrete Structures," Structural Research Series, No. 410, University of Illinois, Urbana, Illinois, July 1974.

76. Sargin, M., "Stress-Strain Relationships for Concrete and the Analysis of Structural Concrete Sections", Study No. 4, Solid Mechanics Division, University of Waterloo, Waterloo, Ontario, Canada.

77. Sarne, Y., Discussion of "Nonlinear Analysis of RC Shells of General Form," by Lin and Scordelis, Journal of the Structural Division, ASCE, Vol. 101, No. ST11, Nov. 1975, pp. 2457-2458.

78. Sarne, Y., "Material Nonlinear Time Dependent Three Dimensional Element Analysis of Reinforced and Prestressed Concrete Structures," Thesis presented to Massachusetts Institute of Technology, at Cambridge, Mass. in 1975, in partial fulfillment of the requirements for the degree of Doctor of Philosophy.

79. Save, M., "A Consistant Limit-Analysis Theory for Reinforced Concrete Slabs," Magazine of Concrete Research, Vol. 19, No. 56, March 1967, pp. 3-12. Discussion by R. J. Lenschow, Vol. 19, No. 1, Dec. 1967.

80. Scanlon, A., "Time Dependent Deflections of Reinforced Concrete Slabs," PhD Dissertation, Department of Civil Engineering, University of Alberta, Edmonton, December, 1971.

81. Scanlon, A.,"Time Dependent Deflections of Reinforced Concrete Slabs," Structural Eng. Report No. 38, Department of Civil Engineering, University of Alberta, Dec. 1971.

82. Scanlon, A., and Murray, D. W., "An Analysis to Determine the Effects of Cracking in Reinforced Concrete Slabs," Proceedings Conference on Finite Element Methods in Civil Engineering, McGill University, 1972, p. 841.

83. Scanlon, A., and Murray, D. W., "Time Dependent Reinforced Concrete Slab Deflection," Journal of the Structural Division, ASCE, Vol. 100, No. ST9, Sept. 1974, pp. 1911-1924.

84. Schnobrich, W. C., "Finite Element Determination of Non-Linear Behavior of Reinforced Concrete Plates and Shells," Symposium on Nonlinear Techniques and Behavior in Structural Analysis, Tranpsort and Road Research Laboratory, Department of the Environment, United Kingdom, 1974.

85. Scordelis, A. C., "Finite Element Analysis of Reinforced Concrete Structures," Proceedings Conference on Finite Element Methods in Civil Engineering, McGill Univ., 1972, p. 71.

86. Sturman, G. M., Shah, S. P., and Winter, G., Journal of the American Concrete Institute, Vol. 62, No. 7, July 1962, pp. 805-822.

87. Suidan, M., and Schnobrich, W. C., "Finite Element Analysis of Reinforced Concrete," Journal of the Structural Division, ASCE, Vol. 99, No. ST10, Oct. 1973, pp. 2109-2122.

88. Szilard, R., Theory and Analysis of Plates, Prentice Hall 1974.

89. Timoshenko, S., and S. Woinowsky-Krieger, Theory of Plates and Shells, McGraw-Hill Book Co., Inc. New York, 1959.

90. Valliappan, S., and Doolan, T. F., "Nonlinear Stress Analysis of Reinforced Concrete," Journal of the Structural Division, ASCE, Vol. 98, No. ST4, April 1972, pp. 885-898.

91. Whang, B., "Elasto-Plastic Orthtropic Plates and Shells," Proceedings of the Symposium on Application of Finite Element Methods in Civil Engineering, Vanderbilt University, Nashville, Tennessee, Nov. 1969.

92. Wanchoo, M. K. and May, G. W., "Cracking Analysis of Reinforced Concrete Plates," Journal of the Structural Division, ASCE, Vol. 101, No. ST1, January 1975, pp. 201-215.

93. Wu, H. C., "Dual Failure Criterion for Plain Concrete," Journal of the Engineering Mechanics Division, ASCE, Vol. 100, No. EM6, December 1974, pp. 1167-1181.

94. Yuzugullu, O., and Schnobrich, W. C., "A Numerical Procedure for the Determination of the Behavior of a Shear Wall Frame System", Journal of the American Concrete Institute, Vol. 69, No. 7, July 1973, pp.474-479.

95. Zienkiewicz, O. C., Valliappan, S., and King, I. P., "Stress Analysis of Rock as a 'No Tension' Material", Geotechnique, Vol. 18, March 1968, pp. 56-66.

96. Zienkiewicz, O., "Elasto-Plastic Solution of Engineering Problems 'Initial Stress' Finite Element Approach", International Journal for Numerical Methods in Engineering, Vol. 1, 1969, pp. 75-100.

97. Zienkiewicz, O., Best, B., Dullage, C., and Stagg, K. G., "Analysis of Non-Linear Problems in Rock Mechanics with Particular Reference to Jointed Rock Systems," Proceedings 3rd International Congress on Rock Mechanics, Belgrade 1970.

98. Zienkiewicz, O. C., The Finite Element Method in Engineering Science, McGraw-Hill Book Co., London, England, 1971.

TABLE 4.1

Material Properties for Specimens

Investigators	Designation	Material Properties					Steel Areas			
		f'_c ksi	(1) $E_c \times 10^{-3}$ ksi	ν	(2) F_y ksi	$E_s \times 10^{-3}$ ksi	x Direction in^2/in	y Direction in^2/in	(3) Angle	Reinforcement Ratio
Gaston, Siess and Newmark[34]	T1MA	4.6	(3.86)		46	28.2	0.068	- - -	- - -	ρ=0.0062
	T3MA	4.8	(3.94)		41	28.2	0.339	- - -	- - -	ρ=0.0322
Cardenas and Sozen[16]	B10	4.92	4.00	0.15	50	30.0	0.0352	0.0352	0°	ρ=0.01
	B7	5.15	4.00		50	30.0	0.0352	0.0352	45°	ρ=0.01
Jain and Kennedy[44]	A_1	4.58	(3.85)		32	(29)	0.0107	0.0128	0°	ρ=0.00878
	A_2	4.43	(3.79)	(0.2)	32	(29)	0.0107	0.0128	30°	ρ=0.01137
	A_3	4.53	(3.83)		32	(29)	0.0107	0.0128	45°	
Jofriet and McNiece[45]	1-Way Slab	5.7	4.1	.15	(50)	29	0.0105	0.0105	0°	ρ=0.008
	2-Way Slab	5.5	4.15	.15	(50)	29	0.0111	0.0111	0°	ρ=0.0085

1) $E_c = 57000$, $f_{rt} = 7.5\sqrt{f'_c}$ are used in the analysis for all problems.

2) Numbers in paranthesis show values used in the analysis; the originals are not available.

3) Measured counter-clockwise from the global coordinate system to the steel directions.

Table 4.2

Yield Moments and Deflections at Midspan
for T1MA and T3MA

Beam	Investigators	Type of Analysis	Moment K-ft/in	Deflection in.	M- κ Relation
T1MA	Gaston, Siess and Newmark[34]	Experimental	15.5	0.25	
		Analytical	15.1	0.24	
	Hsu and Mirza[40]	Analytical	15.6	0.266	Linear
				0.255	Bilinear
	Proposed Model	Analytical Finite Element	15.12	0.257	
T3MA	Gaston, Siess and Newmark[34]	Experimental	60.5	0.50	
		Analytical	59.2	0.32	
	Hsu and Mirza[40]	Analytical	59.12	0.3613	Linear
				0.359	Bilinear
	Proposed Model	Analytical Finite Element	59.4	0.428	

Table 4.3

Moments and Curvatures at Midspan
for B7 and B10

Slab	Investigators	Type of Analysis	Initial Cracking		Yield		Ultimate
			Moment	Curvature	Moment	Curvature	Moment
			in-k/in.	10^{-5}/in.	in-k/in.	10^{-5}/in.	in-k/in
B7	Cardenas and Sozen[16]	Experimental	1.67	10	5.60	140	5.85
		Analytical	1.53	9	5.62	170	5.76
	Hand, Pecknold and Schnobrich [36]	Analytical	1.5	-	5.52	-	-
	Proposed Model		1.625	6.53	5.42	137	5.88
B10	Cardenas and Sozen[16]	Experimental	1.36	8	5.55	90	6.10
		Analytical	1.53	7	5.48	80	5.88
	Hand et al[36]	Analytical	1.43	-	5.43	-	-
	Proposed Model		1.454	7.7	5.49	72	5.96

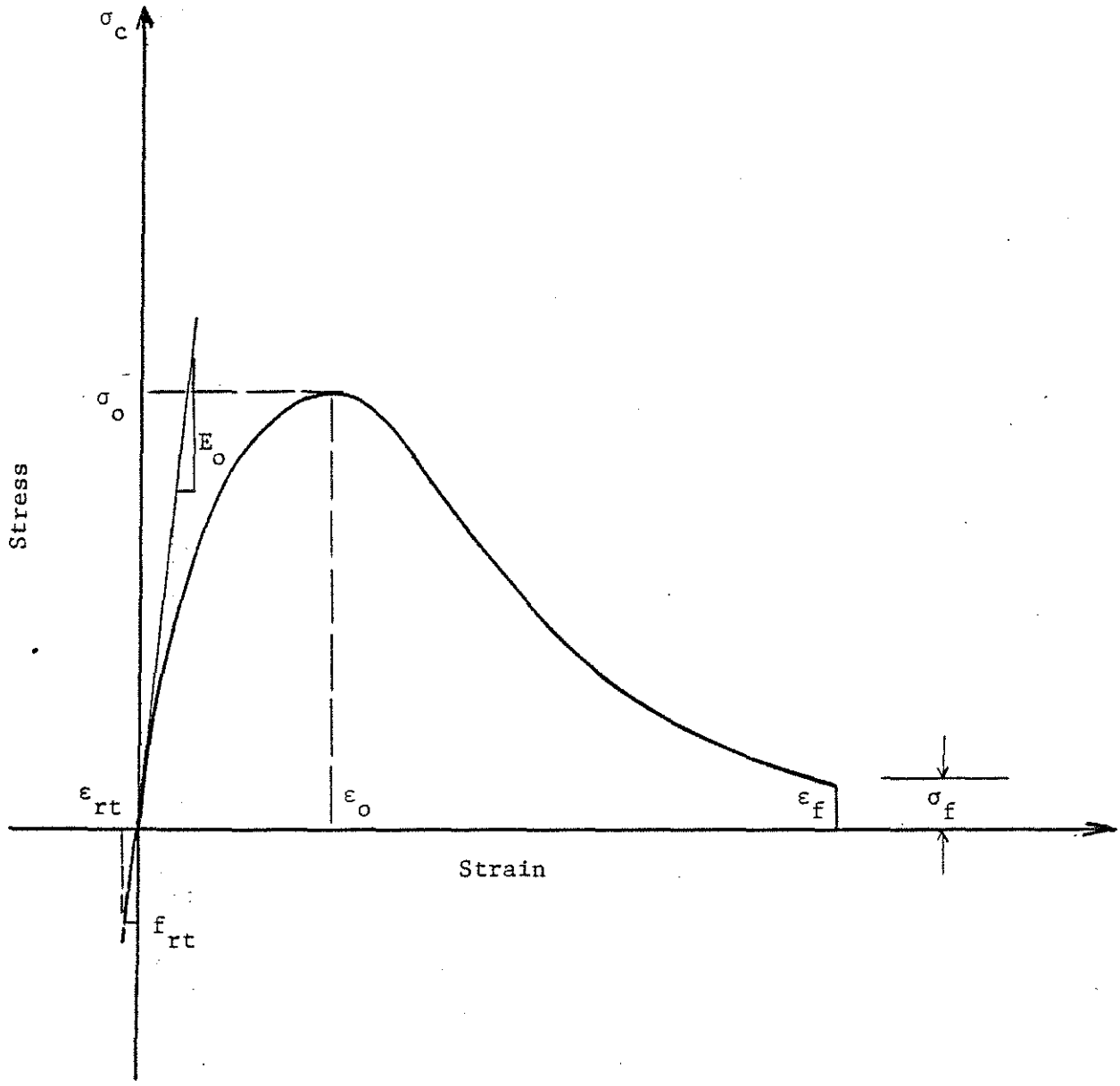

Fig. 2.1 Proposed Stress-Strain Curves for Concrete

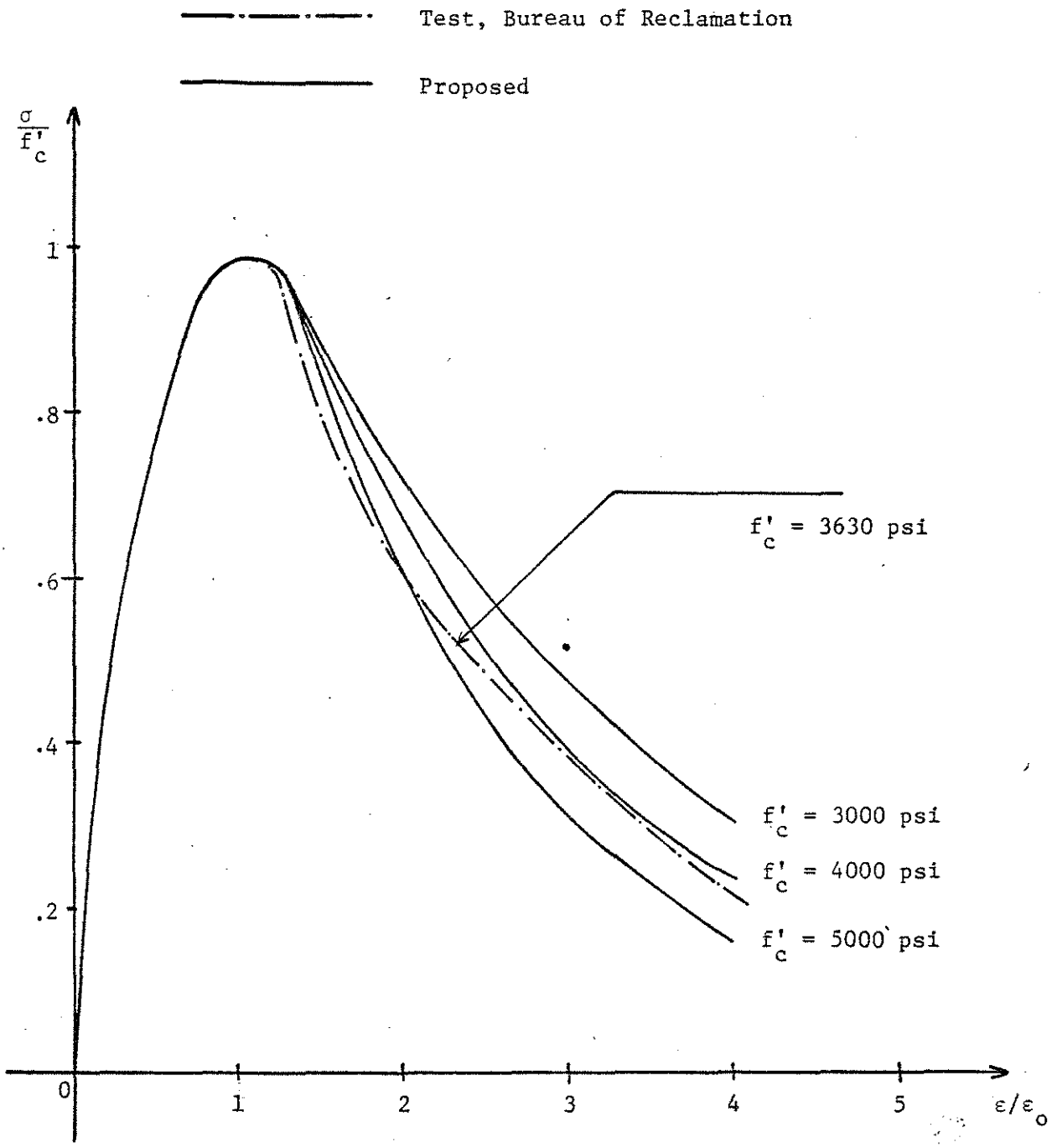

Fig. 2.2 Nondimensional Stress-Strain Curves

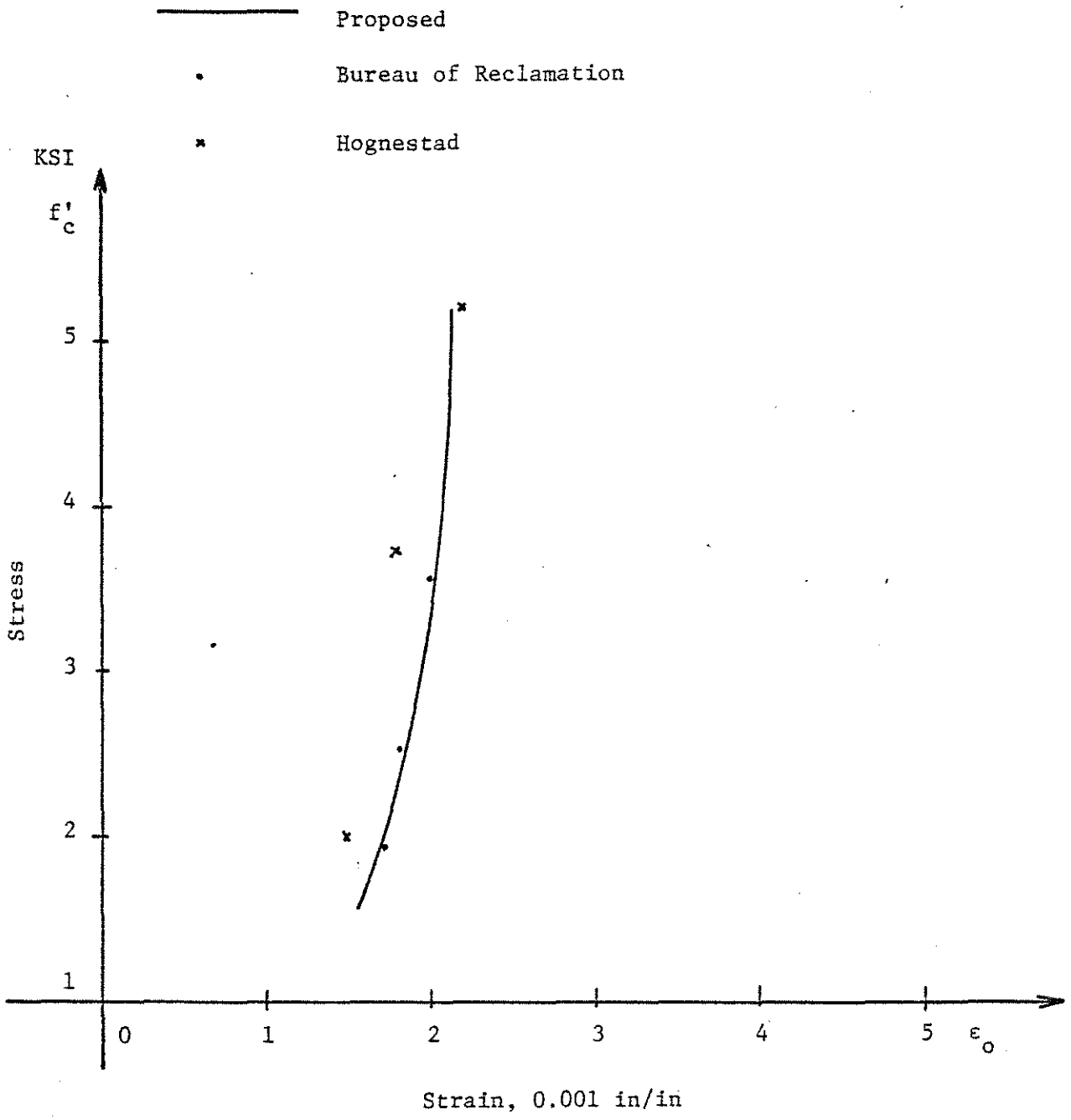

Fig. 2.3 Strain, ε_o, at Maximum Stress, f'_c

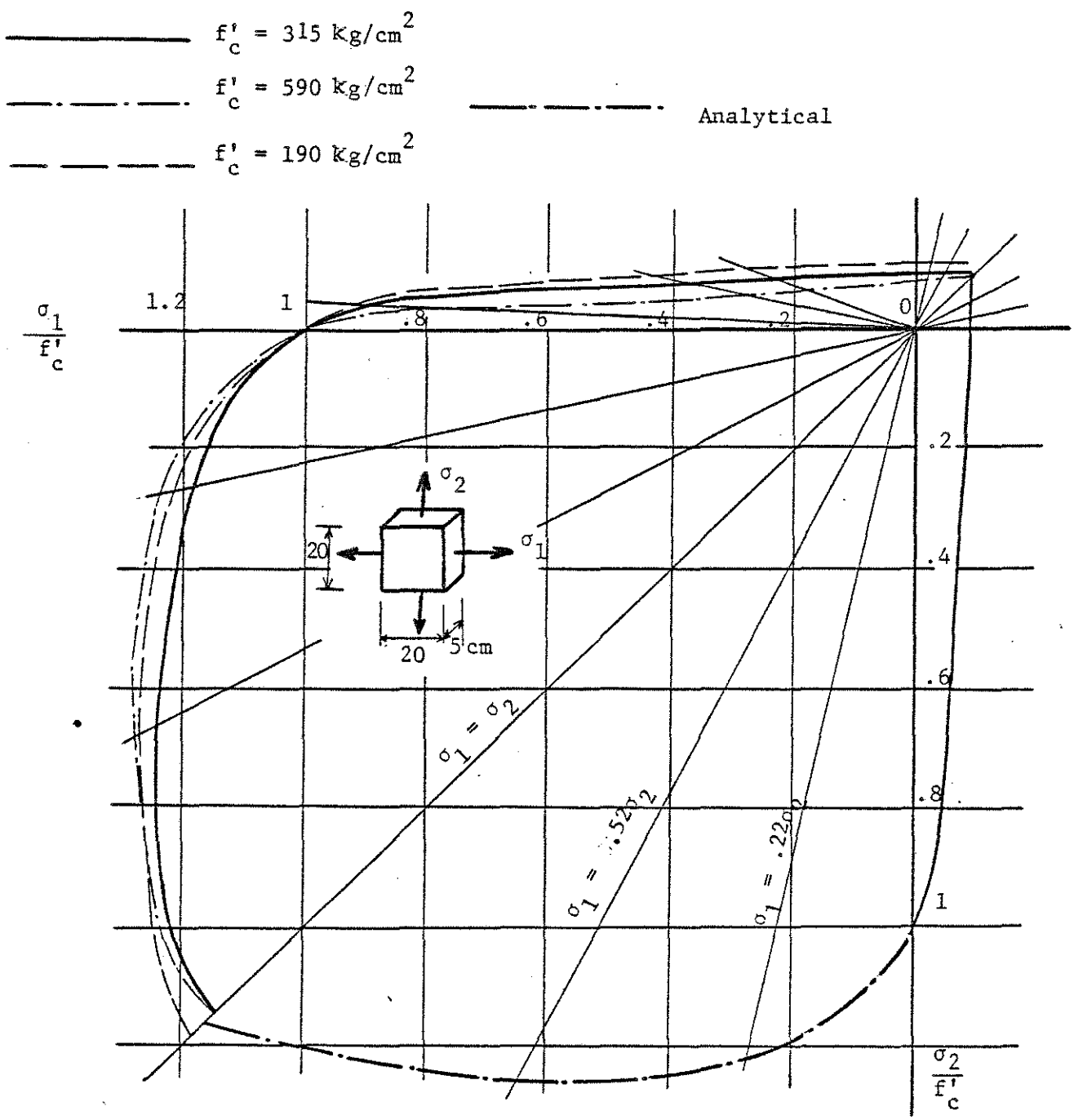

$$\left(\frac{\sigma_1}{f'_c} + \frac{\sigma_2}{f'_c}\right)^2 - \frac{\sigma_2}{f'_c} - 3.65\frac{\sigma_1}{f'_c} = 0$$

or

$$\sigma_2 = \frac{(1+3.65\alpha)}{(1+\alpha)^2} f'_c$$

$$\alpha = \frac{\sigma_1}{\sigma_2}$$

Fig. 2.4 Analytical Biaxial Strength Envelope (48,49)

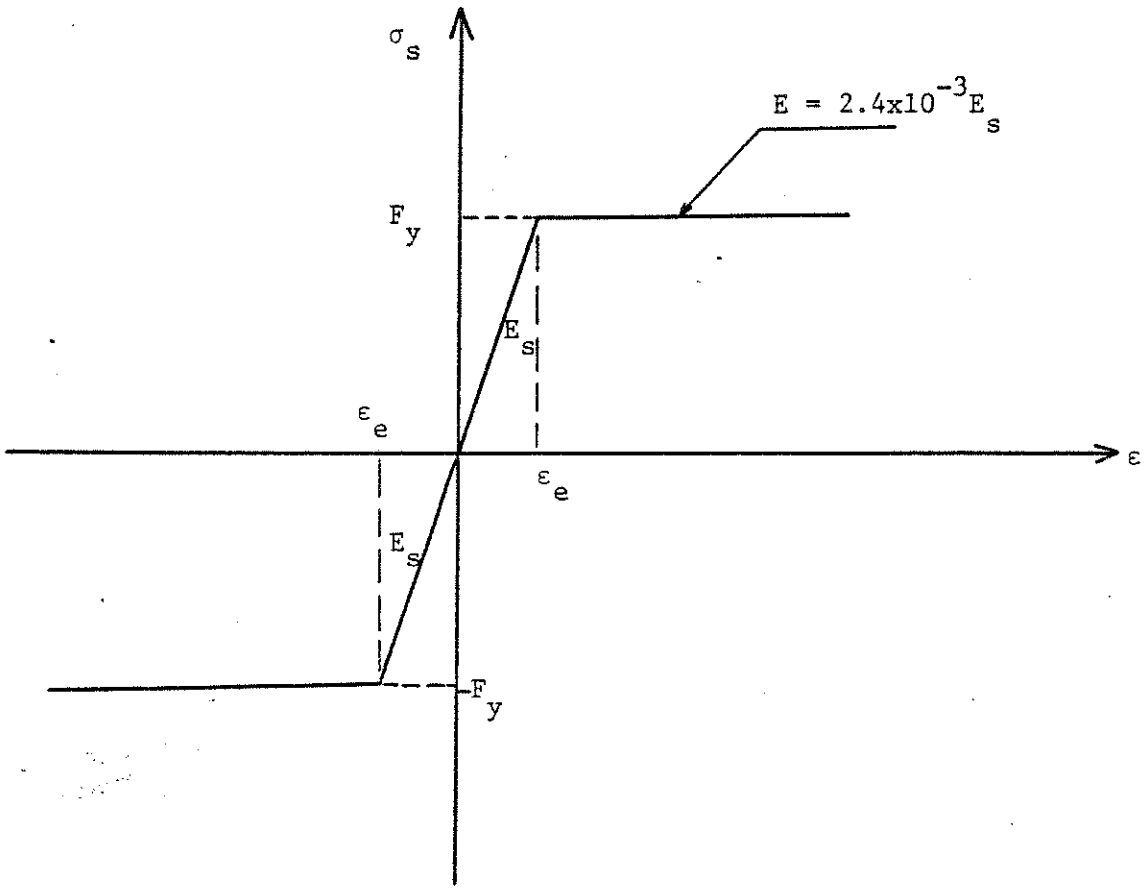

Fig. 2.5 Idealized Stress-Strain Relations for Steel in Tension and Compression

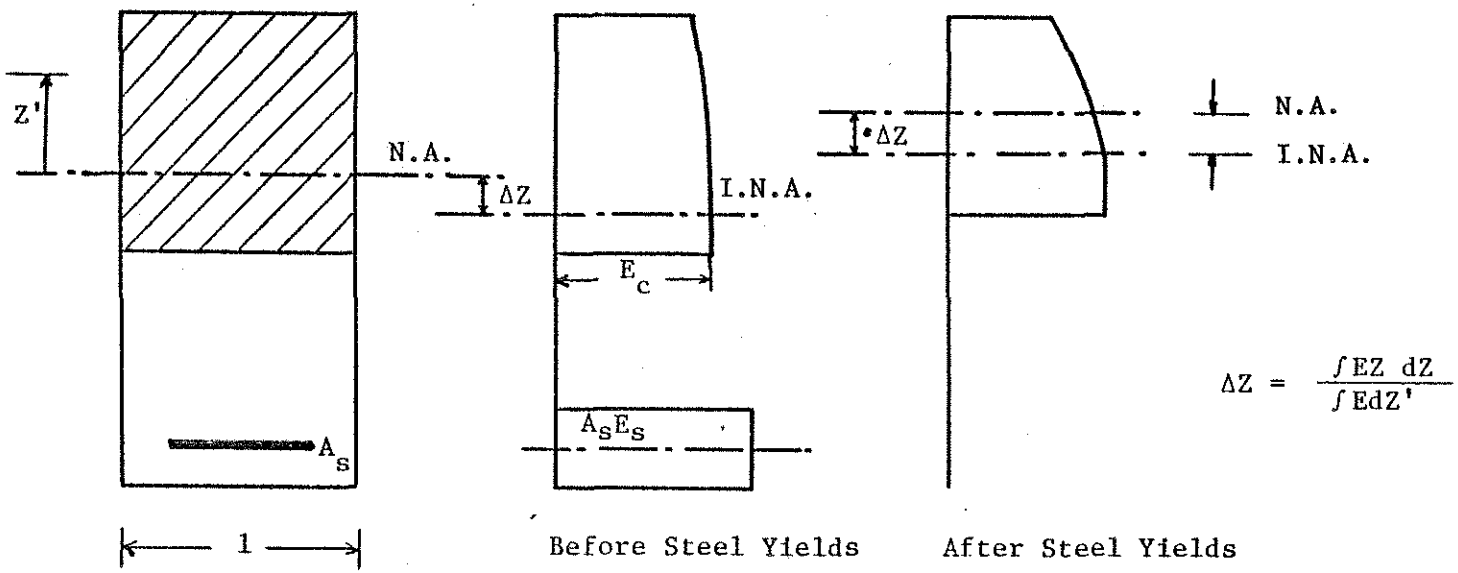

Fig. 2.6 Location of Neutral Axis and Instantaneous Neutral Axis

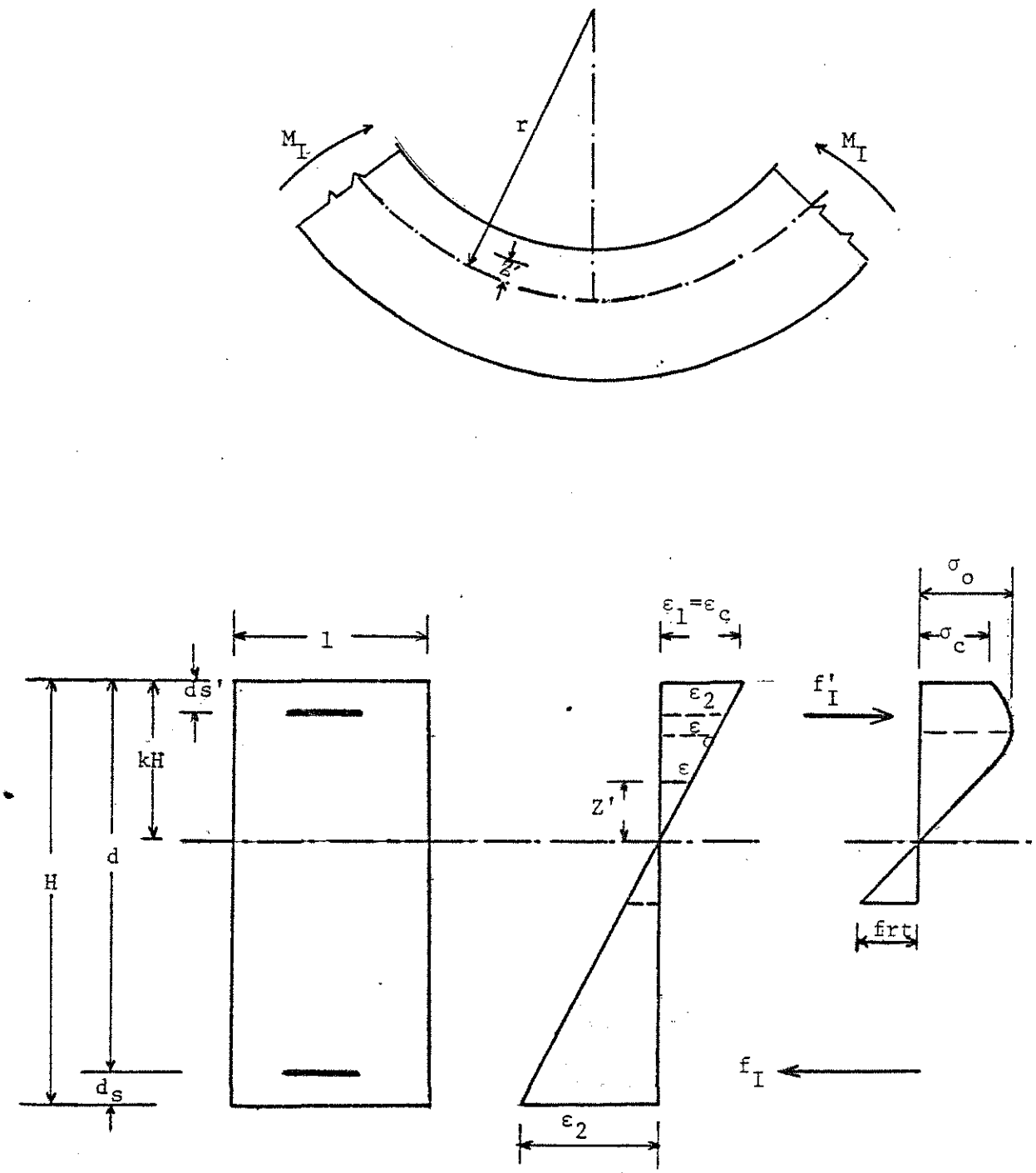

Fig. 2.7 Rectangular Concrete Cross Section Subjected to Pure Bending Moment

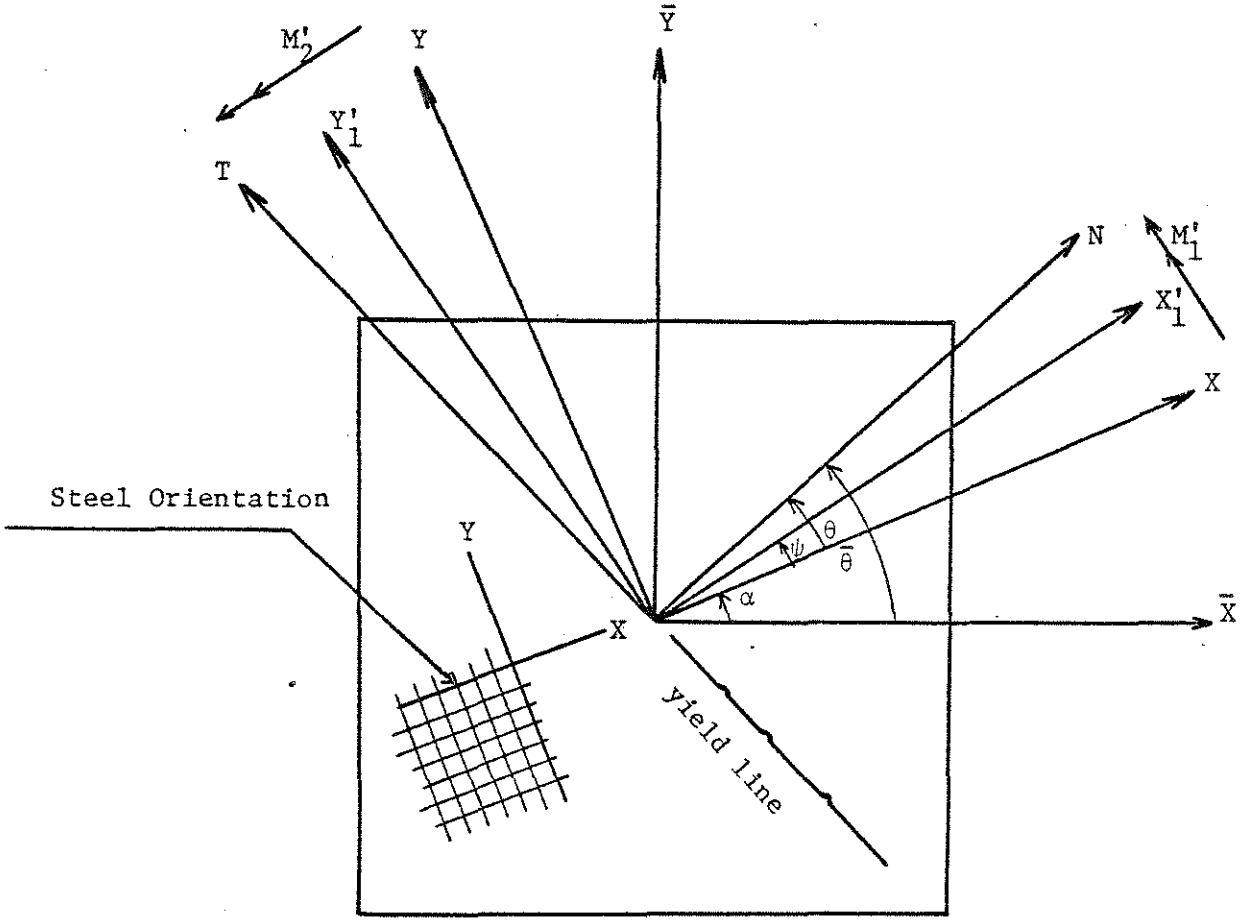

Fig. 2.8 Slab Element and Orientation of Axes and Angles

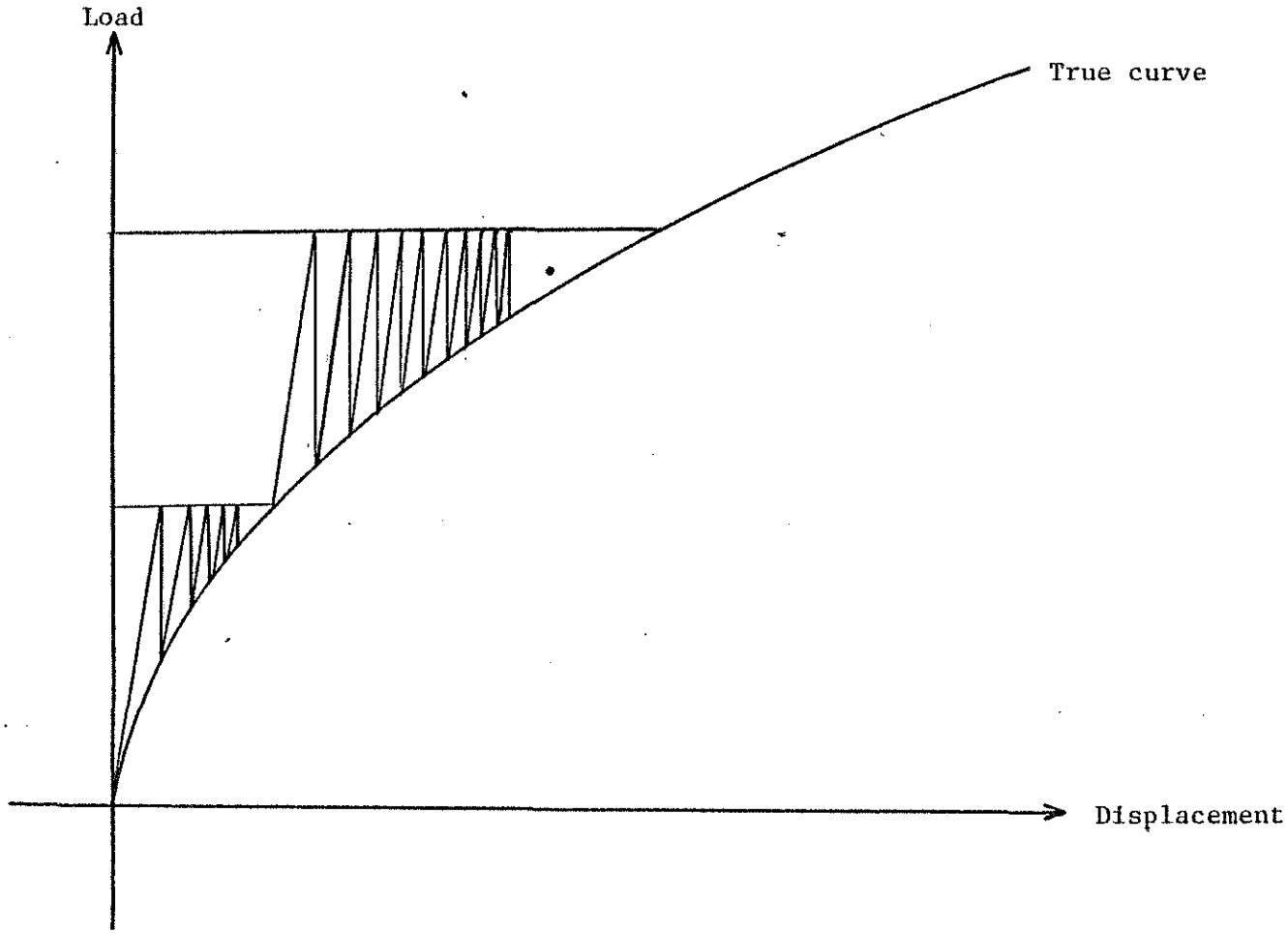

Fig. 3.1 Initial Stress Method, Constant Stiffness Approach.

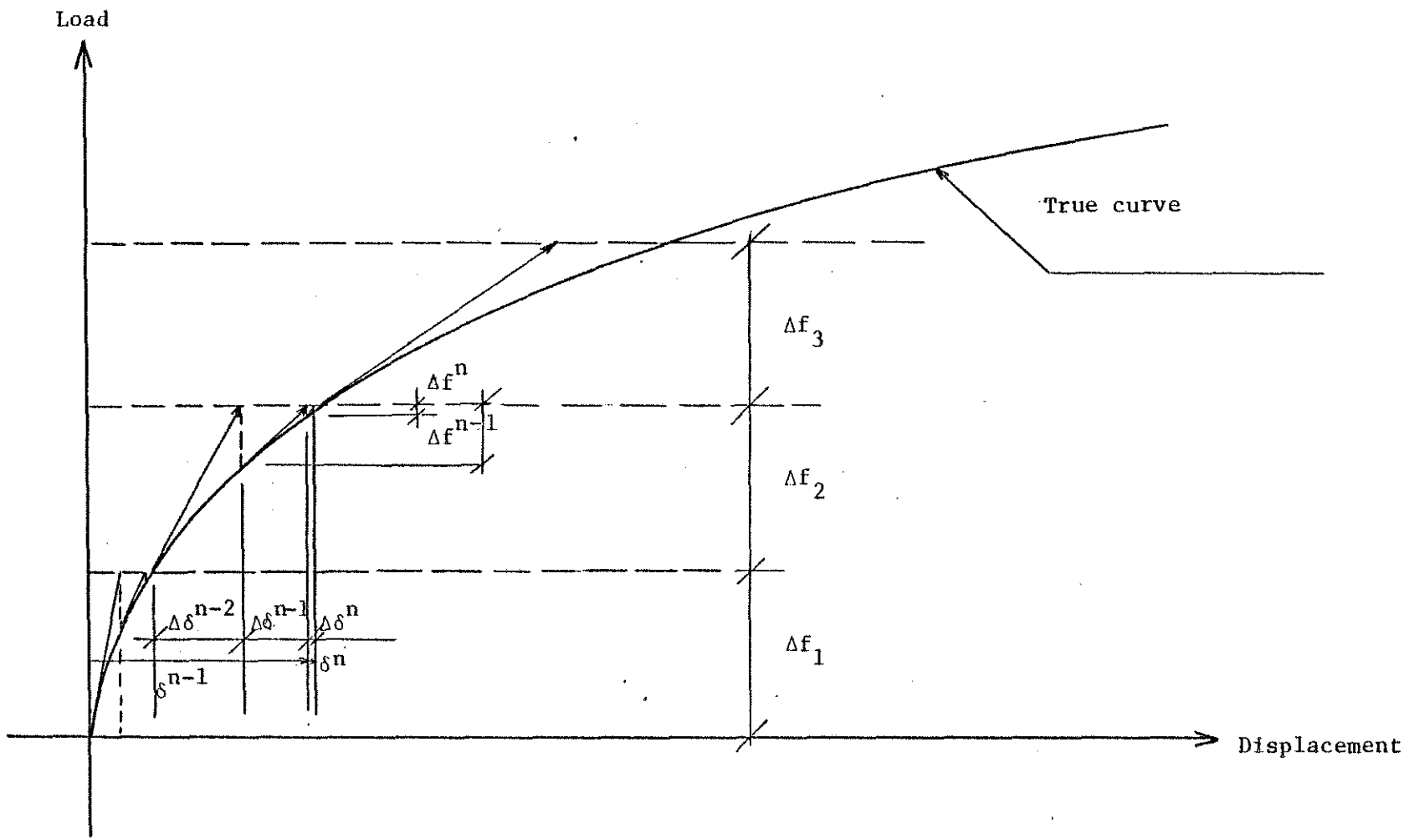

Fig. 3.2 Initial Stress Method, Variable Stiffness Approach

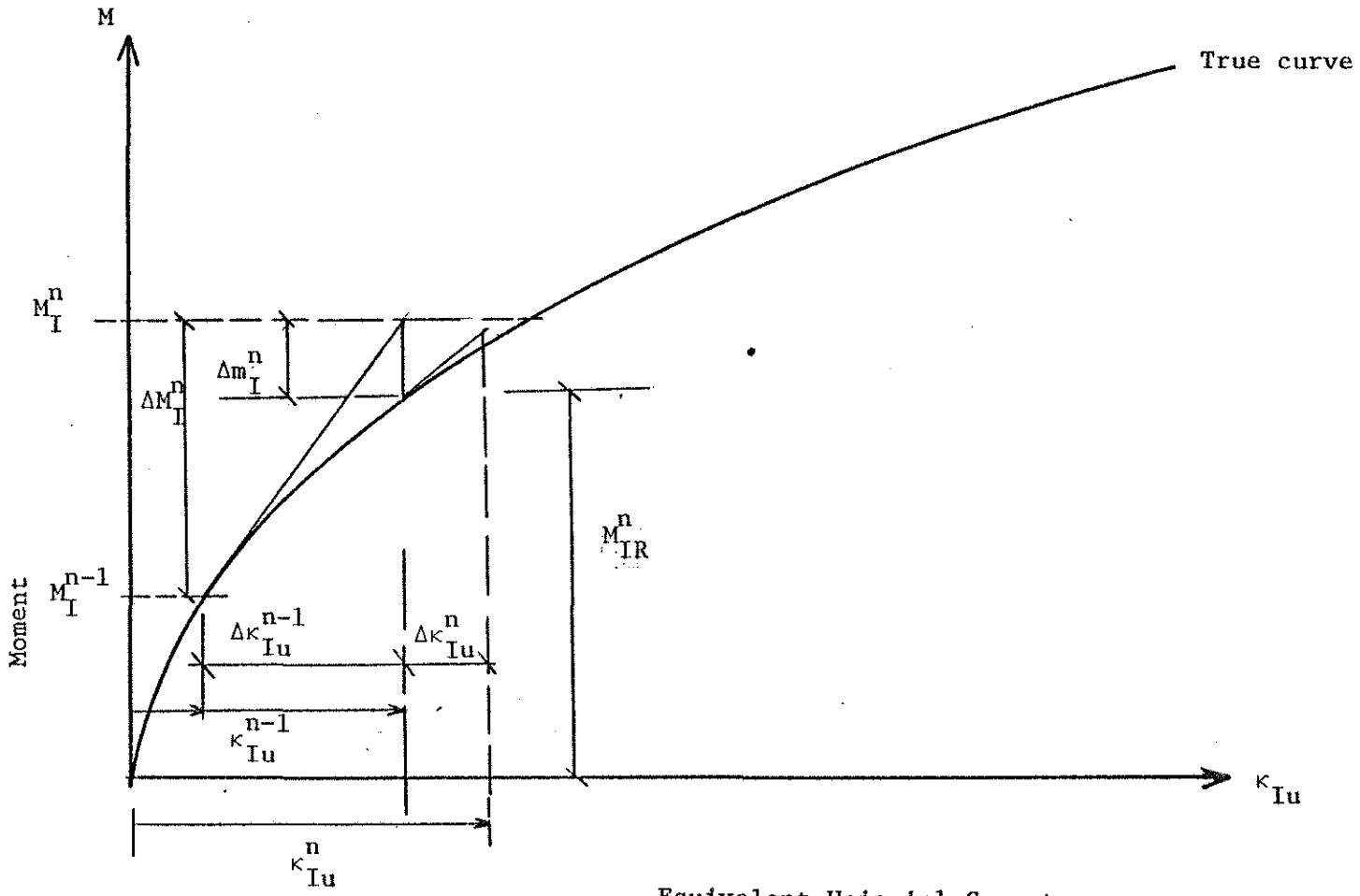

Fig. 3.3 "Initial Moment" Approach

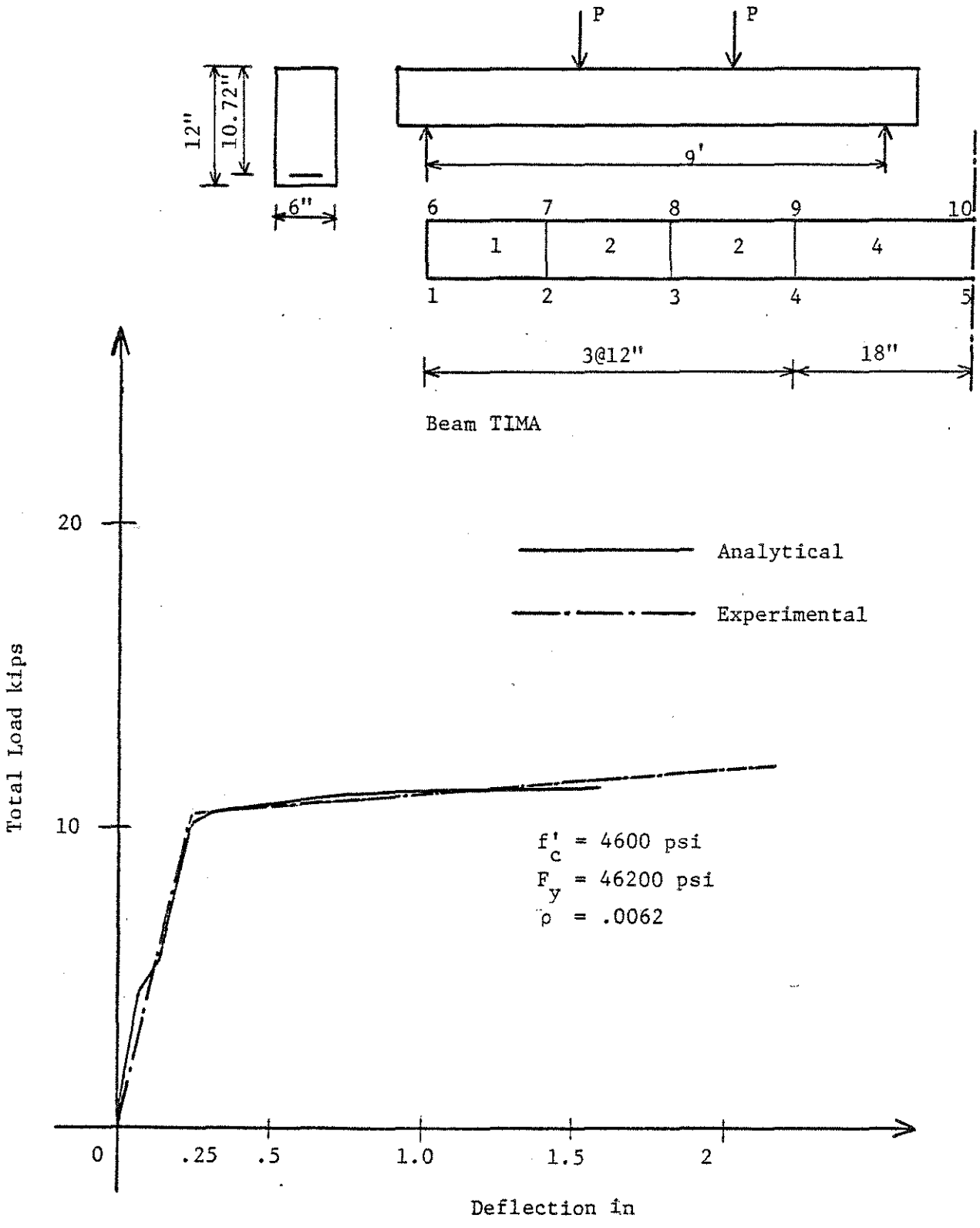

Fig. 4.1 Load-Deflection Curves for Beam Test Specimen TIMA (34)

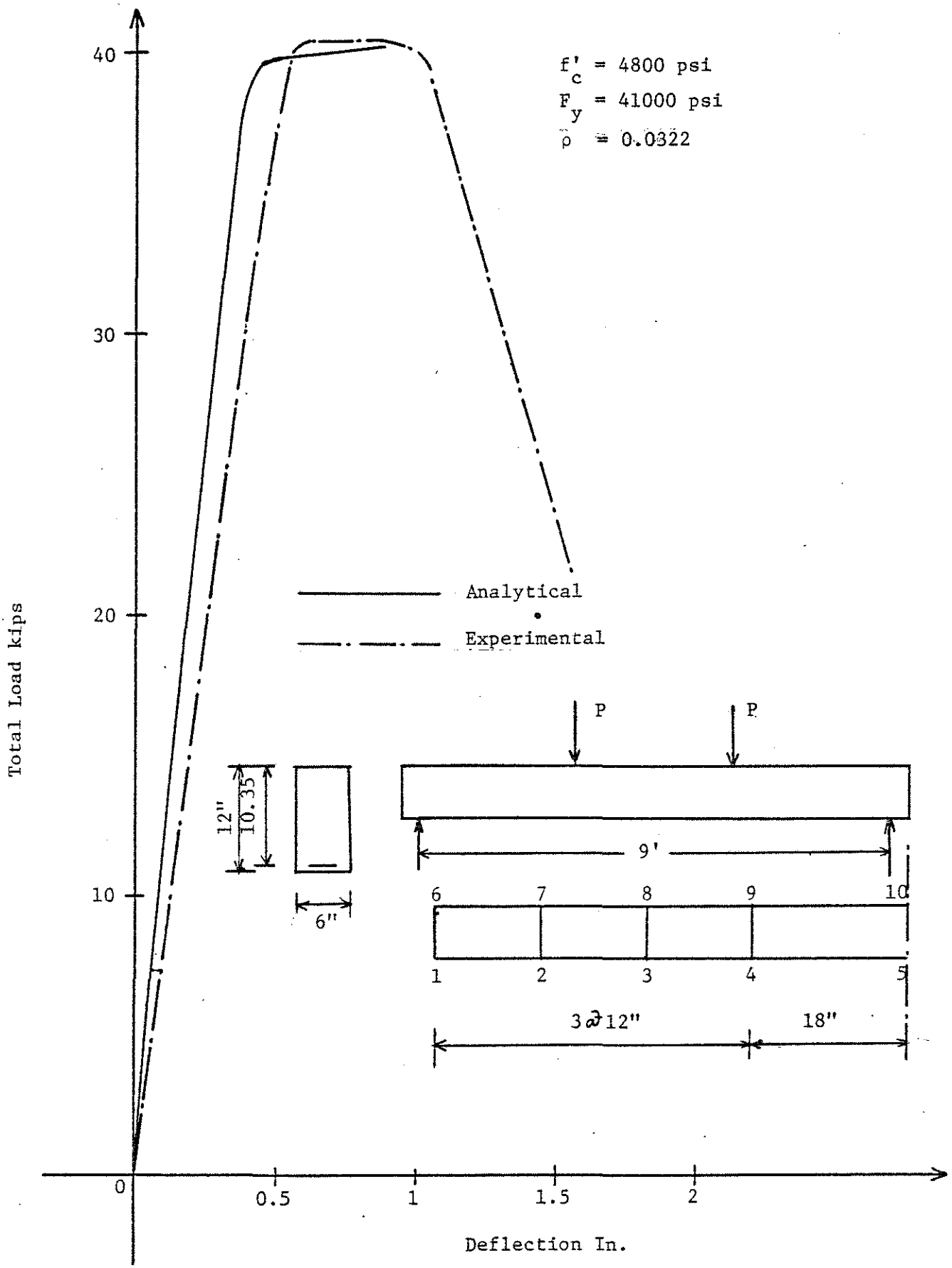

Fig. 4.2 Load-Deflection Curves for Beam Test Specimen T3MA (34)

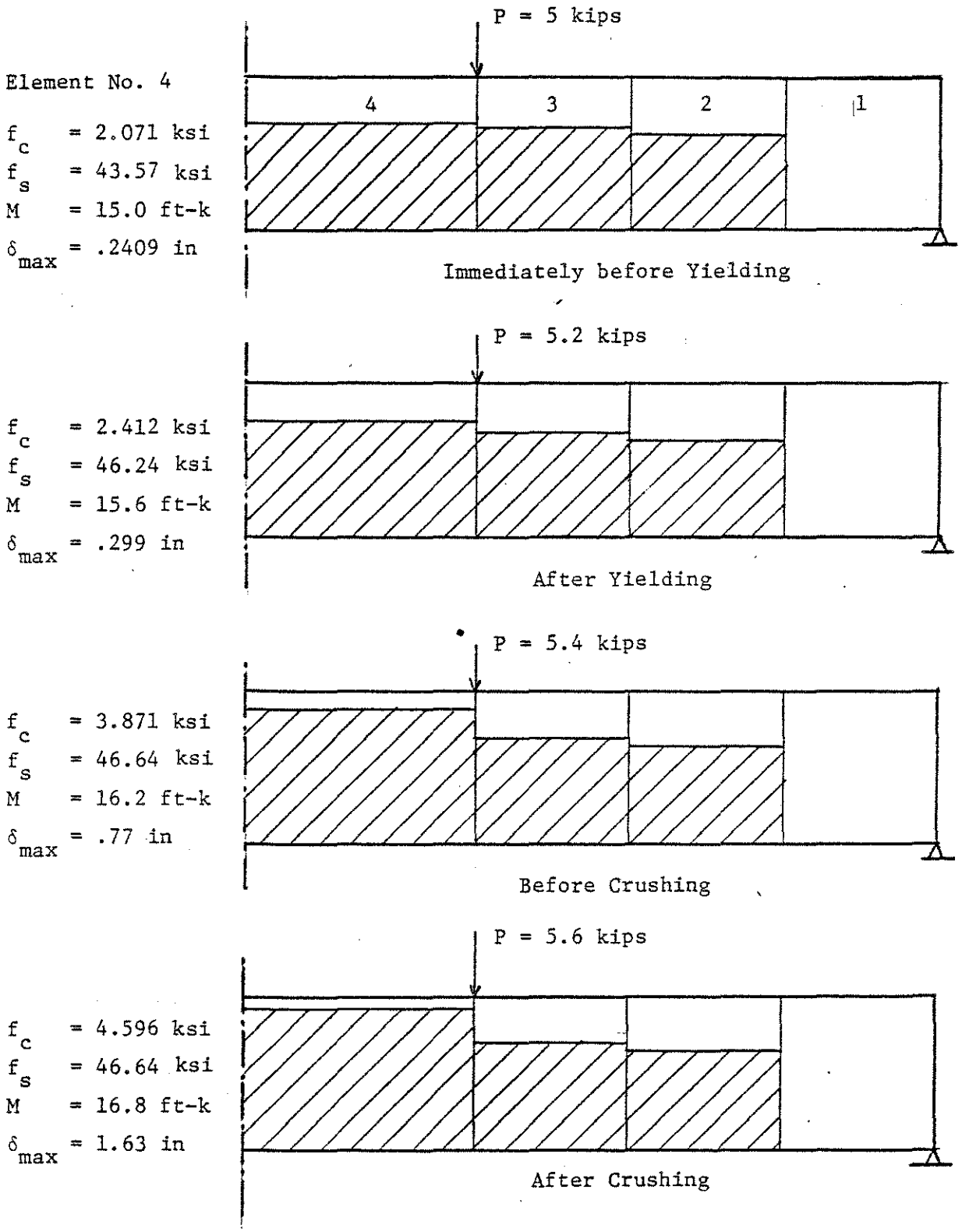

Fig. 4.3 Analytical Crack Depths for Beam T1MA

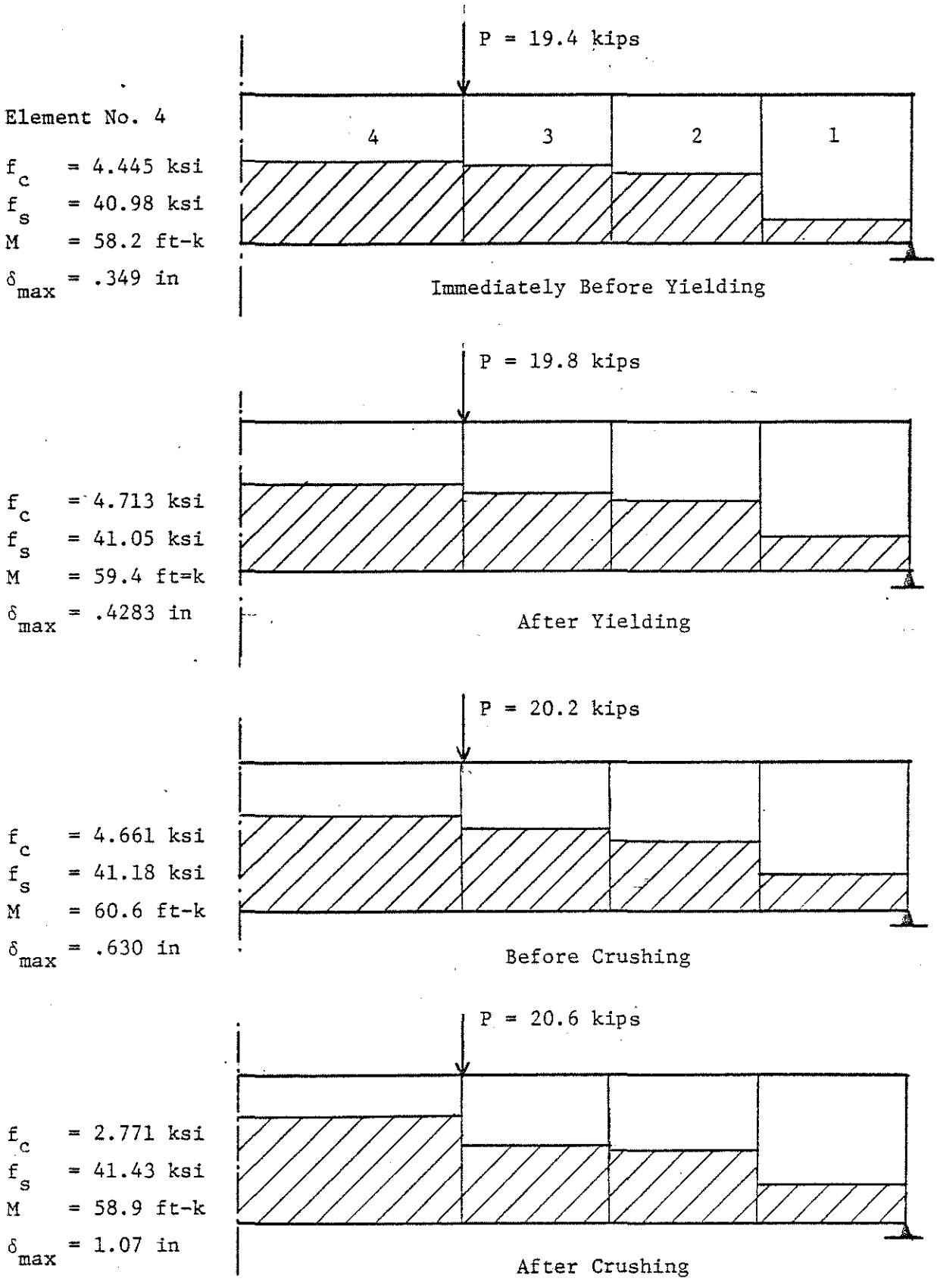

Fig. 4.4 Analytical Crack Depths for Beam T3MA

	B7	B10
f'_c	5150 psi	4920 psi
F_y	50000 psi	50000 psi
E_S	30×10^6 psi	30×10^6 psi

$\rho_x = \rho_y = 0.01$

$d_x = d_y = 3.64"$ (assumed)

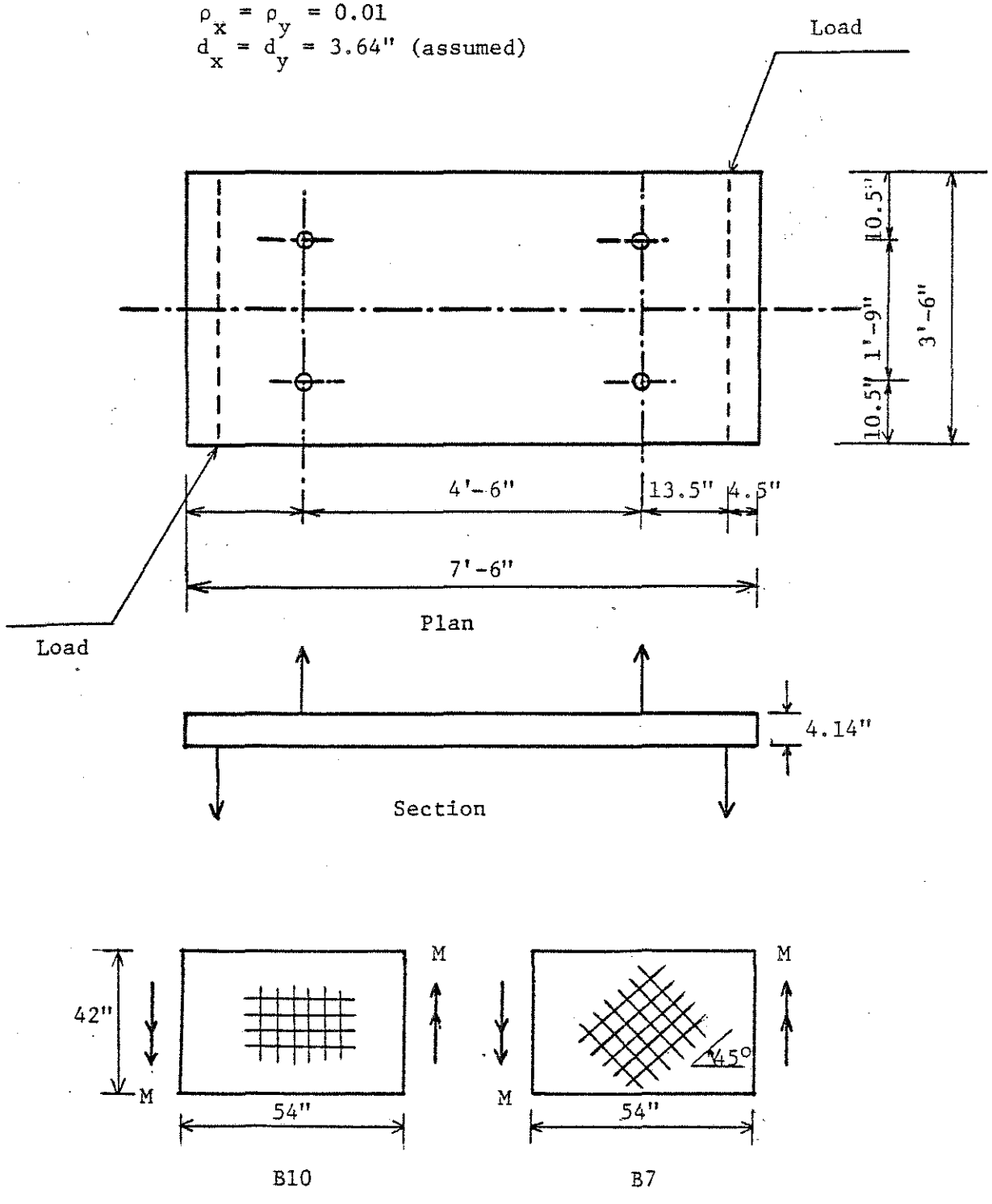

Fig. 4.5 Slab Test Specimens B10 and B7 (16)

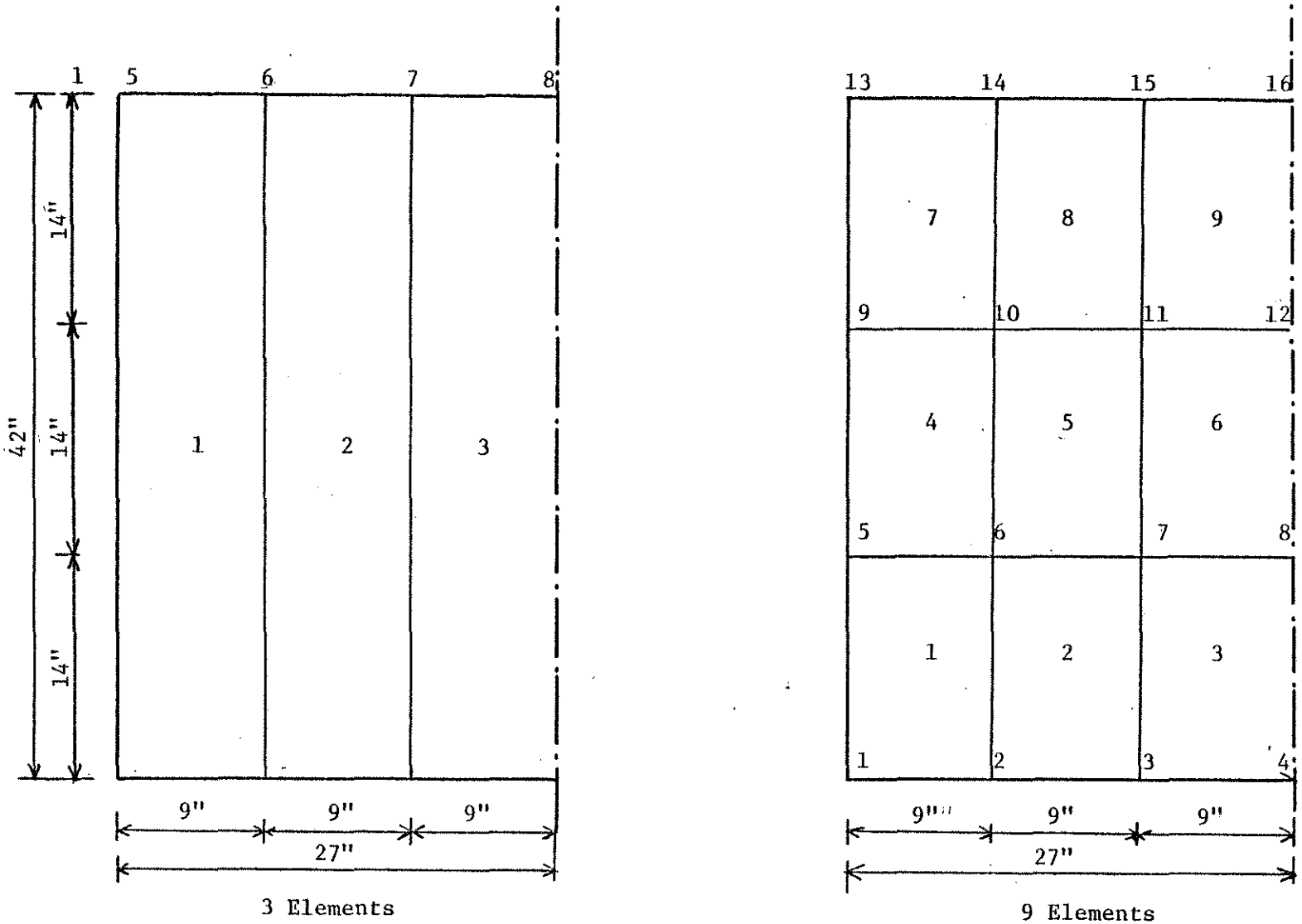

Fig. 4.6 Finite Element Models for Slabs B7 and B10

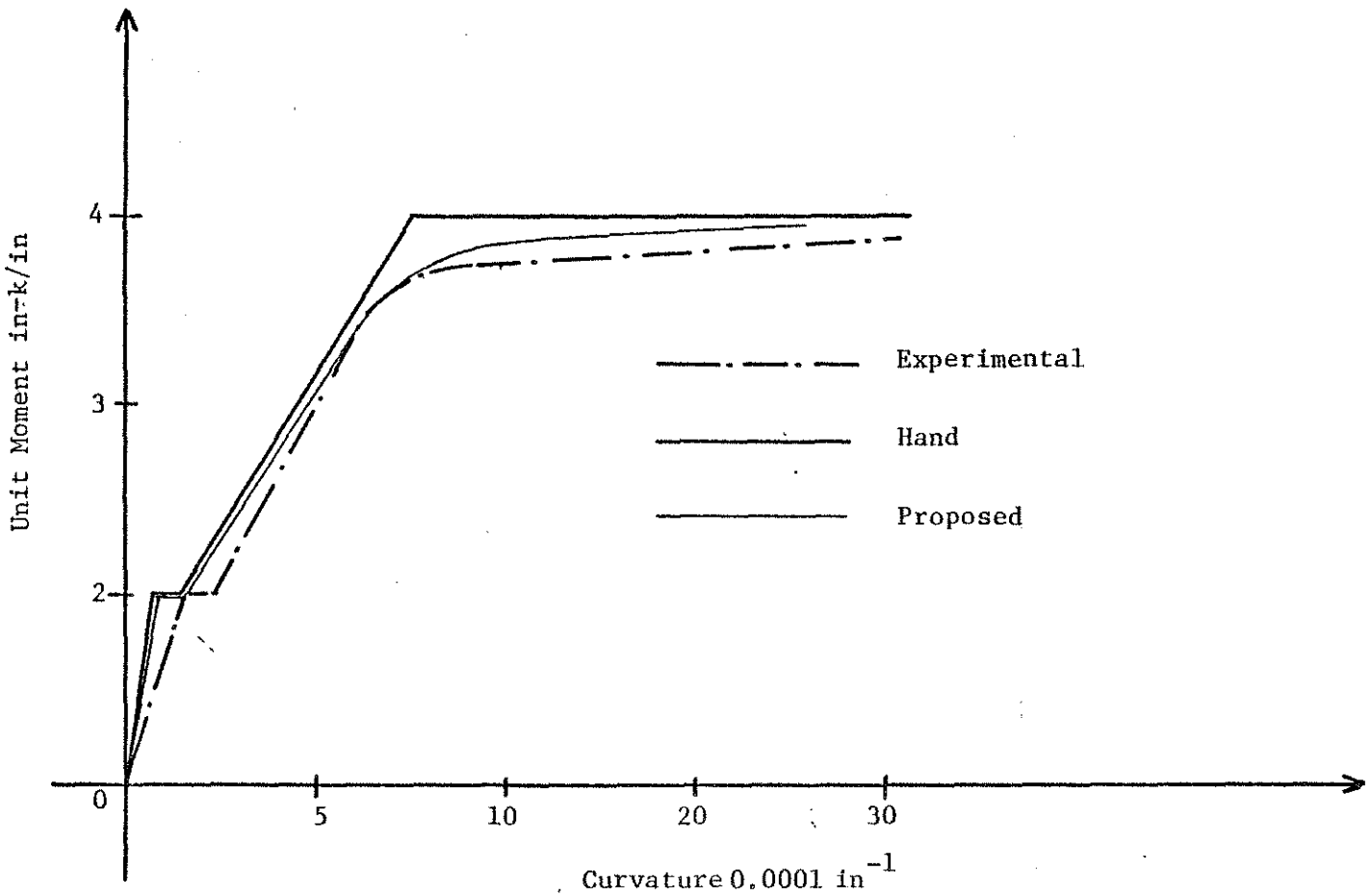

Fig. 4.7 Moment Versus Curvature Curves for Slab B10 (16,36)

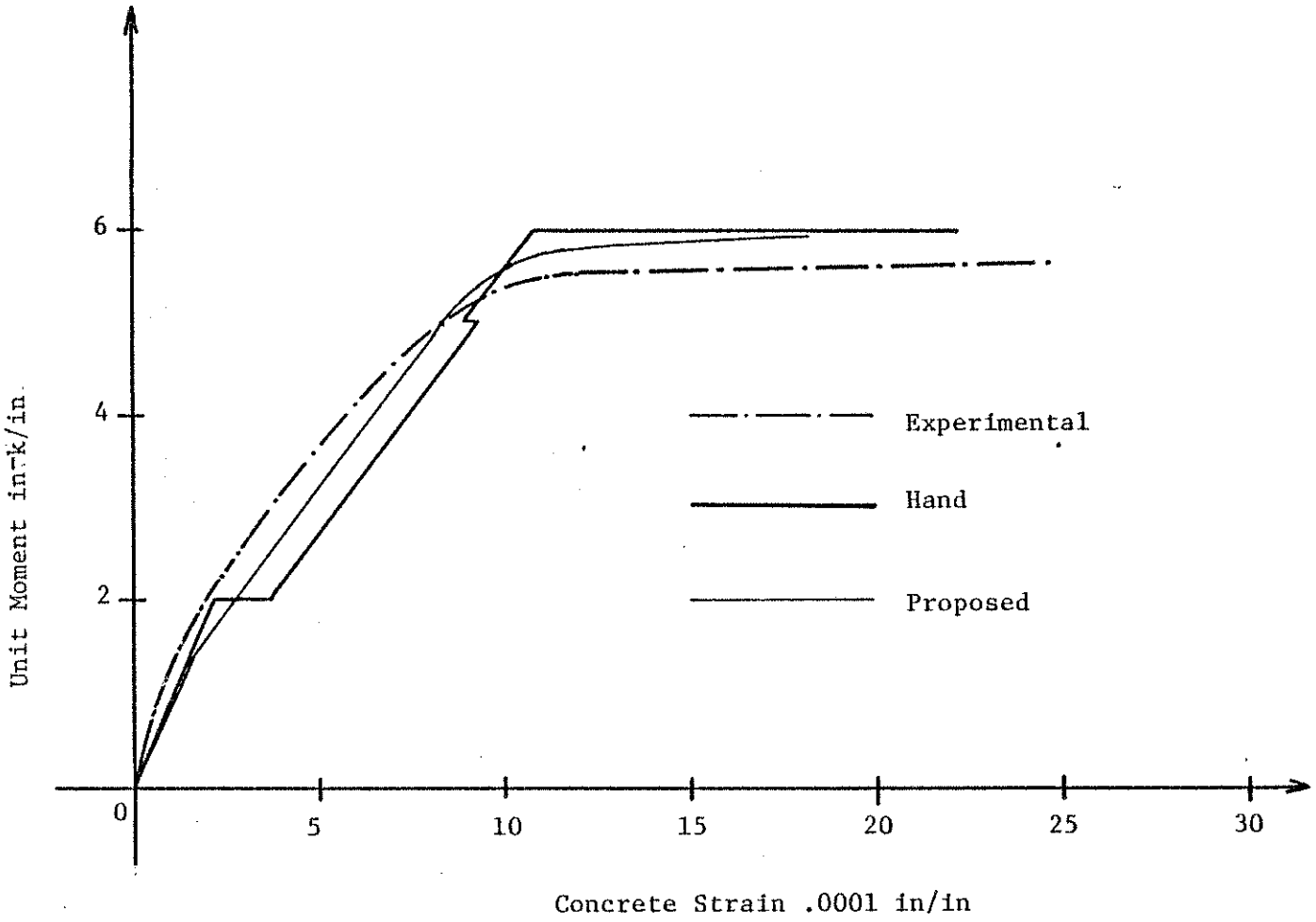

Fig. 4.8 Moment Versus Concrete Strain Curves for Slab B10 (16,36)

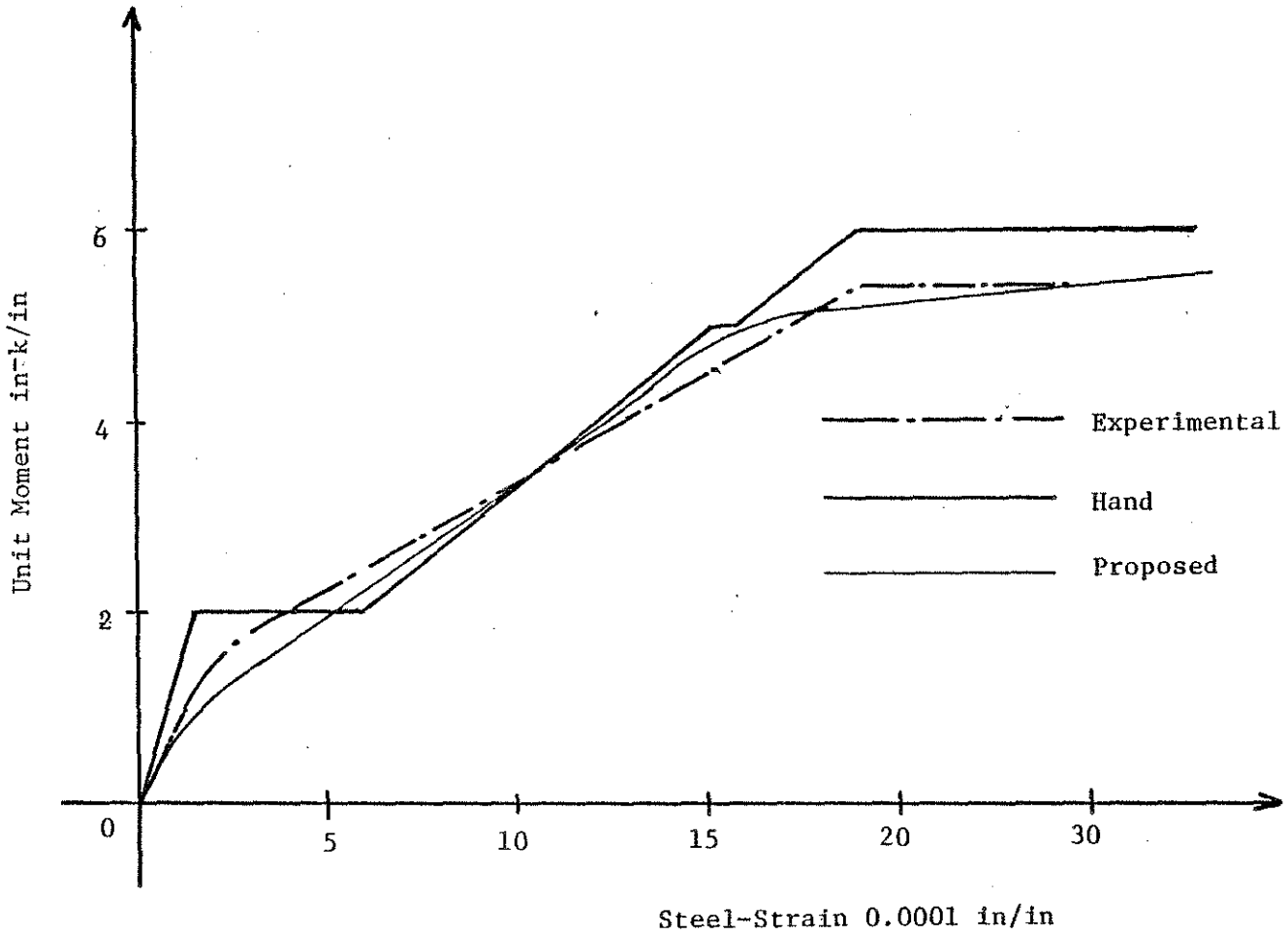

Fig. 4.9 Moment Versus Steel Strain Curves for Slab B10 (16,36)

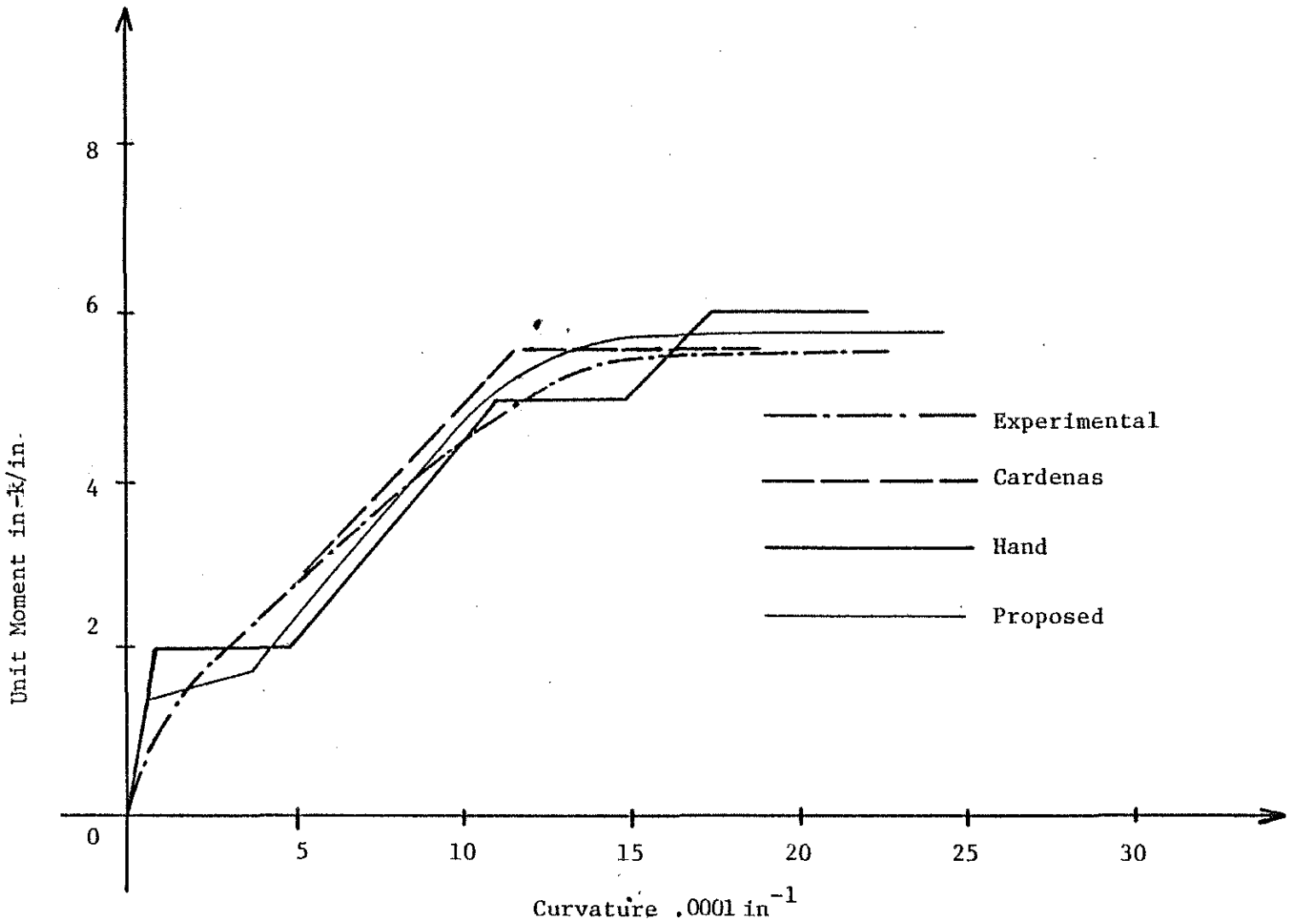

Fig. 4.10 Moment Versus Curvature Curves for Slab B7 (16,36)

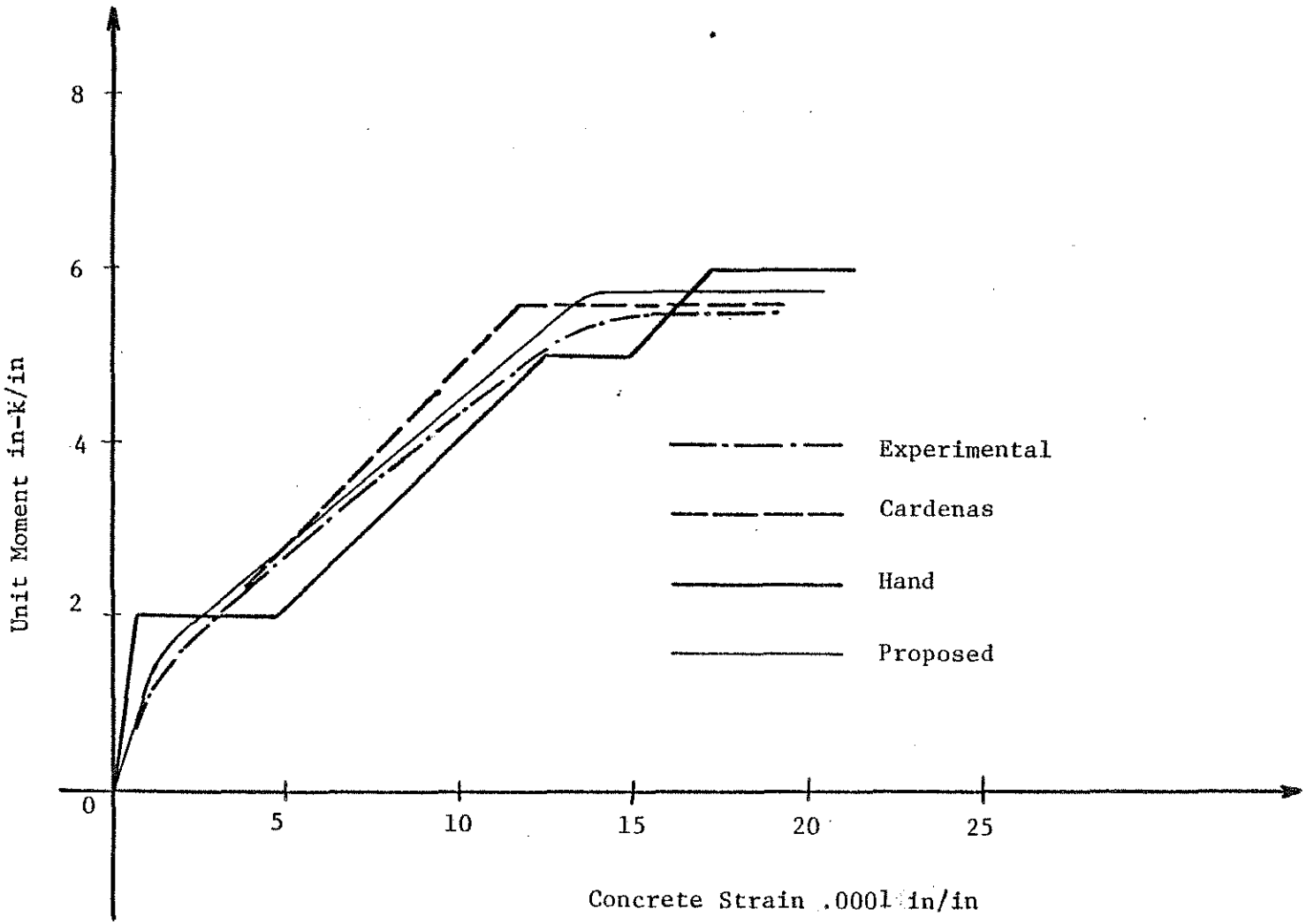

Fig. 4.11 Moment Versus Concrete Strain Curves for Slab B7 (16,36)

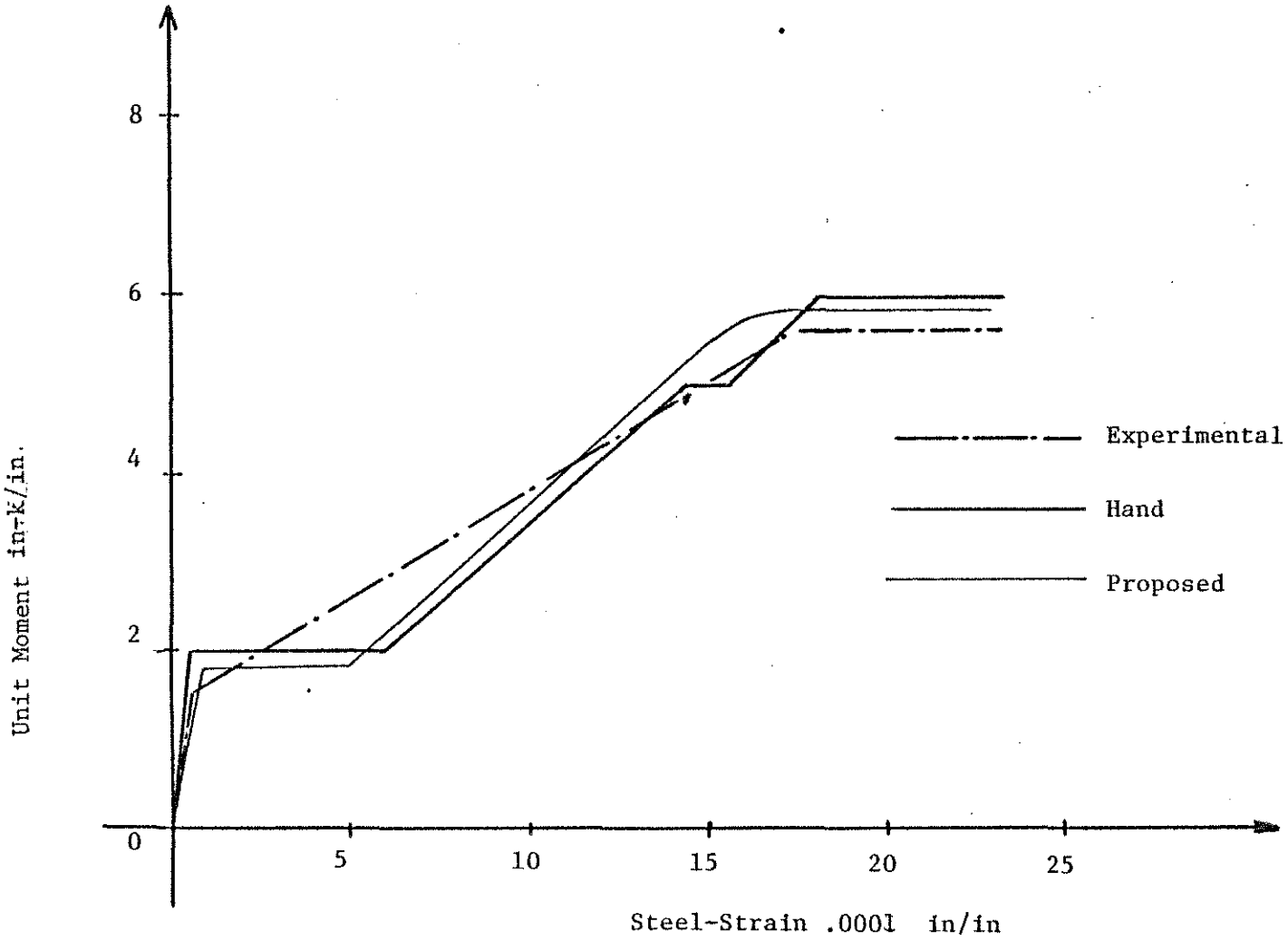

Fig. 4.12 Moment Versus Steel Strain Curves for Slab B7 (16,36)

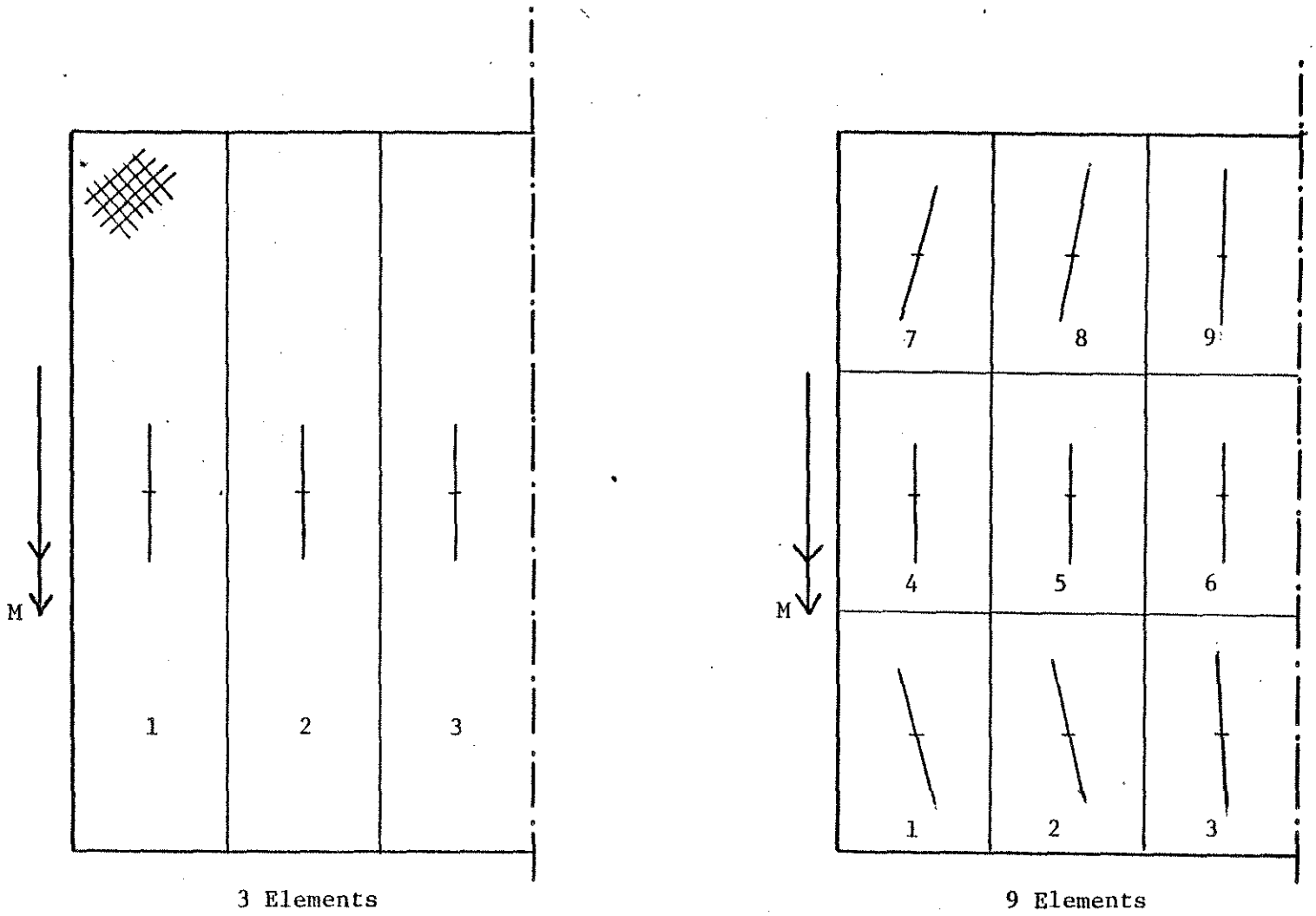

Fig. 4.13 Analytical Crack Patterns for Slab B7

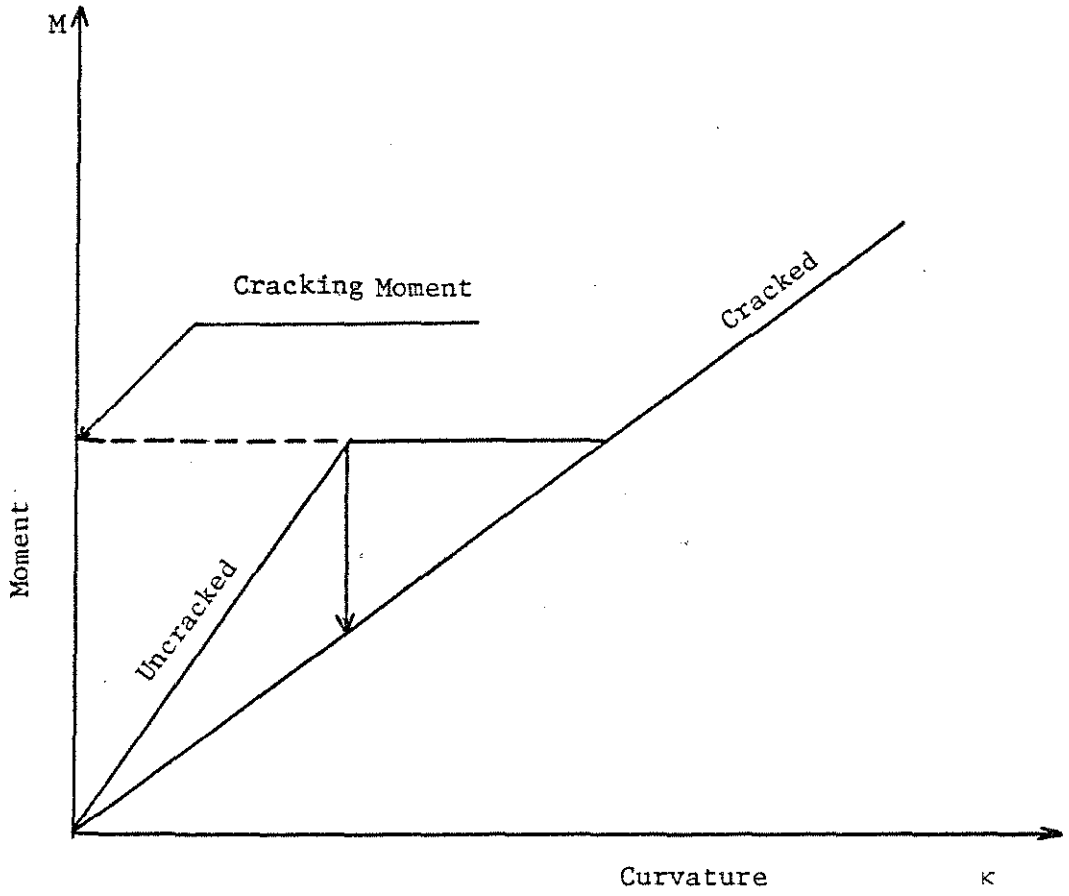

Fig. 4.14 Moment-Curvature Curves for Cracked and Uncracked Sections

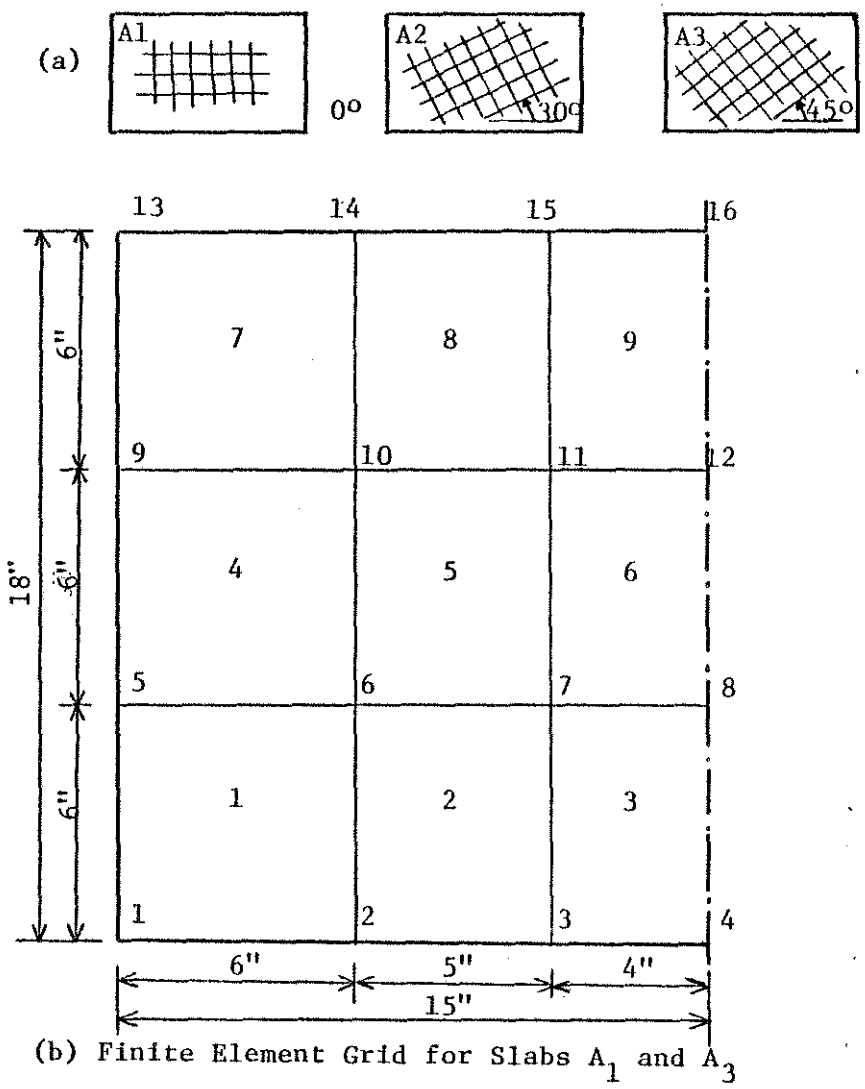

(b) Finite Element Grid for Slabs A_1 and A_3

Fig. 4.15 Slab Test Specimens A_1, A_2 and A_3 (44)

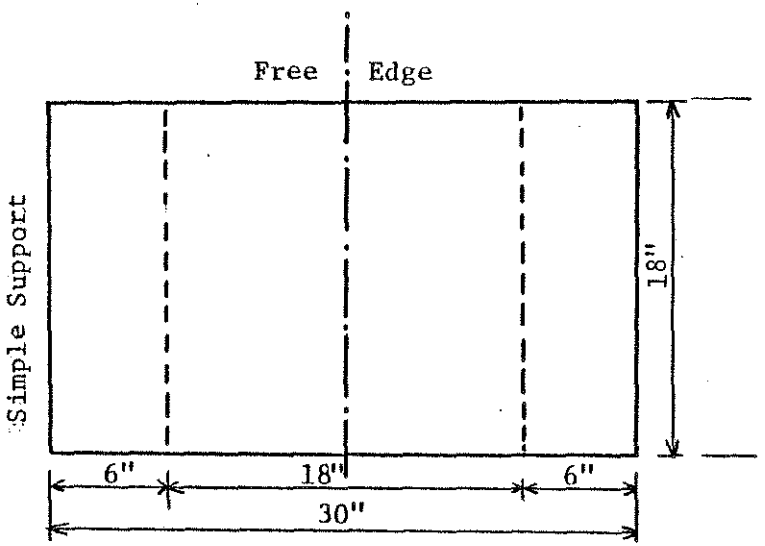

(c) Slabs Under Live Loads

	f'_c
A_1	4580
A_2	4430
A_3	4535

A_1, A_2, A_3

F_y = 32000 psi

H = 1.5"

ρ_x = 0.0085

ρ_y = 0.01137

ν = 0.2

d_x = 1.219"

d_y = 1.125"

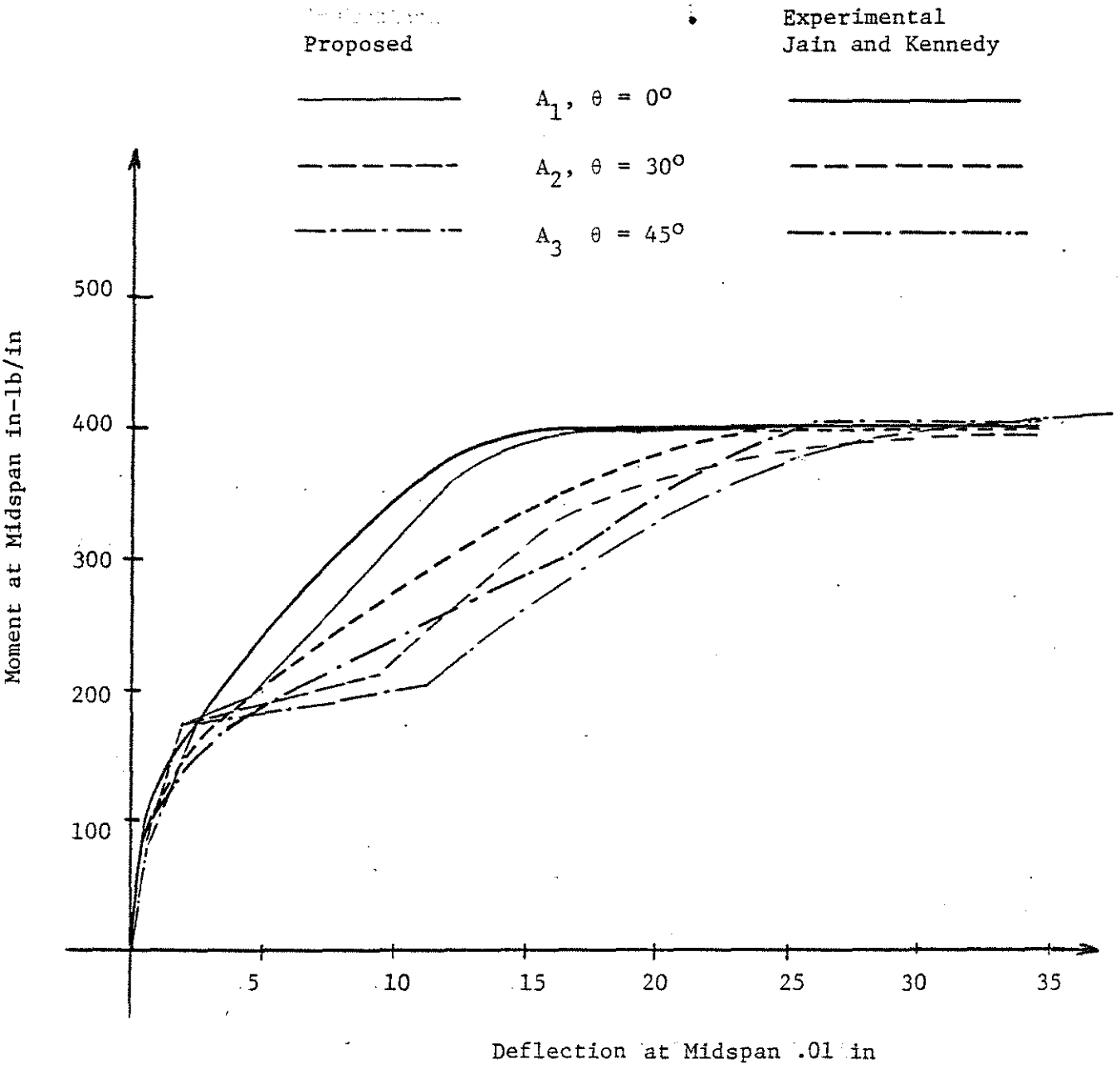

Fig. 4.16 Load Deflection Curves for Slabs A_1, A_2 and A_3 (44)

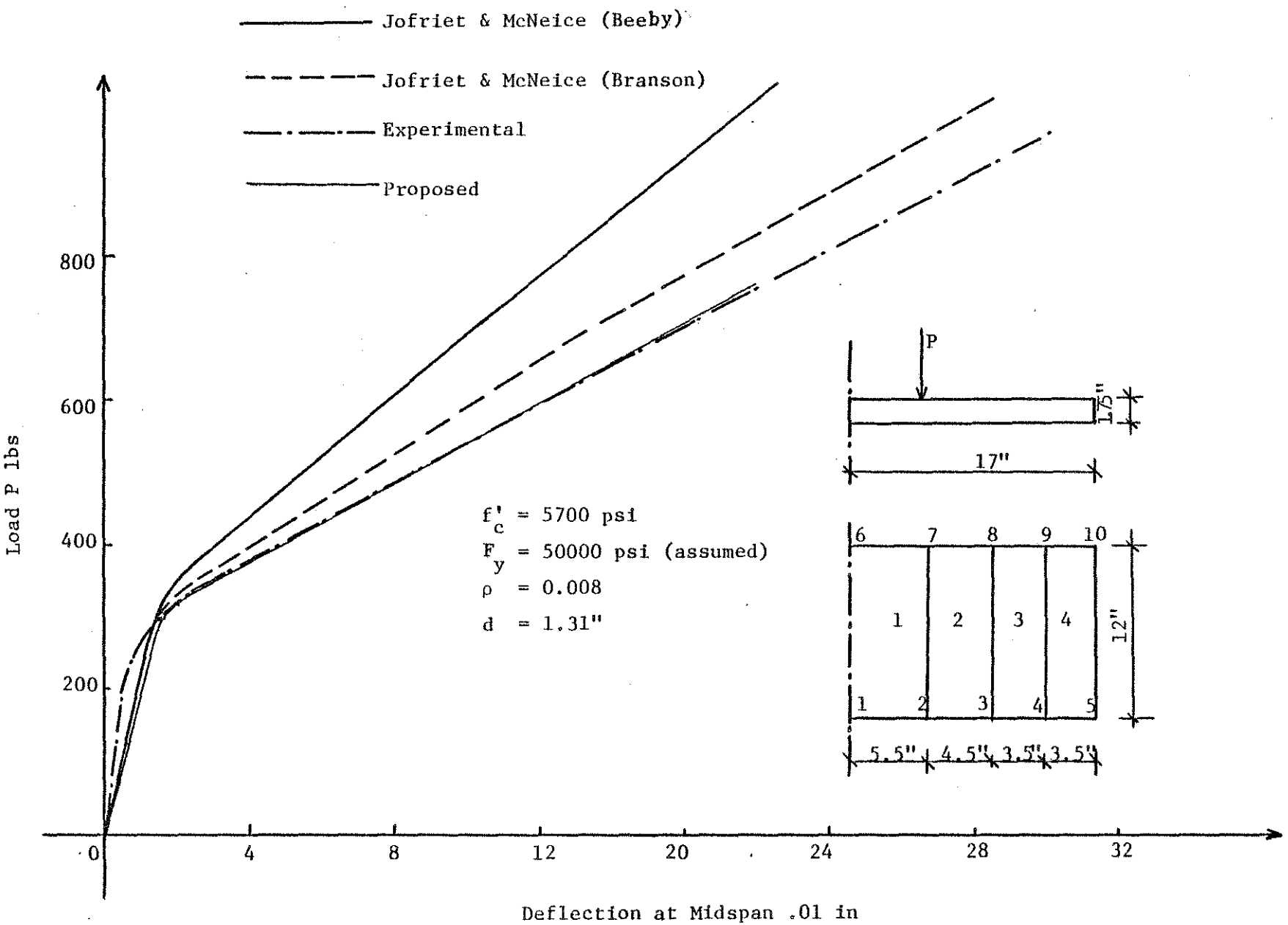

Fig. 4.17 Load Deflection Curvesfor One-Way Slab (45,59)

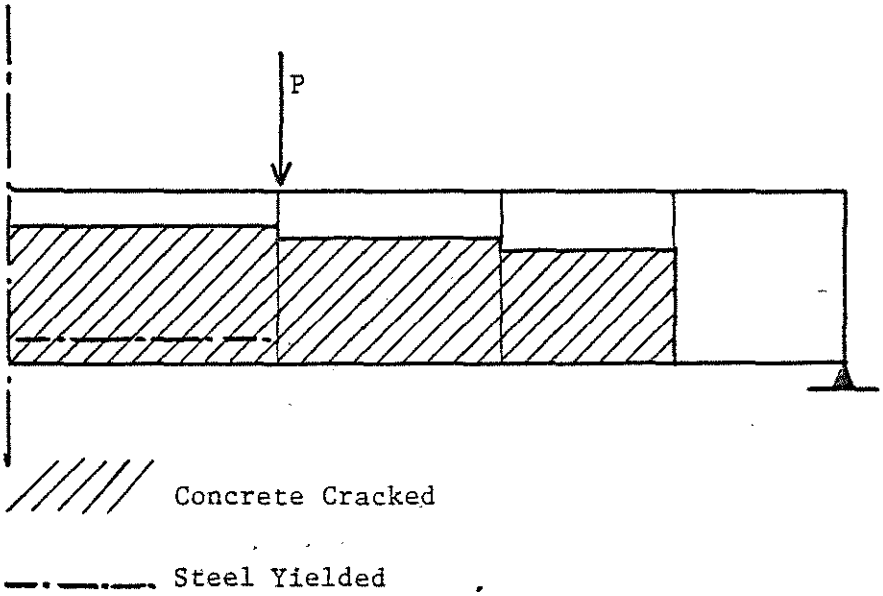

Fig. 4.18 Analytical Crack Depths for One-Way Slab

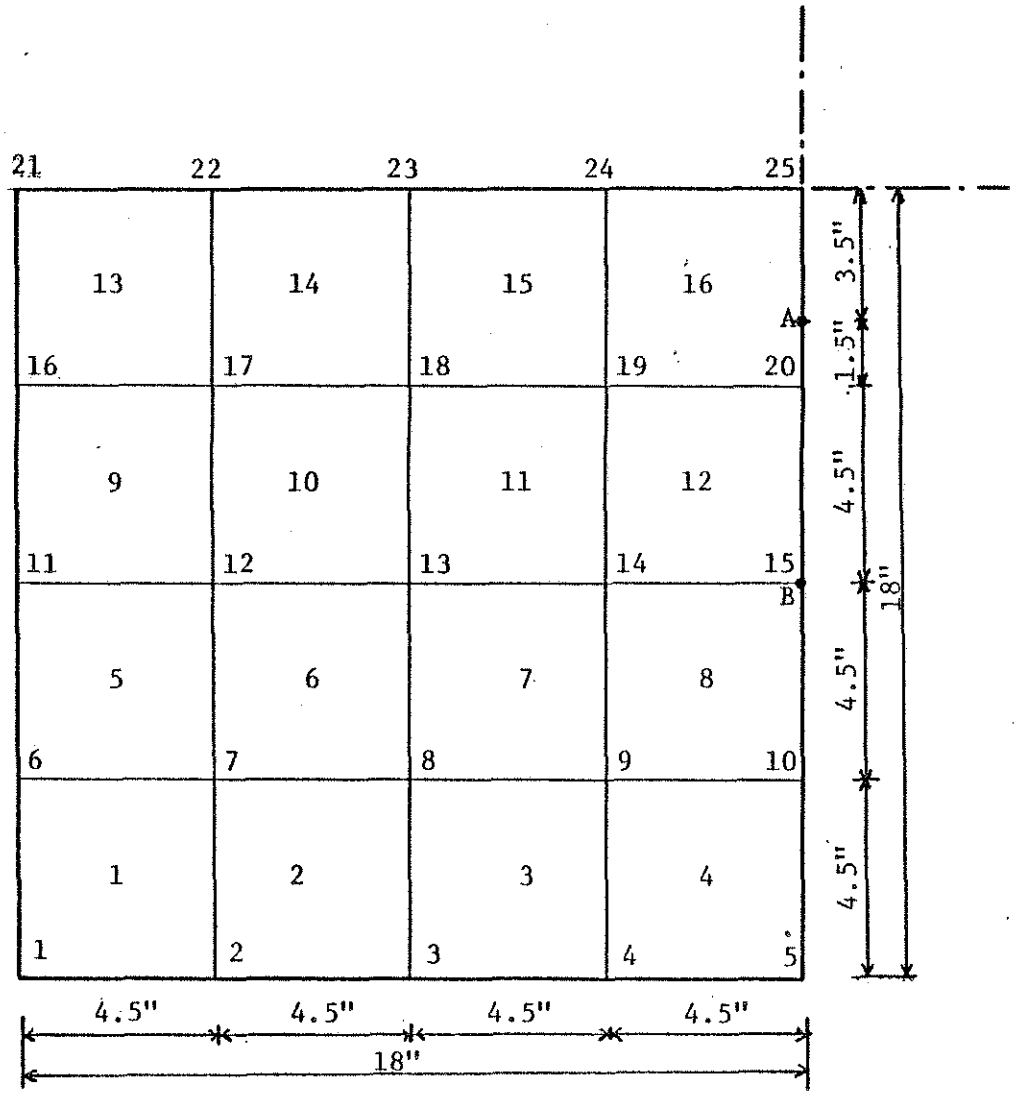

Finite Element Model

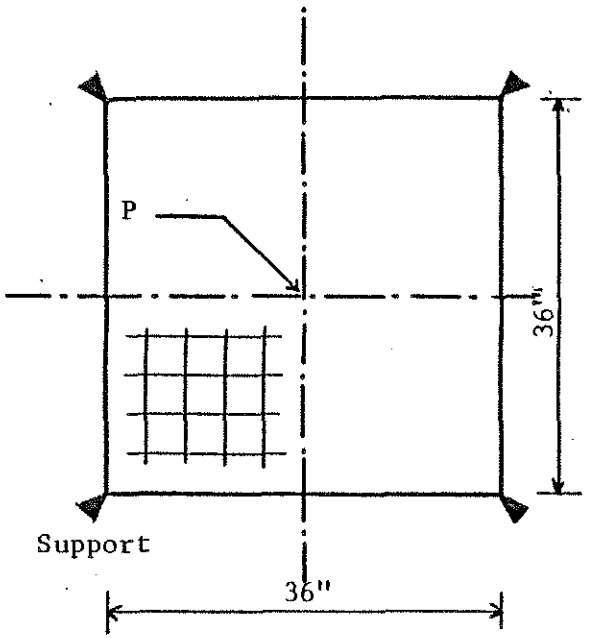

f'_c = 5500 psi

f_y = 50000 psi (assumed)

E_s = 29×10^6

ν = 0.15

$\rho_x = \rho_y$ = 0.0085

H = 1.75"

d = 1.31"

Fig. 4.19 Two-Way Slab Supported at Corners (45,59)

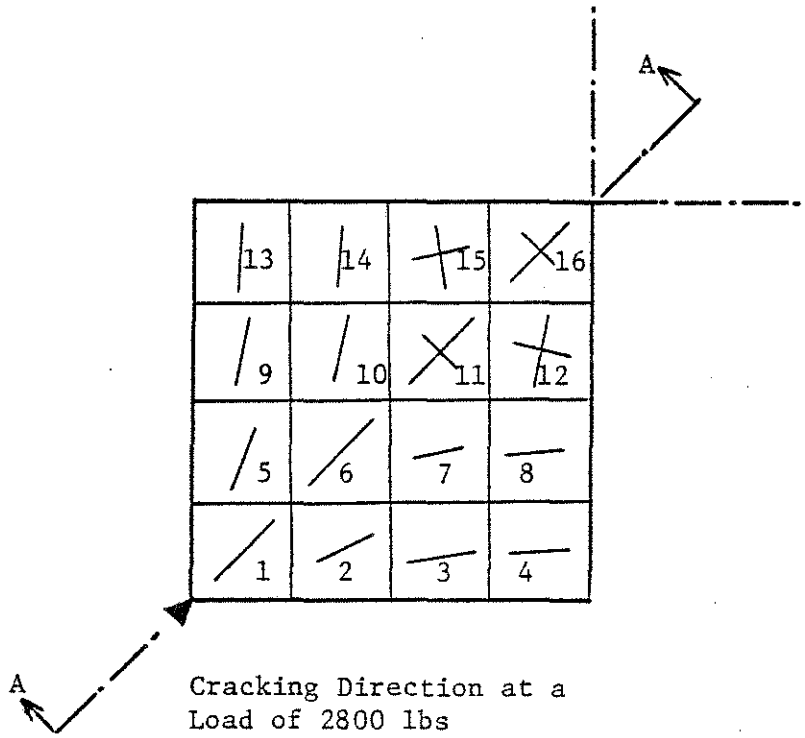

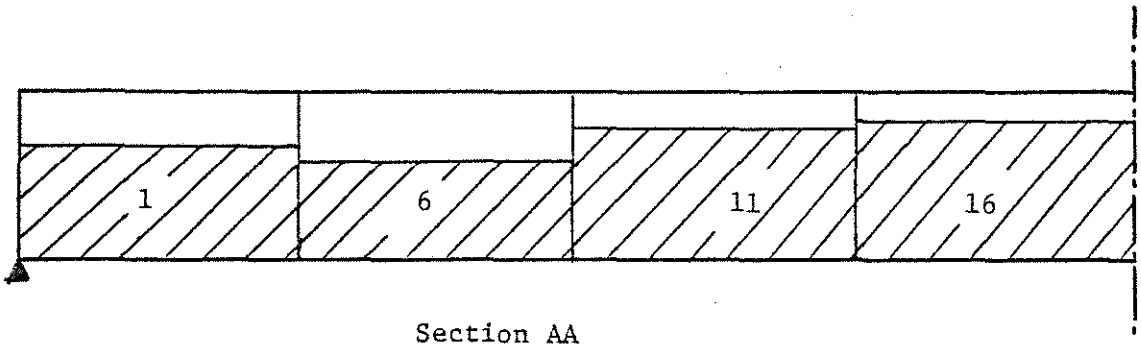

Fig. 4.20 Analytical Crack Configuration for Two-Way Slab, P = 2800 lbs

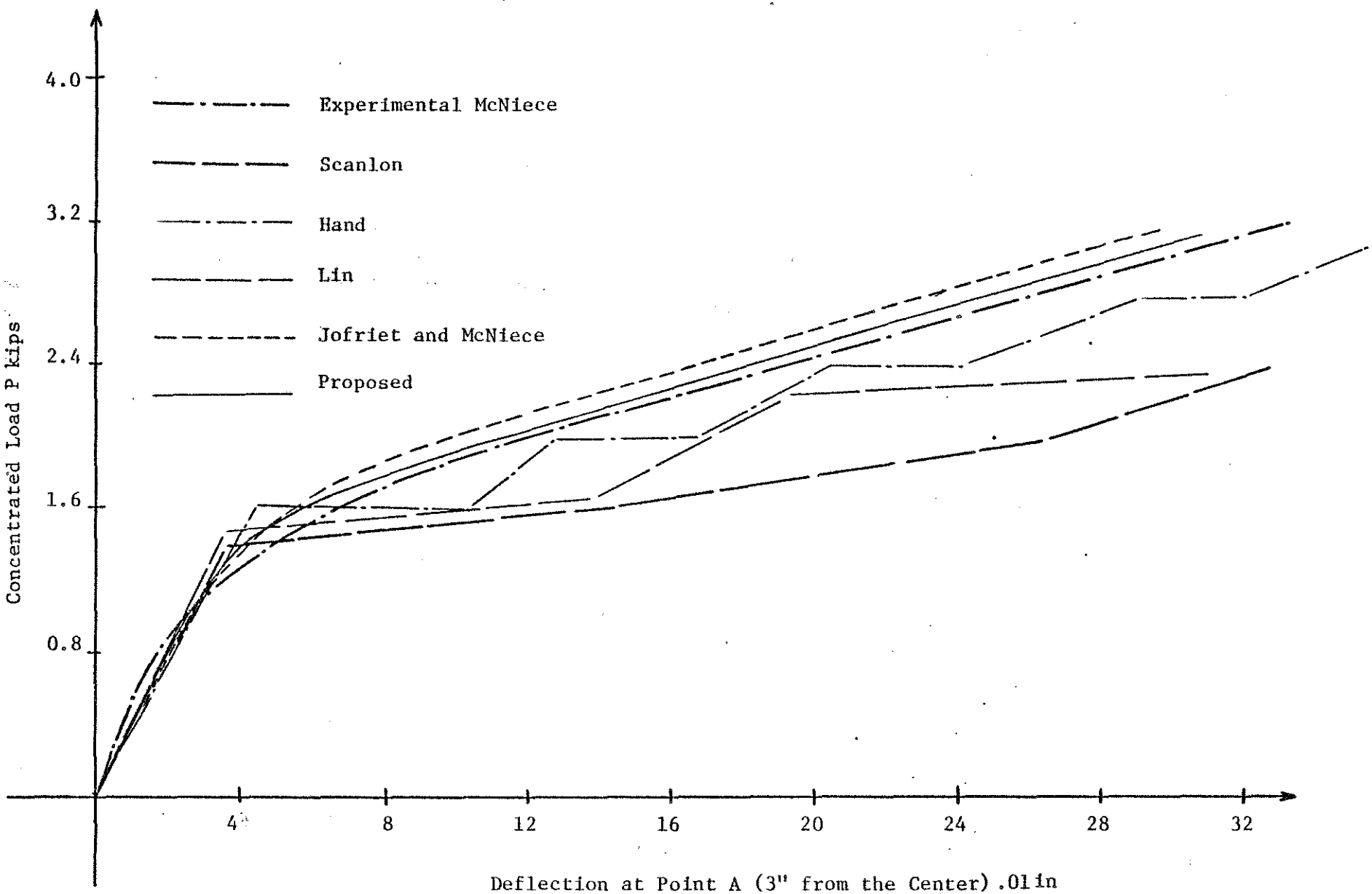

Fig. 4.21 Load-Deflection Curves for Two-Way Slab Supported at Corners, Point A (45,59)

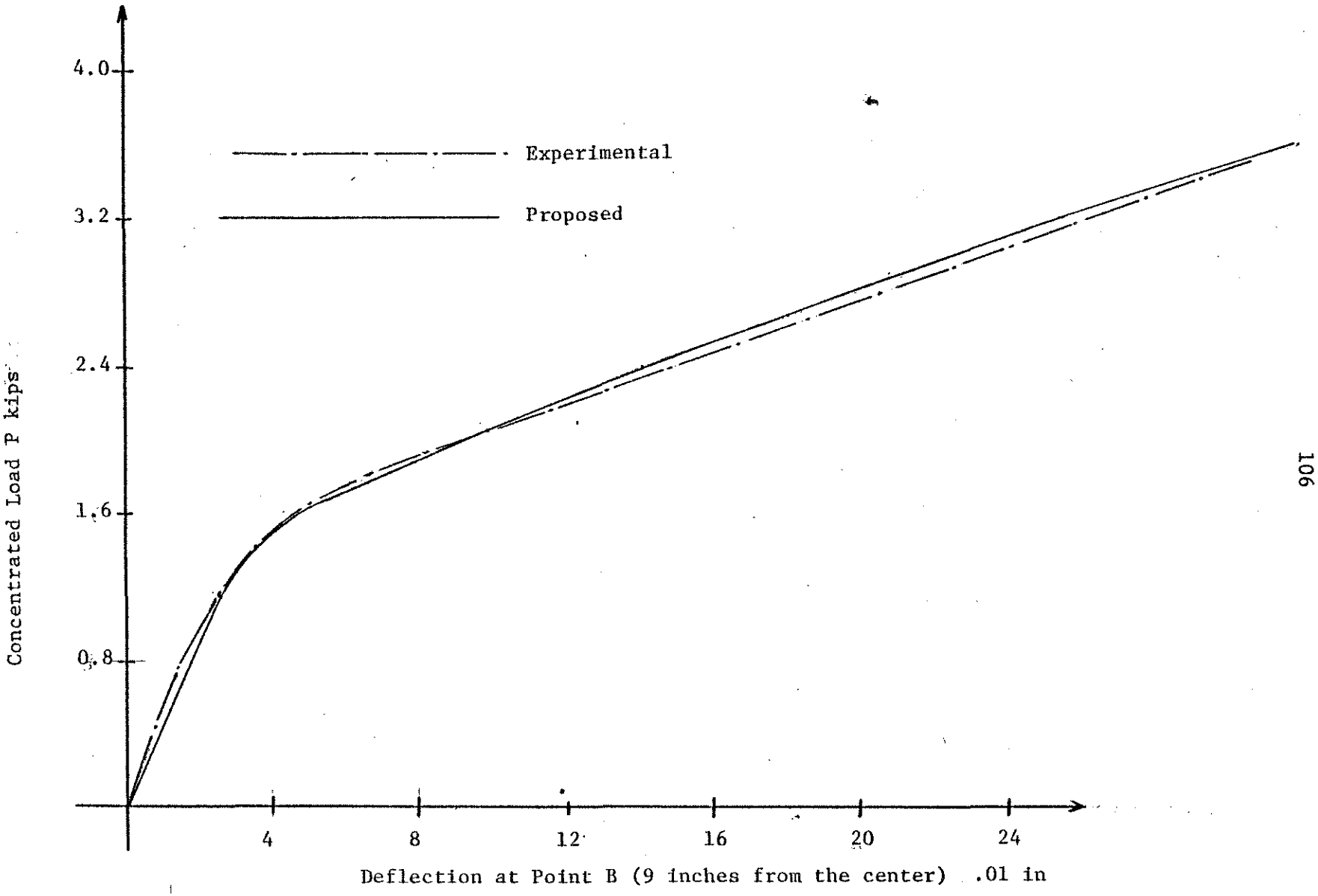

Fig. 4.22 Load Deflection Curves for Two-Way Slab Supported at Corners, Point B (45,59)

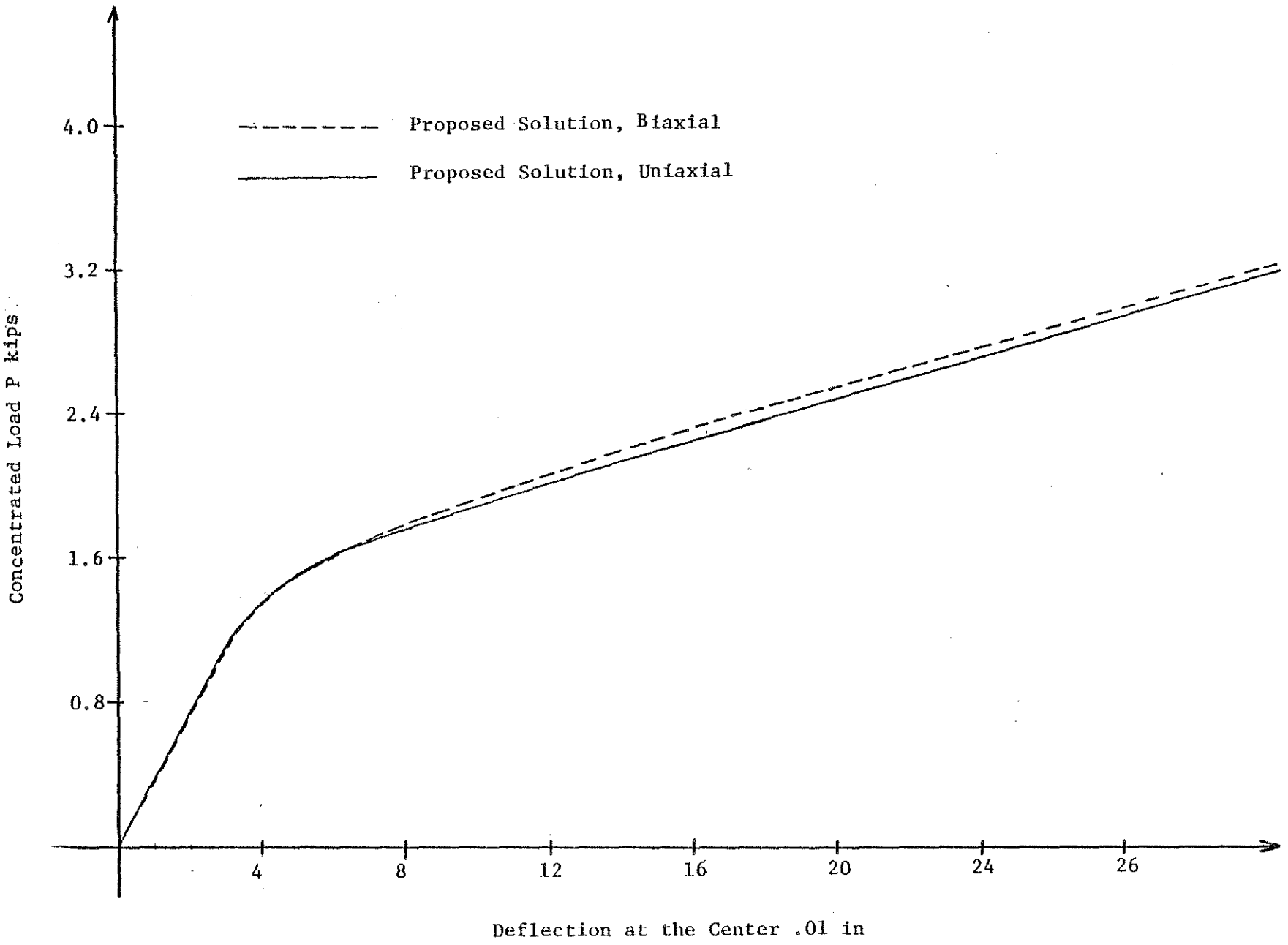

Fig. 4.23 Analytical Load Deflection Curves for Two-Way Slab Supported at Corners

Appendix A

PROPERTIES OF THE PLATE BENDING ELEMENT

A.1 The finite element used in this study is a compact rectangular plate bending element with sixteen degrees of freedom (Figs. A.1 and A.2):

$$\{\delta\}^e = \lfloor w_{11},\ w_{11,x},\ w_{11,y}\ \ w_{11,xy},\ w_{21},\ w_{21,x},\ w_{21,y},\ w_{21,xy},\ w_{22},\ w_{22,x},\ w_{22,y},\ w_{22,xy},\ w_{12},\ w_{12,x},\ w_{12,y},\ w_{12,xy} \rfloor^T \quad \text{(A.1)}$$

where:

$\{\delta\}^e$ = is the element displacement vector;

w_{ij} = is the deflection at the nodal point (i,j);

$w_{ij,x}$ = $-\frac{\partial w}{\partial x}$ at the nodal point (i,j);

$w_{ij,y}$ = $\frac{\partial w}{\partial y}$ at the nodal point (i,j); and

$w_{ij,xy}$ = $\frac{\partial w}{\partial x \partial y}$ at the nodal point (i,j).

Fig. A.2 shows the four displacements, at point (1,1). Corresponding to these nodal displacements, nodal forces consist of shearing forces and bending moments about the X and the Y axes at each node. They are represented by the following column vector;

* The superscript T implies a transposed matrix.

$$\{f\}^e = \left[F_{11},\ M_{11,y},\ M_{11,x},\ M_{11,xy},\ F_{21},\ M_{21,y},\ M_{21,x},\ M_{21,xy},\ F_{22},\ M_{22,y},\ M_{22,x},\ M_{22,xy},\ F_{12},\ M_{12,y},\ M_{12,x},\ M_{22,xy} \right]^T \tag{A.2}$$

where:

F_{ij} is the nodal force corresponding to the displacement w_{ij};

$M_{ij,y}$ is the nodal bending moment in the Y direction corresponding to $w_{ij,x}$;

$M_{ij,x}$ is the nodal bending moment in the X direction corresponding to $w_{ij,y}$; and

$M_{ij,xy}$ is the nodal twisting moment corresponding to $w_{ij,xy}$.

$i,j = 1,2$

The fourth nodal degree of freedom, $w_{ij,xy}$ is included to improve the convergence of the element. A similar element with twelve degrees of freedom, but without these twisting terms has proved to be non-convergent. This extra degree of freedom is permissible as it does not involve excessive continuity (98). The convergent property of the two rectangular elements is shown in Fig. A.3. The element used in this study was developed by Bogner, Fox and Schmit (11) and will be referred to as BFS element. Hermitian polynomials of the first order are used in developing the BFS element.

A.2 Hermitian Polynomials

Hermitian polynomials of the first-order are used to define the displacement functions in terms of the nodal displacements. The Hermitian polynomials $H_{mi}^{(n)}(x)$ are polynomials of order $(2n + 1)$ which have the following properties:

$$\left.\frac{H_{mi}^{(n)}(x)}{dx^K}\right|_{x = x_j} = \delta_{ij} \quad \text{if } K = m,\ m = 0,n \tag{A.3}$$

and

$$\left.\frac{d^K H_{mi}^{(n)}(x)}{dx^K}\right|_{x = x_j} = 0 \text{ if } K \neq m$$

where:

n is the number of derivatives that the set can interpolate;

K is the order of derivative, between zero and n;

x_j is the value of the argument x at j; and

δ_{ij} is the Kronecker delta:

$$\delta_{ij} = \begin{cases} 0 & \text{if } i \neq j \\ 1 & \text{if } i = j \end{cases} \tag{A.4}$$

A set of first order Hermitian polynomials which satisfies these properties are:

$$H_{01}^{(1)}(x) = \frac{1}{a^3}(2x^3 - 2ax^2 + a^3)$$

$$H_{02}^{(1)}(x) = \frac{-1}{a^3}(2x^3 - 3ax^2) \qquad (A.5)$$

$$H_{11}^{(1)}(x) = \frac{1}{a^2}(x^3 - 2a^2 + a^2x)$$

$$H_{12}^{(1)}(x) = \frac{1}{a^2}(x^3 - ax^2)$$

These functions are known as osculatory polynominals, and are shown in Fig. A.4. They interpolate the displacement functions for an element. The values of the functions and their first derivatives are used as variables.

The displacement function proposed by Bogner, Fox and Schmit (11) is:

$$w(x,y) = \sum_{i=1}^{2} \sum_{j=1}^{2} \Big[H_{0i}^{(1)}(x)\, H_{0j}^{(1)}(y)\, w_{ij} + H_{1i}^{(1)}(x)\, H_{0j}^{(1)}(y)\, w_{ij,x} + H_{0i}^{(1)}(x)\, H_{1j}^{(1)}(y)\, w_{ij,y} + H_{1i}^{(1)}(x)\, H_{1J}^{(1)}(y)\, w_{ij,xy} \Big] \qquad (A.6)$$

where:

w_{ij}, $w_{ij,x}$, $w_{ij,y}$ and $w_{ij,xy}$ are the displacements at nodal point (i,j) as defined above and $H_{0i}^{(1)}(x)$, $H_{0j}^{(1)}(y)$, $H_{1i}^{(1)}(x)$ and $H_{1j}^{(1)}(y)$

are given in Eq. (A.5).

These functions satisfy compatibility of slope and deflection along the boundaries of the element. Eq. (A.6) can be written as:

$$w = [N] \quad \{\delta\} \tag{A.7}$$

where:

$[N]$ contains the shape functions; and

$\{\delta\}$ is the nodal displacement vector.

A.3 Formulation of Plate Bending Problem

For completeness and clearity of the analysis introduced in Chapter 3, the following summary of the formulation of the plate bending problem is given:

The incremental changes in curvature and bending moment for an element in an incrementally linear, anisotropic plate, are given in terms of displacements by:

$$\{\Delta\kappa\}^e = [B]\{\Delta\delta\}^e \tag{A.8}$$

$$\{\Delta M\}^e = [D][B]\{\Delta\delta\}^e \tag{A.9}$$

where:

$$B_i = -\begin{Bmatrix} \dfrac{\partial^2 N_i}{\partial x^2} \\ \dfrac{\partial^2 N_i}{\partial y^2} \\ \dfrac{2\partial^2 N_i}{\partial x \partial y} \end{Bmatrix} \qquad i = 1,4 \tag{A.10}$$

and:

$$D = \begin{bmatrix} D_{11} & D_{12} & D_{13} \\ & D_{22} & D_{23} \\ \text{Sym.} & & D_{33} \end{bmatrix} \tag{A.11}$$

By minimizing the total potential energy, the following are obtained for each element, (A.12), and for the whole structure, (A.13):

$$\{\Delta f\}^e = [k]\ \{\Delta\delta\}^e \tag{A.12}$$

$$\{\Delta f\} = [K]\ \{\Delta\delta\} \tag{A.13}$$

where:

$$[k] = \iint_A [B]^T\ [D][B]\ dxdy \tag{A.14}$$

$$[K] = \Sigma\ [k] \tag{A.15}$$

$[k]$ is the element stiffness matrix;

$[K]$ is the stiffness matrix for the structure; and

$\{\Delta f\}$ is the change in load vector at nodal points.

The nodal forces due to distributed loads are:

$$\{f\}_q = -\iint_A [N]^T\{q\}\ dxdy \tag{A.16}$$

Those due to initial curvatures are:

$$\{\Delta f\}_{\kappa_o} = -\iint_A [\beta]^T[D]\{\Delta\kappa_o\}\ dxdy \tag{A.17}$$

And for initial moments are:

$$\{\Delta f\}_{M_o} = \iint_A [\beta]^T\{\Delta M_o\}\ dxdy \tag{A.18}$$

The solution of the nonlinear bending problem is reduced to the solution of the following algorithm:

$$\{\Delta\delta\} = [K]^{-1} \{\Delta f\} \tag{A.19}$$

The total nodal displacements are:

$$\{\delta\} \quad \underset{\text{load increment}}{\Sigma} \quad \{\Delta\delta\} \tag{A.20}$$

The element stiffness formulation is presented in Section (A.4).

A.4 The Element Stiffness Matrix

In this study, the BFS element is extended to cover anisotropic plates. The derivation of the stiffness matrix for the anisotropic case is described below.

The stiffness matrix for an element is:

$$[k]_{16x16} = \iint_A [B]^T [D][B]\, dxdy \tag{A.14}$$

By substituting $[B]^T$, $[D]$ and $[B]$, using Eqs. (A.5), (A.6), (A.10) and (A.11) in (A.15) and integrating term by term, the following stiffness matrix, which is the sum of six matrices, is obtained:

$$\begin{aligned} k(i,j) = \frac{1}{ab}\Big[& k_{11}(i,j)D_{11}\left(\frac{b}{a}\right)^2 + k_{22}(i,j)D_{22}\left(\frac{a}{b}\right)^2 + \\ & k_{33}(i,j)D_{33} + k_{12}(i,j)D_{12} + \\ & k_{13}(,j)D_{13}\left(\frac{b}{a}\right) + \\ & k_{23}(i,j)D_{23}\left(\frac{a}{b}\right)\Big] a\overline{col}(i,j)_b\overline{co2}(i,j) \end{aligned} \tag{A.21}$$

The values of $k_{11}(i,j)$, $k_{22}(i,j)$, $k_{33}(i,j)$, $k_{12}(i,j)$, $k_{13}(i,j)$, $k_{23}(i,j)$, col(i,j) and co2(i,j) are presented in Tables A.1 to A.8. D_{11}, D_{12}, D_{13}, D_{22}, D_{23}, and D_{33} are the flexural and torsional stiffnesses give in Eqs. (2.32) and (2.44). a and b are the element dimensions.

A.5 Moments and Curvatures

The B matrix at the centroid of the element, where the moments and curvatures are evaluated, is presented in Table A.10. Although not used in this study, the B matrix, evaluated at the nodal points, is provided for completeness and shown in Table A.11.

$\frac{156}{35}$	$\frac{78}{35}$	$\frac{22}{35}$	$\frac{11}{35}$	$\frac{-156}{35}$	$\frac{78}{35}$	$\frac{-22}{35}$	$\frac{11}{35}$	$\frac{-54}{35}$	$\frac{27}{35}$	$\frac{13}{35}$	$\frac{-13}{70}$	$\frac{54}{35}$	$\frac{27}{35}$	$\frac{-13}{35}$	$\frac{-13}{70}$
	$\frac{52}{35}$	$\frac{11}{35}$	$\frac{22}{105}$	$\frac{-78}{35}$	$\frac{26}{35}$	$\frac{-11}{35}$	$\frac{11}{105}$	$\frac{-27}{35}$	$\frac{9}{35}$	$\frac{13}{70}$	$\frac{-13}{210}$	$\frac{27}{35}$	$\frac{18}{35}$	$\frac{-13}{70}$	$\frac{-13}{105}$
		$\frac{4}{35}$	$\frac{2}{35}$	$\frac{-22}{35}$	$\frac{11}{35}$	$\frac{-4}{35}$	$\frac{2}{35}$	$\frac{-13}{35}$	$\frac{13}{70}$	$\frac{3}{35}$	$\frac{-3}{70}$	$\frac{13}{35}$	$\frac{13}{70}$	$\frac{-3}{35}$	$\frac{-3}{70}$
			$\frac{4}{105}$	$\frac{-11}{35}$	$\frac{11}{105}$	$\frac{-2}{35}$	$\frac{2}{105}$	$\frac{-13}{70}$	$\frac{13}{210}$	$\frac{3}{70}$	$\frac{-1}{70}$	$\frac{13}{70}$	$\frac{13}{105}$	$\frac{-3}{70}$	$\frac{-1}{35}$
				$\frac{156}{35}$	$\frac{-78}{35}$	$\frac{22}{35}$	$\frac{-11}{35}$	$\frac{54}{35}$	$\frac{-27}{35}$	$\frac{-13}{35}$	$\frac{13}{70}$	$\frac{-54}{35}$	$\frac{-27}{35}$	$\frac{13}{35}$	$\frac{13}{70}$
					$\frac{52}{35}$	$\frac{-11}{35}$	$\frac{22}{105}$	$\frac{-27}{35}$	$\frac{18}{35}$	$\frac{13}{70}$	$\frac{-13}{105}$	$\frac{27}{35}$	$\frac{9}{35}$	$\frac{-13}{70}$	$\frac{-13}{210}$
						$\frac{4}{35}$	$\frac{-2}{35}$	$\frac{13}{35}$	$\frac{-13}{70}$	$\frac{-3}{35}$	$\frac{3}{70}$	$\frac{-13}{35}$	$\frac{-13}{70}$	$\frac{3}{35}$	$\frac{3}{70}$
							$\frac{4}{105}$	$\frac{-13}{70}$	$\frac{13}{105}$	$\frac{3}{70}$	$\frac{-1}{35}$	$\frac{13}{70}$	$\frac{13}{210}$	$\frac{-3}{70}$	$\frac{-1}{70}$
								$\frac{156}{35}$	$\frac{-78}{35}$	$\frac{-22}{35}$	$\frac{11}{35}$	$\frac{-156}{35}$	$\frac{-78}{35}$	$\frac{22}{35}$	$\frac{11}{35}$
									$\frac{52}{35}$	$\frac{11}{35}$	$\frac{-22}{105}$	$\frac{78}{35}$	$\frac{26}{35}$	$\frac{-11}{25}$	$\frac{-11}{105}$
										$\frac{4}{35}$	$\frac{-2}{35}$	$\frac{22}{35}$	$\frac{11}{35}$	$\frac{-4}{35}$	$\frac{-2}{35}$
											$\frac{4}{105}$	$\frac{-11}{35}$	$\frac{-11}{105}$	$\frac{2}{35}$	$\frac{2}{105}$
												$\frac{156}{35}$	$\frac{78}{35}$	$\frac{-22}{35}$	$\frac{-11}{35}$
													$\frac{52}{35}$	$\frac{-11}{35}$	$\frac{-22}{105}$
														$\frac{4}{35}$	$\frac{2}{35}$
Sym.															$\frac{4}{105}$

TABLE A.1 Values $k_{11}(i,j)$ of the stiffness matrix, Eq. A.21.

$\frac{156}{35}$	$\frac{22}{35}$	$\frac{78}{35}$	$\frac{11}{35}$	$\frac{54}{35}$	$\frac{-13}{35}$	$\frac{27}{35}$	$\frac{-13}{70}$	$\frac{-54}{35}$	$\frac{13}{35}$	$\frac{27}{35}$	$\frac{-13}{70}$	$\frac{-156}{35}$	$\frac{-22}{35}$	$\frac{78}{35}$	$\frac{11}{35}$
	$\frac{4}{35}$	$\frac{11}{35}$	$\frac{2}{35}$	$\frac{13}{35}$	$\frac{-3}{35}$	$\frac{13}{70}$	$\frac{-3}{70}$	$\frac{-13}{35}$	$\frac{3}{35}$	$\frac{13}{70}$	$\frac{-3}{70}$	$\frac{-22}{35}$	$\frac{-4}{35}$	$\frac{11}{35}$	$\frac{2}{35}$
		$\frac{52}{35}$	$\frac{22}{105}$	$\frac{27}{35}$	$\frac{-13}{70}$	$\frac{18}{35}$	$\frac{-13}{105}$	$\frac{-27}{35}$	$\frac{13}{70}$	$\frac{9}{35}$	$\frac{-13}{210}$	$\frac{-78}{35}$	$\frac{-11}{35}$	$\frac{26}{35}$	$\frac{11}{105}$
			$\frac{4}{105}$	$\frac{13}{70}$	$\frac{-3}{70}$	$\frac{13}{105}$	$\frac{-1}{35}$	$\frac{-13}{70}$	$\frac{3}{70}$	$\frac{13}{210}$	$\frac{-1}{70}$	$\frac{-11}{35}$	$\frac{-2}{35}$	$\frac{11}{105}$	$\frac{2}{105}$
				$\frac{156}{35}$	$\frac{-22}{35}$	$\frac{78}{35}$	$\frac{-11}{35}$	$\frac{-156}{35}$	$\frac{22}{35}$	$\frac{78}{35}$	$\frac{-11}{35}$	$\frac{-54}{35}$	$\frac{-13}{35}$	$\frac{27}{35}$	$\frac{13}{70}$
					$\frac{4}{35}$	$\frac{-11}{35}$	$\frac{2}{35}$	$\frac{22}{35}$	$\frac{-4}{35}$	$\frac{-11}{35}$	$\frac{2}{35}$	$\frac{13}{35}$	$\frac{3}{35}$	$\frac{-13}{70}$	$\frac{-3}{70}$
						$\frac{52}{35}$	$\frac{-22}{105}$	$\frac{-78}{35}$	$\frac{11}{35}$	$\frac{26}{35}$	$\frac{-11}{105}$	$\frac{-27}{35}$	$\frac{-13}{70}$	$\frac{9}{35}$	$\frac{13}{210}$
							$\frac{4}{105}$	$\frac{11}{35}$	$\frac{-2}{35}$	$\frac{-11}{105}$	$\frac{2}{105}$	$\frac{13}{70}$	$\frac{3}{70}$	$\frac{-13}{210}$	$\frac{-1}{70}$
								$\frac{156}{35}$	$\frac{-22}{35}$	$\frac{-78}{35}$	$\frac{11}{35}$	$\frac{54}{35}$	$\frac{13}{35}$	$\frac{-27}{35}$	$\frac{-13}{70}$
									$\frac{4}{35}$	$\frac{11}{35}$	$\frac{-2}{35}$	$\frac{-13}{35}$	$\frac{-3}{35}$	$\frac{13}{70}$	$\frac{3}{70}$
										$\frac{52}{35}$	$\frac{-22}{105}$	$\frac{-27}{35}$	$\frac{-13}{70}$	$\frac{18}{35}$	$\frac{13}{105}$
											$\frac{4}{105}$	$\frac{13}{70}$	$\frac{3}{70}$	$\frac{-13}{105}$	$\frac{-1}{35}$
												$\frac{156}{35}$	$\frac{22}{35}$	$\frac{-78}{35}$	$\frac{-11}{35}$
													$\frac{4}{35}$	$\frac{-11}{35}$	$\frac{-2}{35}$
														$\frac{52}{35}$	$\frac{22}{105}$
Sym.															$\frac{4}{105}$

TABLE A.2 Values $k_{22}(i,j)$ in the stiffness matrix, Eq. A.21.

$\frac{144}{25}$	$\frac{12}{25}$	$\frac{12}{25}$	$\frac{1}{25}$	$\frac{-144}{25}$	$\frac{12}{25}$	$\frac{-12}{25}$	$\frac{1}{25}$	$\frac{144}{25}$	$\frac{-12}{25}$	$\frac{-12}{25}$	$\frac{1}{25}$	$\frac{-144}{25}$	$\frac{-12}{25}$	$\frac{12}{25}$	$\frac{1}{25}$
	$\frac{16}{25}$	$\frac{1}{25}$	$\frac{4}{75}$	$\frac{-12}{25}$	$\frac{-4}{25}$	$\frac{-1}{25}$	$\frac{-1}{75}$	$\frac{12}{25}$	$\frac{4}{25}$	$\frac{-1}{25}$	$\frac{-1}{75}$	$\frac{-12}{25}$	$\frac{-16}{25}$	$\frac{1}{25}$	$\frac{4}{75}$
		$\frac{16}{25}$	$\frac{4}{75}$	$\frac{-12}{25}$	$\frac{1}{25}$	$\frac{-16}{25}$	$\frac{4}{75}$	$\frac{12}{25}$	$\frac{-1}{25}$	$\frac{4}{25}$	$\frac{-1}{75}$	$\frac{-12}{25}$	$\frac{-1}{25}$	$\frac{-4}{25}$	$\frac{-1}{75}$
			$\frac{16}{225}$	$\frac{-1}{25}$	$\frac{-1}{75}$	$\frac{-4}{75}$	$\frac{-4}{225}$	$\frac{1}{25}$	$\frac{1}{75}$	$\frac{1}{75}$	$\frac{1}{225}$	$\frac{-1}{25}$	$\frac{-4}{75}$	$\frac{-1}{75}$	$\frac{-4}{225}$
				$\frac{144}{25}$	$\frac{-12}{25}$	$\frac{12}{25}$	$\frac{-1}{25}$	$\frac{-144}{25}$	$\frac{12}{25}$	$\frac{12}{25}$	$\frac{-1}{25}$	$\frac{144}{25}$	$\frac{12}{25}$	$\frac{-12}{25}$	$\frac{-1}{25}$
					$\frac{16}{25}$	$\frac{-1}{25}$	$\frac{4}{75}$	$\frac{12}{25}$	$\frac{-16}{25}$	$\frac{-1}{25}$	$\frac{4}{75}$	$\frac{-12}{25}$	$\frac{4}{25}$	$\frac{1}{25}$	$\frac{-1}{75}$
						$\frac{16}{25}$	$\frac{-4}{75}$	$\frac{-12}{25}$	$\frac{1}{25}$	$\frac{-4}{25}$	$\frac{1}{75}$	$\frac{12}{25}$	$\frac{1}{25}$	$\frac{4}{25}$	$\frac{1}{75}$
							$\frac{16}{225}$	$\frac{1}{25}$	$\frac{-4}{75}$	$\frac{1}{75}$	$\frac{-4}{225}$	$\frac{-1}{25}$	$\frac{1}{75}$	$\frac{-1}{75}$	$\frac{1}{225}$
								$\frac{144}{25}$	$\frac{-12}{25}$	$\frac{-12}{25}$	$\frac{1}{25}$	$\frac{-144}{25}$	$\frac{-12}{25}$	$\frac{12}{25}$	$\frac{1}{25}$
									$\frac{16}{25}$	$\frac{1}{25}$	$\frac{-4}{75}$	$\frac{12}{25}$	$\frac{-4}{25}$	$\frac{-1}{25}$	$\frac{1}{75}$
										$\frac{16}{25}$	$\frac{-4}{75}$	$\frac{12}{25}$	$\frac{1}{25}$	$\frac{-16}{25}$	$\frac{-4}{75}$
											$\frac{16}{225}$	$\frac{-1}{25}$	$\frac{1}{75}$	$\frac{4}{75}$	$\frac{-4}{225}$
												$\frac{144}{25}$	$\frac{12}{25}$	$\frac{-12}{25}$	$\frac{-1}{25}$
													$\frac{16}{25}$	$\frac{-1}{25}$	$\frac{-4}{75}$
														$\frac{16}{25}$	$\frac{4}{75}$
Sym.															$\frac{16}{225}$

TABLE A.3 Values of $k_{33}(i,j)$ in the stiffness matrix, Eq. A.21.

$\frac{72}{25}$	$\frac{36}{25}$	$\frac{36}{25}$	$\frac{11}{50}$	$\frac{-72}{25}$	$\frac{6}{25}$	$\frac{-36}{25}$	$\frac{3}{25}$	$\frac{72}{25}$	$\frac{-6}{25}$	$\frac{-6}{25}$	$\frac{1}{50}$	$\frac{-72}{25}$	$\frac{-36}{25}$	$\frac{6}{25}$	$\frac{3}{25}$
	$\frac{8}{25}$	$\frac{61}{50}$	$\frac{4}{25}$	$\frac{-6}{25}$	$\frac{-2}{25}$	$\frac{-3}{25}$	$\frac{-1}{25}$	$\frac{6}{25}$	$\frac{2}{25}$	$\frac{-1}{50}$	$\frac{-1}{150}$	$\frac{-36}{25}$	$\frac{-8}{25}$	$\frac{3}{25}$	$\frac{2}{75}$
		$\frac{8}{25}$	$\frac{4}{25}$	$\frac{-36}{25}$	$\frac{3}{25}$	$\frac{-8}{25}$	$\frac{2}{75}$	$\frac{6}{25}$	$\frac{-1}{50}$	$\frac{2}{25}$	$\frac{-1}{150}$	$\frac{-6}{25}$	$\frac{-3}{25}$	$\frac{-2}{25}$	$\frac{-1}{25}$
			$\frac{8}{225}$	$\frac{-3}{25}$	$\frac{-1}{25}$	$\frac{-2}{75}$	$\frac{-2}{225}$	$\frac{1}{50}$	$\frac{1}{150}$	$\frac{1}{150}$	$\frac{1}{450}$	$\frac{-3}{25}$	$\frac{-2}{75}$	$\frac{-1}{25}$	$\frac{-2}{225}$
				$\frac{72}{25}$	$\frac{-36}{25}$	$\frac{36}{25}$	$\frac{-11}{50}$	$\frac{-72}{25}$	$\frac{36}{25}$	$\frac{6}{25}$	$\frac{-3}{25}$	$\frac{72}{25}$	$\frac{6}{25}$	$\frac{-6}{25}$	$\frac{-1}{50}$
					$\frac{8}{25}$	$\frac{-61}{50}$	$\frac{4}{25}$	$\frac{36}{25}$	$\frac{-8}{25}$	$\frac{-3}{25}$	$\frac{2}{75}$	$\frac{-6}{25}$	$\frac{2}{25}$	$\frac{1}{50}$	$\frac{-1}{150}$
						$\frac{8}{25}$	$\frac{-4}{25}$	$\frac{-6}{25}$	$\frac{3}{25}$	$\frac{-2}{25}$	$\frac{1}{25}$	$\frac{6}{25}$	$\frac{1}{50}$	$\frac{2}{25}$	$\frac{1}{150}$
							$\frac{8}{225}$	$\frac{3}{25}$	$\frac{-2}{75}$	$\frac{1}{25}$	$\frac{-1}{225}$	$\frac{-1}{50}$	$\frac{1}{150}$	$\frac{-1}{150}$	$\frac{1}{450}$
								$\frac{72}{25}$	$\frac{-36}{25}$	$\frac{-36}{25}$	$\frac{11}{50}$	$\frac{-72}{25}$	$\frac{-6}{25}$	$\frac{36}{25}$	$\frac{3}{25}$
									$\frac{8}{25}$	$\frac{61}{50}$	$\frac{-4}{25}$	$\frac{6}{25}$	$\frac{-2}{25}$	$\frac{-3}{25}$	$\frac{1}{25}$
										$\frac{8}{25}$	$\frac{-4}{25}$	$\frac{36}{25}$	$\frac{3}{25}$	$\frac{-8}{25}$	$\frac{-2}{75}$
											$\frac{8}{225}$	$\frac{-3}{25}$	$\frac{1}{25}$	$\frac{2}{75}$	$\frac{-2}{225}$
												$\frac{72}{25}$	$\frac{36}{25}$	$\frac{-36}{25}$	$\frac{-11}{50}$
													$\frac{8}{25}$	$\frac{-61}{50}$	$\frac{-4}{25}$
														$\frac{8}{25}$	$\frac{4}{25}$
Sym.															$\frac{8}{225}$

TABLE A.4 Values of $k_{12}(i,j)$ in the stiffness matrix Eq. A.21.

0	0	0	$\frac{-2}{5}$	0	0	0	$\frac{2}{5}$	0	2	0	$\frac{-2}{5}$	0	-2	0	$\frac{2}{5}$
	1	$\frac{2}{5}$	0	0	0	$\frac{-2}{5}$	$\frac{1}{5}$	-2	1	$\frac{2}{5}$	$\frac{1}{5}$	2	0	$\frac{-2}{5}$	0
		0	0	0	$\frac{-2}{5}$	0	0	0	$\frac{2}{5}$	0	$\frac{-1}{15}$	0	$\frac{-2}{5}$	0	$\frac{1}{15}$
			0	$\frac{2}{5}$	$\frac{-1}{5}$	0	0	$\frac{-2}{5}$	$\frac{1}{5}$	$\frac{1}{15}$	$\frac{-1}{30}$	$\frac{2}{5}$	0	$\frac{-1}{15}$	0
				0	0	0	$\frac{-2}{5}$	0	-2	0	$\frac{2}{5}$	0	2	0	$\frac{-2}{5}$
					-1	$\frac{2}{5}$	0	2	0	$\frac{-2}{5}$	0	-2	-1	$\frac{2}{5}$	$\frac{1}{5}$
						0	0	0	$\frac{-2}{5}$	0	$\frac{1}{15}$	0	$\frac{2}{5}$	0	$\frac{-1}{15}$
							0	$\frac{2}{5}$	0	$\frac{-1}{15}$	0	$\frac{-2}{5}$	$\frac{-1}{5}$	$\frac{1}{15}$	$\frac{1}{30}$
								0	0	0	$\frac{-2}{5}$	0	0	0	$\frac{2}{5}$
									1	$\frac{2}{5}$	0	0	0	$\frac{-2}{5}$	$\frac{-1}{5}$
										0	0	0	$\frac{-2}{5}$	0	0
											0	$\frac{2}{5}$	$\frac{1}{5}$	0	0
												0	0	0	$\frac{-2}{5}$
													-1	$\frac{2}{5}$	0
														0	0
Sym.															0

TABLE A.5 Values of k_{13} (i,j) in the stiffness matrix, Eq. A.21.

0	0	0	$\frac{-2}{5}$	0	0	$\frac{-2}{1}$	$\frac{2}{5}$	0	0	$\frac{2}{1}$	$\frac{-2}{5}$	0	0	0	$\frac{2}{5}$
	0	$\frac{2}{5}$	0	0	0	$\frac{-2}{5}$	$\frac{1}{15}$	0	0	$\frac{2}{5}$	$\frac{-1}{15}$	0	0	$\frac{-2}{5}$	0
		1	0	2	$\frac{-2}{5}$	0	0	-2	$\frac{2}{5}$	1	$\frac{-1}{5}$	0	$\frac{-2}{5}$	0	$\frac{1}{5}$
			0	$\frac{2}{5}$	$\frac{-1}{15}$	0	0	$\frac{-2}{5}$	$\frac{1}{15}$	$\frac{1}{5}$	$\frac{-1}{30}$	$\frac{2}{5}$	0	$\frac{-1}{5}$	0
				0	0	0	$\frac{-2}{5}$	0	0	0	$\frac{2}{5}$	0	0	-2	$\frac{-2}{5}$
					0	$\frac{2}{5}$	0	0	0	$\frac{-2}{5}$	0	0	0	$\frac{2}{5}$	$\frac{1}{15}$
						-1	0	0	$\frac{-2}{5}$	0	$\frac{1}{5}$	2	$\frac{2}{5}$	-1	$\frac{-1}{5}$
							0	$\frac{2}{5}$	0	$\frac{-1}{5}$	0	$\frac{-2}{5}$	$\frac{-1}{15}$	$\frac{1}{5}$	$\frac{1}{30}$
								0	0	0	$\frac{-2}{5}$	0	0	2	$\frac{2}{5}$
									0	$\frac{2}{5}$	0	0	0	$\frac{-2}{5}$	$\frac{-1}{15}$
										1	0	-2	$\frac{-2}{5}$	0	0
											0	$\frac{2}{5}$	$\frac{1}{15}$	0	0
												0	0	0	$\frac{-2}{5}$
													0	$\frac{2}{5}$	0
														-1	0
Sym.															0

TABLE A.6 Values of the $k_{23}(i,j)$ in the stiffness matrix, Eq. A.21

0	1	0	1	0	1	0	1	0	1	0	1	0	1	0	1
	2	1	2	1	2	1	2	1	2	1	2	1	2	1	2
		0	1	0	1	0	1	0	1	0	1	0	1	0	1
			2	1	2	1	2	1	2	1	2	1	2	1	2
				0	1	0	1	0	1	0	1	0	1	0	1
					2	1	2	1	2	1	2	1	2	1	2
						0	1	0	1	0	1	0	1	0	1
							2	1	2	1	2	1	2	1	2
								0	1	0	1	0	1	0	1
									2	1	2	1	2	1	2
										0	1	0	1	0	1
											2	1	2	1	2
												0	1	0	1
													2	1	2
														0	1
Sym.															2

TABLE A.7 Values of $\overline{col}(i,j)$ in the stiffness matrix, Eq. A.21

0	0	1	1	0	0	1	1	0	0	1	1	0	0	1	1
	0	1	1	0	0	1	1	0	0	1	1	0	0	1	1
		2	2	1	1	2	2	1	1	2	2	1	1	2	2
			2	1	1	2	2	1	1	2	2	1	1	2	2
				0	0	1	1	0	0	1	1	0	0	1	1
					0	1	1	0	0	1	1	0	0	1	1
						2	2	1	1	2	2	1	1	2	2
							2	1	1	2	2	1	1	2	2
								0	0	1	1	0	0	1	1
									0	1	1	0	0	1	1
										2	2	1	1	2	2
											2	1	1	2	2
												0	0	1	1
													0	1	1
														2	2
Sym.															2

TABLE A.8 Values of $\overline{co2}(i,j)$ in the stiffness matrix, Eq. A.21

$$\{\Delta f\} = \begin{bmatrix} 0 & \frac{b}{2} & 0 & \frac{b^2}{12} & 0 & \frac{-b}{2} & 0 & \frac{-b^2}{12} & 0 & \frac{-b}{2} & 0 & \frac{b^2}{12} & 0 & \frac{b}{2} & 0 & \frac{-b^2}{12} \\ 0 & 0 & \frac{a}{2} & \frac{a^2}{12} & 0 & 0 & \frac{a}{2} & \frac{-a^2}{12} & 0 & 0 & \frac{-a}{2} & \frac{a^2}{12} & 0 & 0 & \frac{-a}{2} & \frac{-a^2}{12} \\ -2 & 0 & 0 & 0 & 2 & 0 & 0 & 0 & -2 & 0 & 0 & 0 & 2 & 0 & 0 & 0 \end{bmatrix}^T \{\Delta M_\sigma\}$$

TABLE A.9 Calculation of residual nodal forces from residual moments at the element centroid

$$[B] = \begin{bmatrix} 0 & \frac{1}{2a} & 0 & \frac{b}{8a} & 0 & \frac{-1}{2a} & 0 & \frac{-b}{8a} & 0 & \frac{-1}{2a} & 0 & \frac{b}{8a} & 0 & \frac{1}{2a} & 0 & \frac{-b}{8a} \\ 0 & 0 & \frac{1}{2b} & \frac{a}{8b} & 0 & 0 & \frac{1}{2b} & \frac{-a}{8b} & 0 & 0 & \frac{-1}{2b} & \frac{a}{8b} & 0 & 0 & \frac{-1}{2b} & \frac{-a}{8b} \\ \frac{-9}{2ab} & \frac{-3}{4b} & \frac{-3}{4a} & \frac{-1}{8} & \frac{9}{2ab} & \frac{-3}{4b} & \frac{3}{4a} & \frac{-1}{8} & \frac{-9}{2ab} & \frac{3}{4b} & \frac{3}{4a} & \frac{-1}{8} & \frac{9}{2ab} & \frac{3}{4b} & \frac{-3}{4a} & \frac{-1}{8} \end{bmatrix}$$

TABLE A.10 B matrix evaluated at the element centroid

$$
\begin{bmatrix}
\frac{6}{a^2} & \frac{4}{a} & 0 & 0 & \frac{-6}{a^2} & \frac{-2}{a} & 0 & 0 & 0 & 0 & 0 & 0 & 0 & 0 & 0 & 0 \\
\frac{6}{b^2} & 0 & \frac{4}{b} & 0 & 0 & 0 & 0 & 0 & 0 & 0 & 0 & 0 & \frac{-6}{b^2} & 0 & \frac{-2}{b} & 0 \\
0 & 0 & 0 & -2 & 0 & 0 & 0 & 0 & 0 & 0 & 0 & 0 & 0 & 0 & 0 & 0 \\
\frac{-6}{a^2} & \frac{2}{a} & 0 & 0 & \frac{6}{a^2} & \frac{-4}{a} & 0 & 0 & 0 & 0 & 0 & 0 & 0 & 0 & 0 & 0 \\
0 & 0 & 0 & 0 & 0 & 0 & 0 & 0 & \frac{-6}{b^2} & 0 & \frac{-2}{b} & 0 & \frac{-6}{b^2} & 0 & \frac{-2}{b} & 0 \\
0 & 0 & 0 & 0 & 0 & 0 & 0 & -2 & 0 & 0 & 0 & 0 & 0 & 0 & 0 & 0 \\
0 & 0 & 0 & 0 & 0 & 0 & 0 & 0 & \frac{6}{a^2} & \frac{-4}{a} & 0 & 0 & \frac{-6}{a^2} & \frac{2}{a} & 0 & 0 \\
0 & 0 & 0 & 0 & \frac{-6}{b^2} & 0 & \frac{2}{b} & 0 & \frac{6}{b^2} & 0 & \frac{-4}{b} & 0 & 0 & 0 & 0 & 0 \\
0 & 0 & 0 & 0 & 0 & 0 & 0 & 0 & 0 & 0 & 0 & -2 & 0 & 0 & 0 & 0 \\
0 & 0 & 0 & 0 & 0 & 0 & 0 & 0 & \frac{-2}{a^2} & \frac{-2}{a} & 0 & 0 & \frac{6}{a^2} & \frac{4}{a} & 0 & 0 \\
\frac{-6}{b^2} & \frac{2}{b} & 0 & 0 & 0 & 0 & 0 & 0 & 0 & 0 & 0 & 0 & \frac{6}{b^2} & 0 & \frac{-4}{b} & 0 \\
0 & 0 & 0 & 0 & 0 & 0 & 0 & 0 & 0 & 0 & 0 & 0 & 0 & 0 & 0 & -2
\end{bmatrix}
$$

$$
\{\kappa\}_{12x1} = [B]_{12x16} \{\delta\}_{16x1}
$$

TABLE A.11 B matrix evaluated at the nodal points

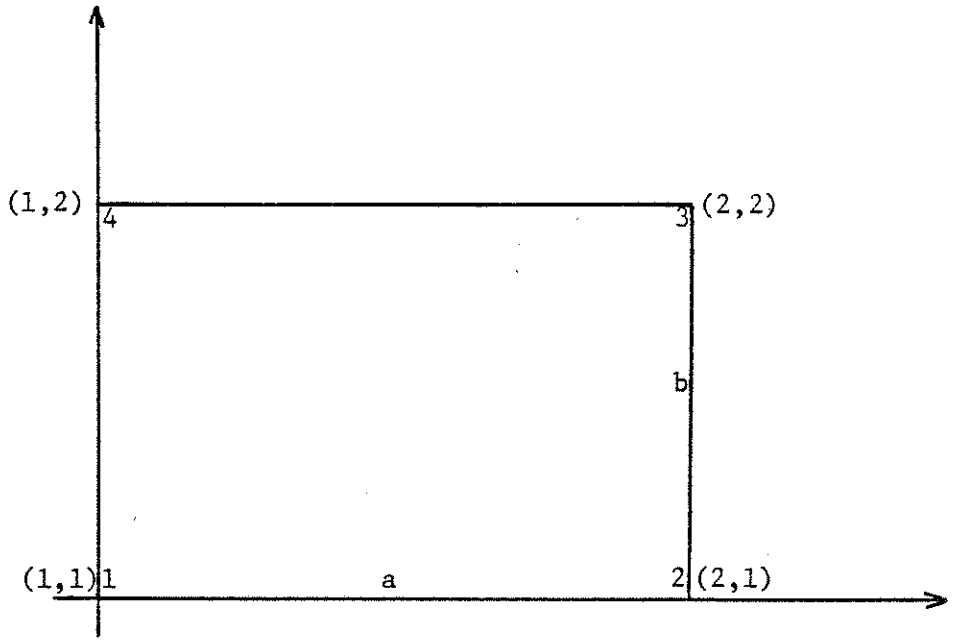

Fig. A.1 Rectangular Plate Element

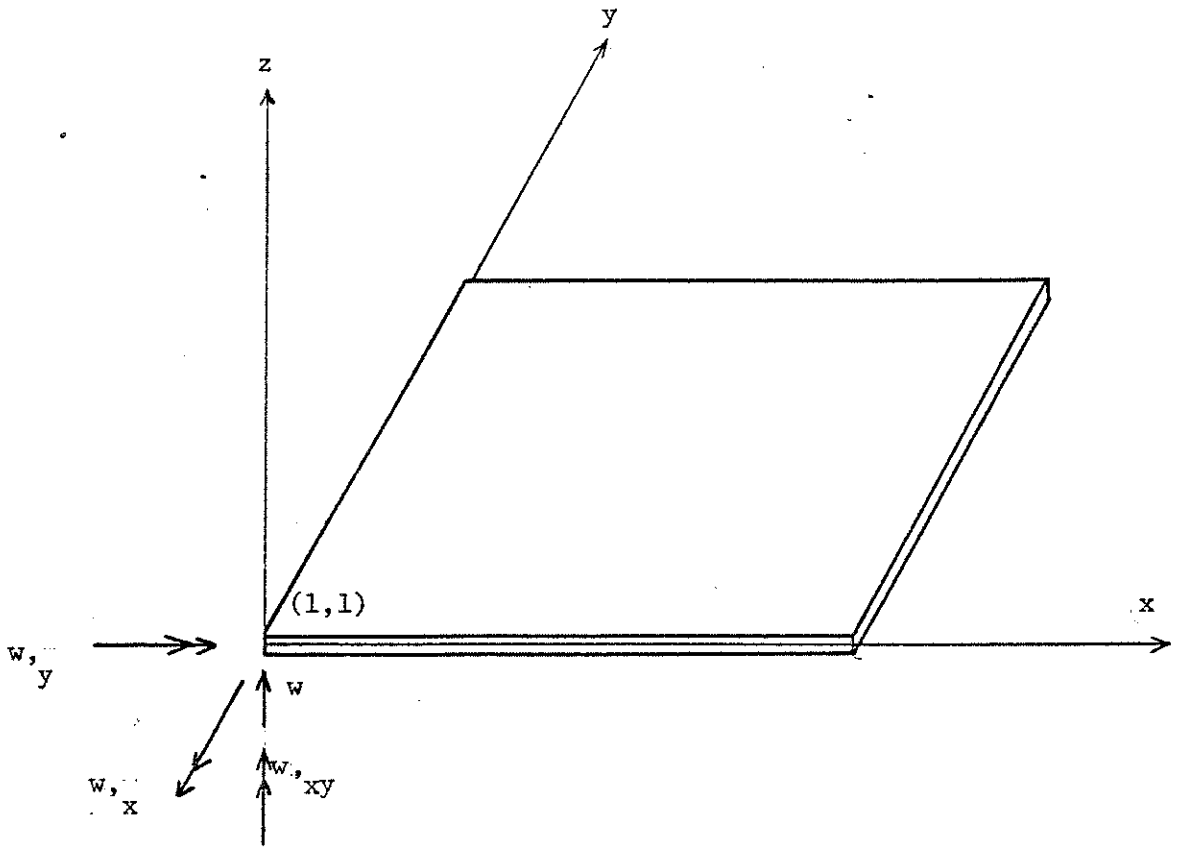

Fig. A.2 Nodal Degrees of Freedom

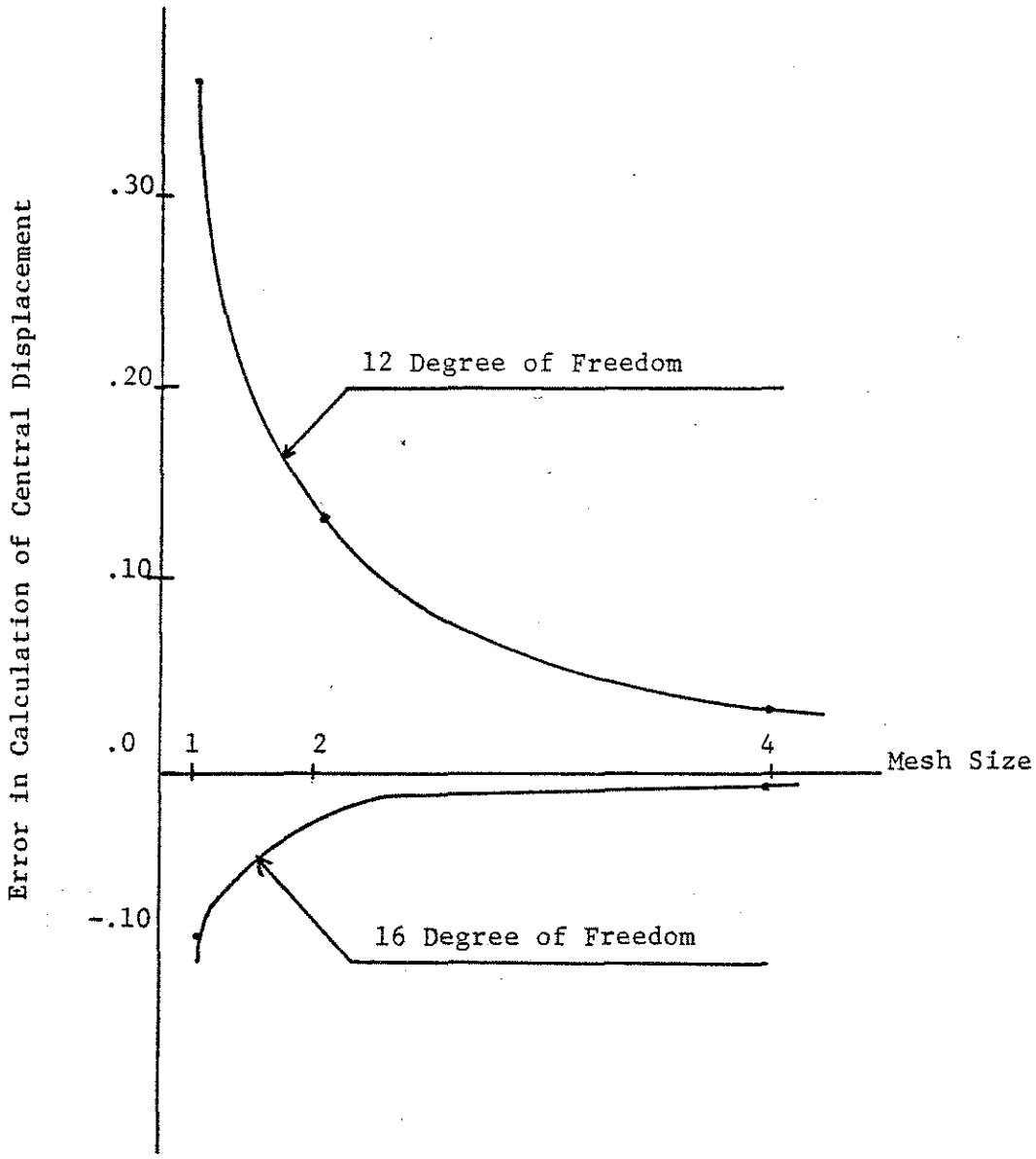

Fig. A.3 Convergence Properties of the Rectangular Bending Elements of Twelve and Sixteen Degrees of Freedom (33)

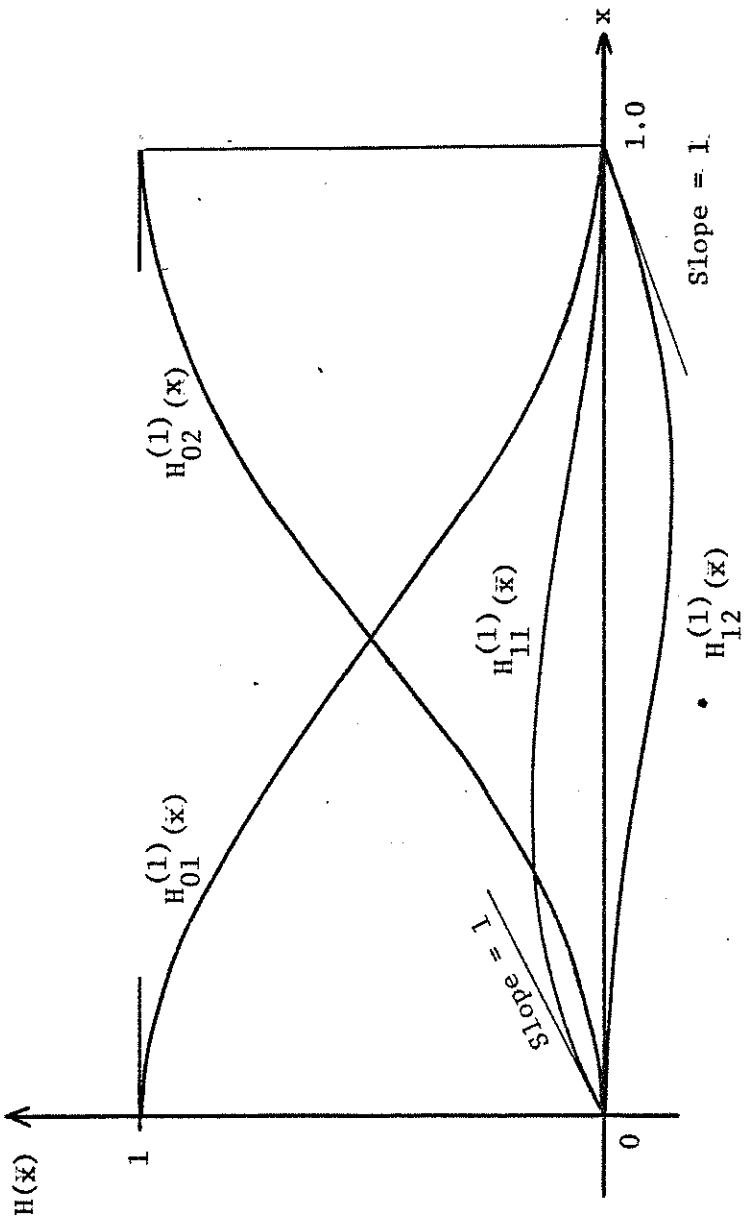

Fig. A.4 First Order Hermitian Polynomials